SKIN FLAP SURGERY – NON-INVASIVE *IN VIVO* METHODOLOGY TO PREDICT SKIN FLAP SHRINKAGE

LIM KENG HUI

NATIONAL UNIVERSITY OF SINGAPORE

2008

SKIN FLAP SURGERY –
NON-INVASIVE *IN VIVO* METHODOLOGY
TO PREDICT SKIN FLAP SHRINKAGE

LIM KENG HUI

(B. Eng., Imperial College, UK;
MS. Eng, Massachusetts Institute of Technology, USA)

A THESIS SUBMITTED

FOR THE DEGREE OF DOCTOR OF PHILOSOPHY

DEPARTMENT OF MECHANICAL ENGINEERING

NATIONAL UNIVERSITY OF SINGAPORE

2008

ACKNOWLEDGEMENT

TABLE OF CONTENTS

SUMMARY

Skin flap transplant is a common procedure in reconstructive surgery, where surgeons transfer a healthy skin flap from a donor site to the traumatized wound site. Skin flaps generally undergo shrinkage/retraction after harvest, and estimating the geometry of the flaps to be harvested to resurface the defect site is difficult. There is currently no standard objective method and depends on the experience of the surgeon. The goal of this project is thus to develop a surgical planning methodology to aid the prediction of skin flap shrinkage prior or during a flap transplant surgery.

To measure the biomechanical properties of skin for analysis, a new device in the form of an extensometer was developed. This device was demonstrated to be effective in removing unwanted peripheral forces during *in vivo* measurement to produce results that were significantly closer to the *true* uniaxial skin properties, as compared to existing devices. Besides innovations in design, the new device also incorporated a standardization protocol in its construction and operations that was designed to produce consistent and reproducible results.

The Langer's line, or line of tension, is an important parameter in the study of skin biomechanics. It has been stated in literature that biomechanical properties and shrinkage behavior are orthotropic along and perpendicular to the Langer's line. It was established in this work that terminal stiffness of skin can be approximated to be orthotropic. This new observation led to the development of a reliable non-invasive method to predict the direction of the Langer's line using the new device.

A method was further developed to predict the shrinkage of skin flap by analyzing the compressive force-displacement data measured by the new device. Although the device took measurement at a small localized region of the skin, it was demonstrated that the predicted shrinkage can represent that of a much larger flap (needed in surgery) with uniform Langer's line directions. The validation experiments on animals have been shown to produce results with an average absolute error of 6% between the actual and predicted shrinkages. This may be close to what an experienced surgeon would estimate subjectively, thus indicating the usefulness of this method as a clinical tool for training or surgery. Aside from shrinkage, the proposed method was also demonstrated to be capable of estimating the natural tension and elastic modulus of skin. Measurement of these parameters is important for finite element modeling to study skin biomechanics and shrinkage, which is a project that is done in parallel to this work.

In summary, the work in this thesis involved the developments of instrumentation, measurement methodologies and data analysis. Beside the theoretical conception, validation results from software simulations and actual experiments involving synthetic materials and animal models are presented. This work is part of a large-scale project to develop an integrated skin flap surgical planning system, and this study has demonstrated that it is feasible.

LIST OF TABLES

LIST OF FIGURES

LIST OF SYMBOLS

α	Angle
a	Major axis value of an ellipse
b	Minor axis value of an ellipse
$\Delta\varepsilon_{res}$	Residual strain
e	Extension (distance)
ε	Strain
F	Force
F_0	Force along the x-axis
F_p	Peripheral force
$F_{peripheral}$	Peripheral force
F_{total}	Total force
$f(x)$	Function in x
$g(x)$	Function in x
h	Interval length (distance)
$k_{e,\theta}$	Uniaxial spring constant of material at angle θ and extension e
LL	Langer's line
l_0	Original length (distance)
Δl	Displacement
Δl_{res}	Residual deformation
m	Length
m'	Length
N	Size of object, or total value
NL	Natural length
NT	Natural tension
σ	Stress
S_i	Data point on an ellipse

t	Thickness	
θ	Angle	xv
T_i	Terminal stiffness	
T_N	Natural tension	
w	Width	

CHAPTER 1
INTRODUCTION

1.1. <u>Problem statement</u>

Skin flap transplant is a common procedure in reconstructive surgery, where surgeons transfer a healthy skin flap from a donor site to the traumatized wound site (also call the *primary defect*). Skin is a complex structure that is subjected to a *natural tension* on a human body (Cox, 1941; Langer, 1978 B). Estimating the size and geometry of a skin flap to be harvested to resurface the defect site can be difficult, and there is currently no standard objective method. This is due to the deformation of skin flap after harvest. The changes in size and geometry of flap after harvest are highly patient specific, and vary with factors such as the skin's biomechanical properties and natural tension (Cox, 1941; Langer, 1978 B). These factors are in turn dependent on the patient's age, gender, body mass index and location of the donor site. Most of the time, the skin flap shrinks after harvest (Barrett-Brown *et al*., 1945; Crawford, 1965).

Adequate blood supply is critical to the survival of the flap after the harvest and revascularization. Re-stretching a shrunken flap to its original size so as to fit the primary defect would cause tension on the anastomosis and decrease flow through it, resulting in thrombosis. Furthermore, following revascularization of the flap after sitting it on the defect site, the subsequent tissue swelling may also compromise circulation because of the increased pressure closing in at the vessels. Ideally, a surgeon will want the shrunken flap to closely match the size and geometry of the primary defect so that it can be transplanted without producing tension (Barron *et al*, 1965).

When designing the donor flaps, surgeons are taught to allow for the retraction behavior of skin but the excess amount is normally left to the individual surgeon to decide from his/her own experience. Presently, surgeons based their judgment on tactile pinches on the patient's skin to estimate skin tension, patient's physiology, and location of the donor site. Due to the lack of quantitative tools and inadequate understanding of the biomechanical behavior of skin, the surgeon has a difficult problem of determining the appropriate size and geometry of the flap to harvest, while avoiding tissue wastage. As a result, flap/wound mismatch problem is common. This leads to further complications during surgery and unnecessary trauma to the patient.

1.2. <u>Motivation</u>

Numerous groups have studied about flap shrinkage or retraction after harvest (Barrett-Brown *et al*, 1945; Blocker *et al*, 1950; Cannon *et al*, 1947; Coakley *et al*, 1950; etc). However, to the best of our knowledge, there is no work done to estimate skin flap shrinkage quantitatively. Therefore, to objectively assist surgeons during the critical stage of skin flap planning, an *in vivo* non-invasive methodology should be developed.

A literature survey also revealed that current non-invasive devices that measure the uniaxial biomechanical properties of skin *in vivo* are significantly inaccurate. This is due to the fact that in an *in vivo* setting, the tension from directions other than the measurement axis results in a non-uniform stress field in the skin, thus adding error to the measurement result. Due to this inaccuracy, results from existing devices may not accurately represent the *true* uniaxial biomechanical behavior; this property is what

one would obtain in a uniform stress field in the test material, such as an *in vitro* setting. Therefore, to assist researchers and doctors in the field of skin behavior studies, a new device should be developed to address this problem.

1.3.   Objectives and scope of work

Based on the problem and motivation discussed, the overall goal of this project is to develop a surgical planning methodology to aid the prediction of skin flap shrinkage prior or during a flap transplant surgery. The specific objectives for this thesis work are to develop the following:

- A means to measure the *true* uniaxial biomechanical properties of skin accurately. This information can be used to study skin elasticity, shrinkage and other biomechanical behaviors.

- A means to predict the geometry and size of post-harvest skin flap shrinkage during surgical planning.

- A means to measure specific biomechanical properties of skin for finite element modeling of shrinkage behavior. These properties include the direction of Langer's line (which strongly corresponds to the principal stress axis), Young's modulus of elasticity, and natural tension of skin.

It is not within the scope of this thesis work to develop a finite element model, or a full mathematical model of the skin biomechanics. This work is carried out in another parallel study.

To achieve these objectives, the scope of the work includes:

- Literature search to review work done in the area of skin biomechanics and skin measurement devices.

- Design, construct and test a measurement device to estimate the *true* uniaxial biomechanical properties of skin. The new device will become the standard tool for the whole research work.

- Develop a model and method to estimate the direction of Langer's line.

- Develop a model and method to estimate the geometry and size of skin flap shrinkage post-harvest, i.e. the *natural length* of skin.

- Develop a model and method to estimate the natural tension and elastic modulus.

- Preliminary testing of the developed methods using software simulation, rubber sheets and animal skin sheets.

- Actual testing with clinical trials on animals (pigs).

In this thesis, the *natural length* refers to the shrunken dimension of a skin flap after it is harvested from the body, i.e. the flap dimension without tension.

1.4.   **Organization of thesis**

This thesis is organized as follows:

Chapter 2 describes an overview of the skin flap surgery and the biomechanical properties of skin. A literature review of current skin measurement devices and existing work done to estimate flap shrinkage and natural tension are also examined.

Chapter 3 presents a new measurement device capable of estimating the *true* uniaxial biomechanical properties of skin. The chapter first examines the limitations of current designs and then presents a new superior design. Verification tests using software simulation, rubber sheets and animal models are also presented.

Chapter 4 examines the principles and assumptions of the skin measurement in this research work. Specifically, the topics of the accuracy of *in vivo* non-invasive

measurement using the new device, skin viscoelasticity, skin preconditioning, and measurement standardization protocols are discussed. The use of the pig model as a human surrogate in validation studies is also covered.

Chapter 5 discusses and establishes the relationship between the Langer's line and properties such as the orientation of the skin's collagen fibers network, force-extension data, and the terminal stiffness of skin. In addition, this chapter describes an *in vivo* non-invasive method to predict the direction of the Langer's line.

Chapter 6 presents an *in vivo* non-invasive method using the new device to predict local skin flap shrinkage, as well as the natural tension and Young's modulus of elasticity of skin. Validation trials on rubber sheets and animal models are described, followed by results presentation and discussions.

Chapter 7 presents an integrated methodology that enables surgeons to predict the shrinkage of a large skin flap. Validation trials on animal models are also presented.

Chapter 8 concludes the thesis by discussing the contributions made and the recommendations for future work.

The Appendix includes information of the research work which is not described in detail in the main chapters so as to facilitate reading, and these information include experimental details, data, and calculation examples.

CHAPTER 2

LITERATURE REVIEW

2.1. <u>Introduction</u>

This chapter describes an overview of the skin flap surgery and the biomechanical properties of skin. A literature review of current skin measurement devices is also discussed. Finally, the existing work done to predict skin shrinkage and natural tension is examined.

2.2. <u>Skin flap surgery</u>

Resurfacing of skin loss with a skin flap is a common reconstructive procedure. This is an autotransplantation, where surgeons transfer a healthy skin flap from a donor site to the traumatized wound site on the same body (Masquelet, 1995) (see Figure 2-1). The transplant of the pedicle flap is of interest to this research work. The pedicle flap consists of the full thickness of the skin and the subcutaneous fat tissue, as well as the vascular network that receives the blood supply. During transplantation, once a pedicle flap is positioned at the wound site (also call the primary defect), it is carefully reattached to a vascular supply using microsurgical techniques, and then sutured at the edges to the surrounding tissue.

Adequate blood supply is critical to the survival of the flap after harvest and revascularization. The maintenance of vascular flow to the flap is dependent on rate of blood flow, viscosity of blood, and repair of the blood vessels (Virchow, 1998). It is essential to maintain the blood pressure above the critical closing pressure of 30

mmHg (Burton, 1951; Ashton, 1962). It is well known to surgeons that when a skin flap is harvested, most of the time the flap shrinks (Barrett-Brown *et al*., 1945; Crawford, 1965). Re-stretching a shrunken flap to its original size so as to fit the primary defect would cause tension on the anastomosis and decrease flow through it, resulting in thrombosis. Furthermore, following revascularization of the flap after sitting it on defect site, the flap swelling may also compromise circulation because of the increased pressure closing in at the vessels. Therefore, a surgeon will ideally want the shrunken flap to closely match the shape and size of the primary defect so that it can be transplanted without producing tension (Barron *et al*, 1965). When designing the donor flaps, the surgeons are taught to allow for retraction behavior of the flap but the excess amount is normally left to the individual surgeon to decide from his/her own experience.

Transplant (donor) site

Flap (shown with vascular network)
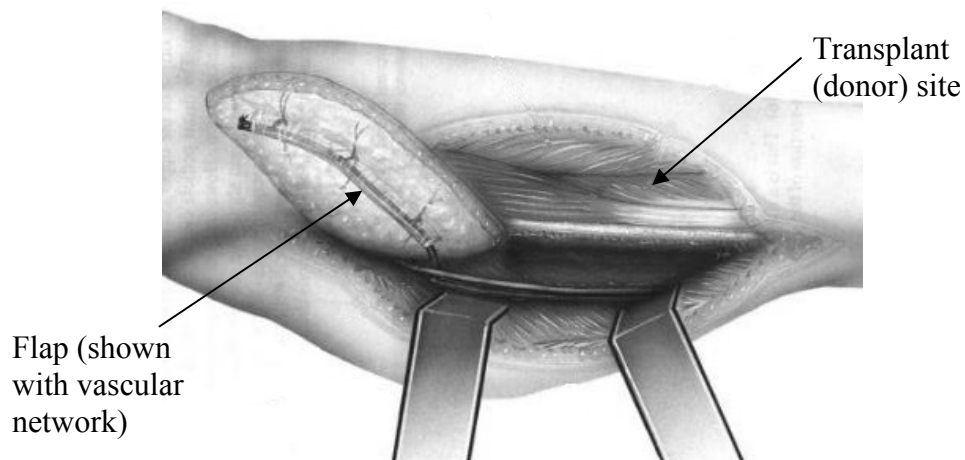
Figure 2-1: Illustration of skin flap harvest at a donor site; pedicle flap is shown with vascular network. (Picture taken from Strauch *et al*, 1992)

2.2.1. Skin flap composition

Skin flap comprises three main layers (Danielson, 1973), namely the epidermis, dermis, and subcutaneous (fat). The latter two layers contain a network of blood vessels (refer to Figure 2-2). The epidermis, which is a thin layer of stratified epithelium, is the outer layer of skin, and the thickness varies according to location. It

is the thinnest on the eyelids at 0.05 mm and the thickest on the palms and soles at 1.5 mm (Fawcett, 1986). The dermis is composed mainly of collagen fibres, ground substance and elastic fibres, and the dermis thickness also depends on location; it is roughly 0.3 mm on the eyelids to 3 mm on the back. The fat layer is generally much thicker than the dermal layer (Agache *et al*, 2004), and the thickness depends on the Body Mass Index of the subject. The entire flap sits above the muscle surface, separated by a thin tissue layer called fascia. At regions such as the scalp, the back of the neck, the palms of the hands and sole of the feet, the skin flap is firmly anchored to the underlying muscle tissues. At most other locations on the body, such as the dorsal and volar regions, the skin flap may move freely over the muscle.
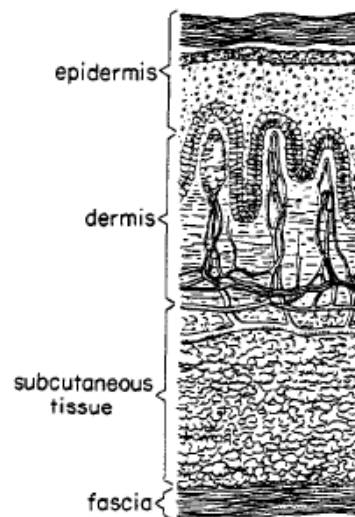
Figure 2-2: Cross section of human skin (Danielson, 1973)

2.2.2. Skin flap shrinkage

When a skin flap is harvested, most of the time the flap shrinks and the resultant wound (also call the *secondary defect*) expands. As early as 1950, Blocker and Mithoefer advised that the flap should be cut one quarter to one third longer than the defect so that it could be sutured in place in its relaxed retracted state (Blocker *et al*, 1950). It quickly became apparent to surgeons that the amount of excess tissue to be harvested cannot be simplified as what was suggested by Blocker and Mithoefer.

The shrinkage behavior is believed to be due to the pre-stress and the biomechanical properties of skin, and this varies with age, health, gender, body location and body mass index. In a skin area, the pre-stress is caused by both *internal* built-in and *external* tensions; the internal tension is also known as the natural tension. The tension magnitude at different sites on the body varies considerably, and it is also known that the tension is not equal in all directions.
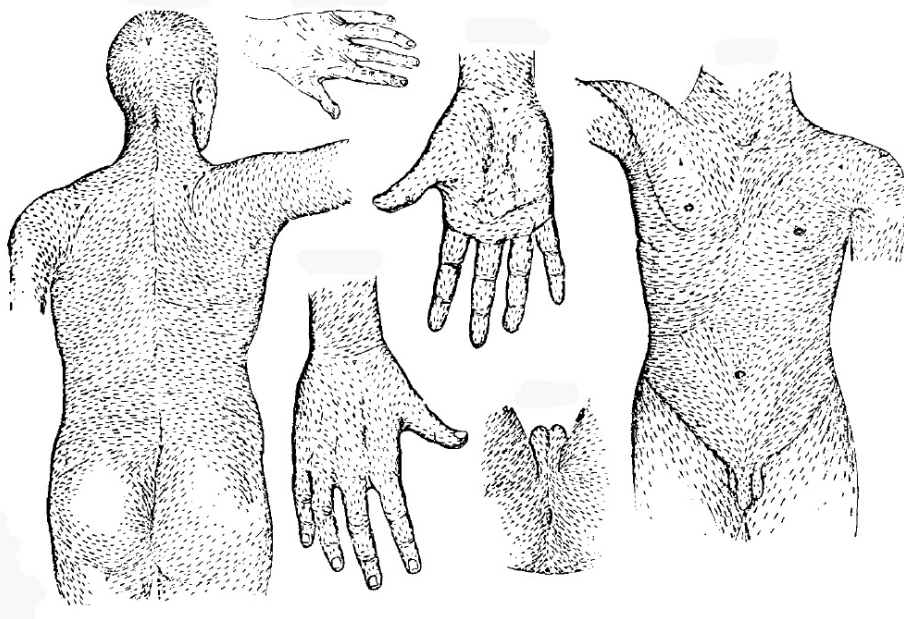
Figure 2-3: Langer's line (redrawn from Langer, 1978 A)

In 1860, Langer recognized the presence of a biaxial passive tension in human skin and his experiments led to the discovery of lines of tension (Langer, 1978 A, B) (refer to Figure 2-3). These tension lines (also called Langer's lines or cleavage lines) tend to correspond closely with the crease lines on the surface of the skin in most parts of the body. His experiments were later repeated by Cox (Cox, 1941), whose experiments further illustrated that the line pattern remained unaltered even after the skin was excised from the body. It was also subsequently reported that the Langer's lines correspond closely to the alignment of collagen fibers within the reticular

dermis. Reihsner and his coworkers (Reihsner *et al*, 1995) showed that the maximum tension is not parallel to the Langer's lines but it is in a small angle from it (refer to Figure 2-4). This observation had created some controversy but since the angle is small (less than 10 degrees), it was thought to be insignificant. Langer's line is important in the study of skin biomechanics because it will be discussed later in this chapter that biomechanical properties and shrinkage behavior of skin show symmetry along and perpendicular to the Langer's line. It is also interesting to note that knowledge of the Langer's line is important during surgery because wounds made across these tension lines are much more likely to produce a stretched or hypertrophic scar than those which parallel them.
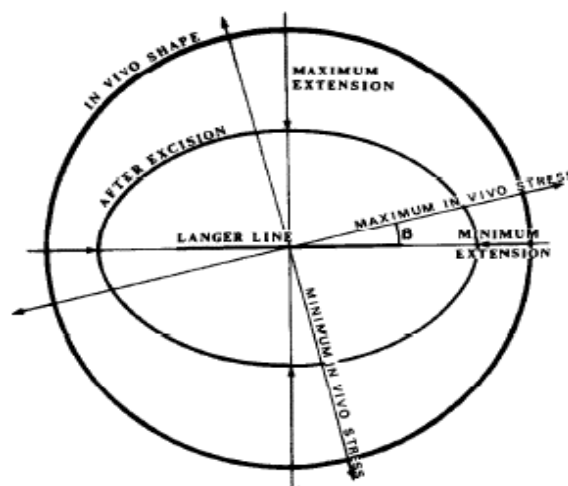
Figure 2-4: Deformation of circular sample after harvest, where the maximum tension line coincides closely with the Langer's line, which is along the ellipse's major axis (picture taken from Reihsner *et al*, 1995).

The internal natural tension is attributable to a constant state of strain produced due to the stretching of skin tissue over the bony framework, active fibroblast-collagen and fibroblast-fibroblast interactions (Silver *et al*, 2003; Kolodney *et al*, 1992). Reihser and coworkers (Reihsner *et al*, 1995) have reported that in a region where there is a high permanent *in vivo* strain, the dermis is thicker and collagen content is higher. This reflects the complex relationship of internal tension and the composition of skin

tissue, which may provide reason for the observed location-specific shrinkage of skin flaps. Beside internal tension, skin tissues throughout the body are also subjected to *external* mechanical forces due to joint, mimetic and other voluntary muscle movements.

Even though shrinkage phenomenon is widely recognized, to our knowledge, the amount of shrinkage has not been systematically studied or quantified. In literature, reported researches on skin flap shrinkage measurements are relatively few and at the same time, the results contradict each other. For instance, Crawford (Crawford, 1965) reported that a defect enlarges when the skin flap is excised, and a flap always shrinks once it has been raised. This shrinkage observation was also reported by various groups (Barrett-Brown *et al*, 1945; Cannon *et al*, 1947; Coakley *et al*, 1950; Jobert, 1849; Langer, 1862). On the other hand, some groups reported that flap retracts but on occasion it becomes longer (McGregor *et al*, 1970; Stell, 1982). Some researchers have indicated that a flap shrinks less in the direction of Langer's line than at right angle to it (Sawhney, 1977; Reihsner *et al*, 1995) but others have observed that the flap shows greater retraction in the direction of Langer's line (Stell, 1982; Ridge *et al*, 1966; Langer, 1978 A). In general, most literature stated shrinkage as the more common occurrence. The literature also agreed that a small circular flap will generally shrink to an elliptical shape after harvest, and one of the axes on the ellipse coincides with the Langer's line (refer to Figure 2-4).

When examining the relationship between the excised skin flap and produced wound areas (secondary defect), Hudson-Peacock and his co-workers observed that 90% of the secondary defects are larger than the planned excision area (Hudson-Peacock *et al*,

1995). It was computed from their study that on average, skin flap shrunk between 15 to 29% while secondary defect expanded between -2 to 31%. Thacker and his co-workers (Thacker *et al*, 1977) have studied skin properties using an extensometer and then examined the shape of the excised skin. They have noticed that when force-extension profiles of two orthogonal directions were different, then the excised circular skin flaps took up elliptical shapes; otherwise, circular flaps were obtained. They have also shown that the external tension of the harvest site (whether taut or lax state) would make a profound difference to the outcome of the shrunken shape.

2.2.3. Flap-defect matching problem

When designing donor flaps, surgeons are taught to allow for the retraction behavior of skin but the excess amount is normally left to the individual surgeon to decide from his/her own experience. In order to ensure the best survival as well as to minimize scarring, the surgeon's foremost responsibility during an each flap surgery is to outline a safe margin of skin tissue that will conform closely to the shape and size of the recipient site after harvesting, while avoiding tissue wastage.

Presently, surgeons based their judgment on tactile pinches on the patient's skin to estimate the tension, the patient's physiology, and evaluation of the donor site. Due to this subjective judgment, mistakes are common occurrence; either the harvested flap is too big or small to fit the primary defect, or the secondary defect at the donor site is too big for simple closing method to be employed. After reviewing the available literature, it is clear that there is no comprehensive study to predict skin flap shrinkage objectively. The goal of this study is therefore to develop a surgical planning methodology to predict flap shrinkage objectively.

2.3. <u>Biomechanical properties of skin</u>

Human skin is classified as a non-linear viscoelastic material (Fung, 1996). The stress-strain curve exhibits a J-shape profile, where stress increases much faster with increasing strain than Hooke's law predicts. Due to the viscoelastic and composite nature of skin tissue, the stress-strain profile shows dependency on the applied strain and the strain rate.
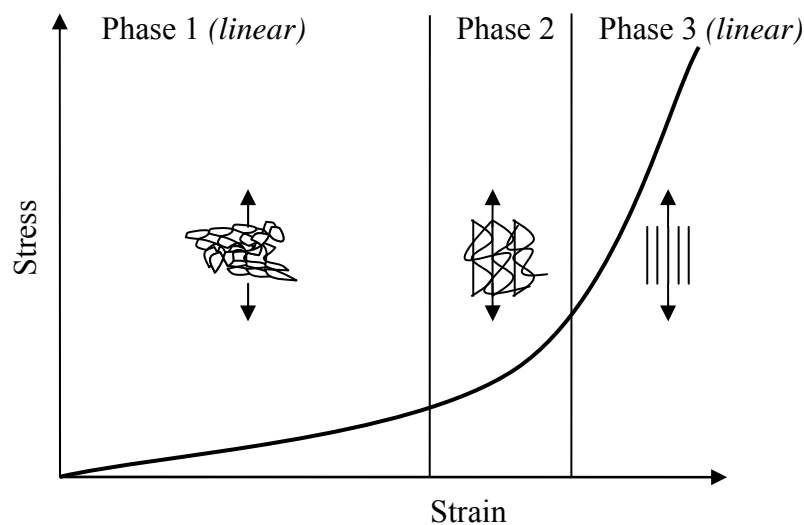
Figure 2-5: Schematic of geometrical deformation of collagen network with applied force. The J-shaped stress-strain curve; redrawn from Daly, 1982.

The structural origins of the J-shaped stress-strain curves of skin have been attributed to the progressive orientation of the collagen fibers and elastin network, and it can be subdivided into three regions (refer to Figure 2-5; Daly, 1982). In the initial phase '*toe region*', a small force produces a large extension, which is generally linear. The region corresponds to the gradual removal of a macroscopic crimp in the collagen network (visible through the light microscope). The second phase represents progressive stiffening of tissue, where the stress-strain curve is concave upwards. In this region, the resistance to deformation is relatively low, since the fibers themselves are not being stretched but are being aligned along the strain axis. Finally, the third phase

represents the stretching of dermal tissue, where stress-strain response becomes linear once again. At this region, as the fibers become aligned along the strain axis, further deformation can only occur by straining the fibers themselves and this requires increasingly greater force. An alternative explanation put forward is based on the network arrangement; the junction points of the collagen fiber bundles may have differing degrees of tautness and so, as the fibrous network is extended, more and more fibers become taut and the stress increases (Attenburrow, 1993). It is generally believed that the skin (on the body) is only under strain within upper limit of the elastic region, i.e. the first phase (Silver *et al*., 2003).

The complex structure of skin gives rise to extreme variations in its biomechanical properties between individuals and further variations between different areas on the same individual. Furthermore, *in vivo* biomechanical characterization of skin also changes with respect to the internal built-in tension as well as the local external tension due to joint movements (Thacker *et al*., 1977). The orientation of fibrous network of dermal tissue is reported to be biased in one direction (Cox, 1941). As a result, skin shows directionally dependent biomechanical properties and it is reported to be stiffer along the Langer's lines compared to across the lines (Alexander & Cook, 1977; Cox, 1941; Daly, 1982; Langer, 1978; Reihsner *et al*., 1995; Stark, 1977).

The literature makes clear that the mechanics of skin is not completely anisotropic but shows some degree of symmetry. Alexander (Alexander *et al*, 1977) stated that skin possesses at least orthotropic material properties, which was validated by Lanir (Lanir *et al*, 1974). They have reported that biomechanical properties show symmetry along and perpendicular to the Langer's line.

Directionally dependent *in vivo* biomechanical properties of the skin have also been examined by Stark and his co-workers using an extensometer (Stark, 1977; Gibson *et al*, 1969). They have initially observed that skin extends further in one direction than in other directions (on application of a specified uniaxial load). Further systematic studies have been undertaken by them to characterize the basic shape of the stress-strain curve. They postulated that the curve can be characterized (see Figure 2-6) by the length AB, which indicates the initial elastic region ('limit strain'), and the slope BC, which measures the skin's resistance to deformation ('terminal stiffness'); the more closely BC approaches the vertical, the greater the stiffness. Their results indicate a correlation between these 2 parameters and the testing direction.
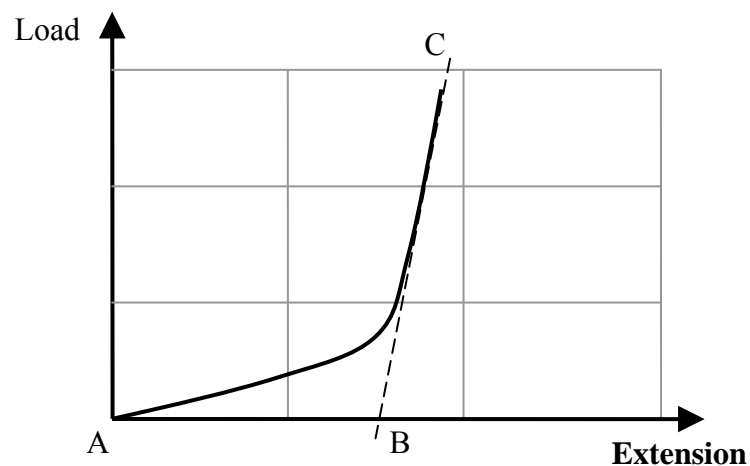
Figure 2-6: A typical *in vivo* stress-strain profile of skin; AB measures limit strain and slope CB measures terminal stiffness; redrawn from Stark, 1977.

It was revealed that the Langer's lines correlate very closely with the direction of minimum limit strain and maximum terminal stiffness. When the limit strain was plotted with respect to the testing direction, it was periodic and the data points formed a circle or ellipse (Gibson *et al*, 1969). At those sites where the ellipses were elongated, the direction of minimum limit strain correlates closely with the direction of the Langer's line. When the terminal stiffness was plotted with respect to the

testing direction (Stark, 1977), the shape of the resultant polar plot was also found to be symmetric and regular, though not necessarily elliptical/circular (refer to Figure 2-7); the long axis of the shape was found to be aligned in the direction of the Langer's line.
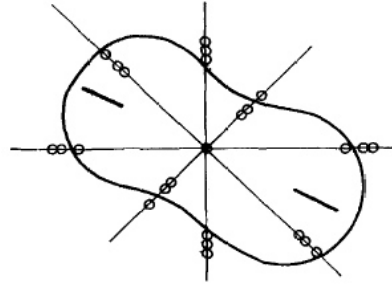
Figure 2-7: Sample of polar plot of terminal stiffness; the shape of the plot may also be elliptical. Diagram from Stark, 1977.

2.4. Skin measurement devices overview

The biomechanical properties of skin have been measured by both *in vivo* and *in vitro* methods. The simplest method is the *in vitro* tensile test, where a sample of the test material is isolated for measurement. Here, the applied stress and resultant strain are measured under a carefully controlled environment and thus the material constants can be determined accurately. The *in vitro* test is an accurate method to measure the *true* uniaxial properties because the stress field in the test material is uniformly along the test direction. The *in vivo* test, on the other hand, is challenging due to the complex interaction of skin with its surrounding structure on the body, as well as the physiological condition of the body at the time of measurement (Elsner *et al.*, 2002). Compared to the *in vitro* test, the *in vivo* test will reveal properties of the skin that are more representative of the actual skin condition of the subject, since the tissue is not removed from the body.

2.4.1. Current devices

Berardesca and Elsner conducted comprehensive literature reviews on current skin measurement devices (Berardesca *et al.*, 1995; Elsner *et al.*, 2002). Most experimental data on skin biomechanics are based on the stress-strain relationship: the skin is subjected to a force (stress), and the resulting deformation (strain) is measured. Some common devices and their operating principles are summarized in Table 2-1.

Table 2-1: Common *in vivo* skin measurement devices

Generic Name (*Manufacturer*)	Operating principle	Brief description
Extensometer (*No company*)	Traction or lateral force (*uniaxial*)	It measures the directionally dependent elastic and viscoelastic properties by extending the skin laterally in plane to the skin surface and measuring the force vs. displacement.
Cutometer and Dermaflex A (*Courage and Khazaka Electronic GmbH, Germany*)	Suction force (*multi-axial*)	It measures the elastic and viscoelastic properties by using suction to pull the skin surface through a small aperture and measuring the negative pressure vs. suction height.
Dermal torque meter (*Dia-Stron Limited, USA*)	Torsional force (*multi-axial*)	It measures the elastic and viscoelastic properties by twisting the skin surface using a disc and measuring the torque vs. angular rotation.
Torsional ballistometer (*Dia-Stron Limited, USA*)	Impact force (*multi-axial*)	It measures firmness and elasticity by impacting the skin surface with a low mass and inferring the biomechanical properties by the degree of rebound.
Durometer (*Rex Gauge Company, Inc, USA*)	Compression force (*multi-axial*)	It measures skin hardness by measuring the penetration of a specified indentor onto the skin surface under specified conditions of force and time.
Goodyer Skin Rheometer (*E&C Consultancy, UK*)	Sinusoidal force (*uniaxial*)	It measures the elastic and viscoelastic properties. This is done by measuring the dynamic spring rate of the skin by applying a sinusoidal lateral force to the skin and measuring the resultant displacement and phase shift.

These devices measure skin properties by applying deformation forces in various manners. One group of devices produces multi-axial loading on skin by mechanisms such as the rotating disk, indentator and vacuum suction cup. These instruments are

not capable of identifying directional differences. In contrast, loading of the skin by devices that impose lateral traction in a specified direction can ascertain directional differences in material properties.

Measurement of skin properties using a suction cup ("cutometer") has been recognized as the standard in dermatology and cosmetology. It has been used to support the latest discoveries in both fields. Due to its precision and ease of use compared to other measurement methods, the cutometer is mentioned in most studies on this subject. However, its inability to differentiate direction-dependent biomechanical properties makes it unfavorable for this study. In contrast, another popular device, the extensometer, can be used to ascertain directional differences in material properties. The extensometer works by applying a displacement to the skin using two extensible pads/tabs/legs that are attached to the skin by double sided tape, and then measuring the force using a load cell as the skin deforms.

The literature revealed that for uniaxial measurements, the existing *in vivo* non-invasive devices provide a qualitative assessment of the biomechanical properties, but the measured result differs significantly from the *true* uniaxial properties. The latter properties are what one would get in a uniform stress field in the test area, and in the absence of force contribution from the deformation (or stretching) of surrounding skin tissues, such as in an *in vitro* setting. Thus, for existing devices, the forces measured are often much higher than the *true* values. Part of the work in this research was to develop a new device to address this problem.

2.4.2. Standardization of measurement

Rodrigues reported difficulties in standardizing biomechanical measurement of skin, by pointing out that the Young's modulus of elasticity (initial elastic region of stress-strain curve), measured by *in vivo* techniques, vary by four orders of magnitude (Rodrigues, 2001). In yet another review, vastly different values of the *in vivo* Young's modulus (from 0.02 to 540 MPa) measured using different devices have been reported, as summarized in Table 2-2 (Diridollou *et al*, 2000). This inconsistency is true for both measurements done using devices of similar and different operating principles.

Table 2-2: Modulus of elasticity of the forearm skin measured by different authors and devices; results are seen to vary by a factor of 3000.

Research group	Sites on forearm	Modulus (MPa)	Device
Diridollou *et al*, 2000	Not specified	0.11 to 0.12	Suction
Barel *et al*, 1998	Not specified	0.13 to 0.17	
Agache, 1992 Panisset, 1992	Anterior part	0.25	
Grahame *et al*, 1969	Not specified	18 to 57	
Alexander *et al*, 1976	Anterior part and upper back	320 to 540	
Sanders, 1973	Dorsal side	0.02 to 0.1	Torsion
Agache, 1980 Leveque, 1980	Dorsal side	0.42 to 0.85	
Escoffier, 1989	Anterior part	1.1 to 1.32	

For devices of different principles, the measured results may inevitably differ because of different designs. However, for devices based on the same principle, one reason for the reported inconsistency is the lack of standardization. Without standardization, the results produced may be inconsistent and non-reproducible. The list of variables to standardize includes design parameters (such as the size, shape and configuration of key device components), measurement settings (such as speed, and amount of deformation and load applied), and method of handling during operation (such as the device placement on the skin with respect to load and angle). Therefore,

standardization must be carefully considered in both the design and operation of instruments in order to ensure result reproducibility and consistency between different measurement sessions.

2.5. <u>Measurement of natural tension</u>

As discussed, much work has been done to study the shrinkage of skin flap qualitatively. To the best of our knowledge, there is no work that is done to predict flap shrinkage quantitatively. On the other hand, the literature survey revealed work by various groups to measure the natural tension of skin *in vivo*. As one of the factors influencing flap shrinkage is the skin tension, it is necessary to review these work.

2.5.1. Wrinkle test

Alexander and Cook attached an extensometer to the skin and retracted the pads until the skin in between started to wrinkle (Alexander *et al*, 1977; Cook *et al*, 1975). By assuming that the skin tension is zero when the skin wrinkled, the natural tension was read directly from the load cell. The authors claimed to have tested the validity of this method on biaxially stretched membrane. They also found that the natural tension on the upper back of a human was approximately 5 N/m perpendicular to the Langer's line, and 24 N/m in the parallel direction. The accuracy of the measurements was not verified by excising the skin for *in vitro* measurement.

This method suffers from two main disadvantages. Firstly, it is unknown how much the skin must wrinkle before the natural tension reaches zero. Furthermore, the evaluation of wrinkle formation is highly subjective. This is also complicated by the fact that when two pads attached to the skin are moved together, the wrinkles always

form near the pads first; the skin at the middle is always the last part to wrinkle (refer to Figure 2-8). Therefore, skin wrinkling is uneven and it is unclear which part of the skin should be evaluated for wrinkles.
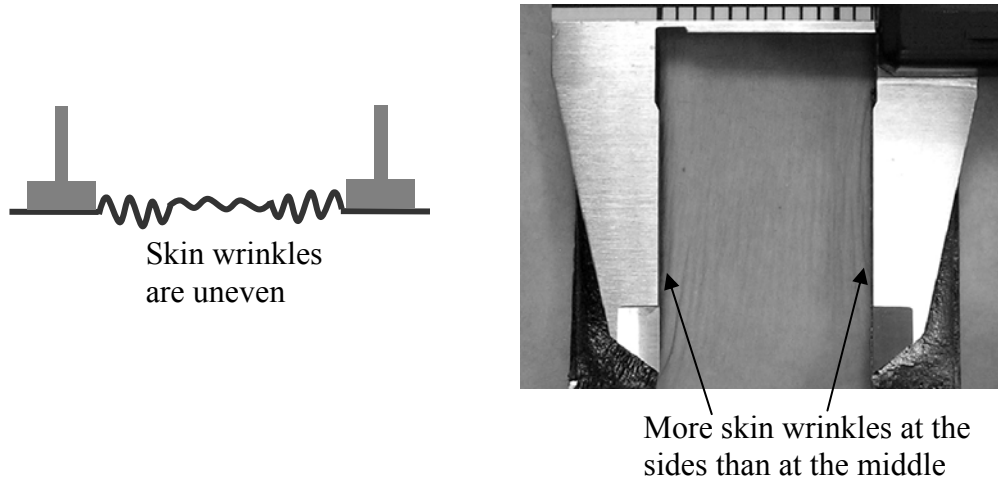
Figure 2-8: Pictures showing uneven wrinkle distribution between pads.

The second problem is that the skin tension measured using an extensometer will always be higher than the *true* uniaxial tension. This is because a typical 2-pad extensometer not only measures the tension of the skin between the pads, but also the tension from all other directions due to stretching of the surrounding skin. Therefore, one would expect the tension obtained to be higher than the actual uniaxial value.

2.5.2. Suction cup

Diridollou (Diridollou *et al*, 2000) measured the natural tension *in vivo* using a suction cup. The method involved the use of a suction chamber and an ultrasound device to measure both the vertical displacement of the skin's surface during suction and the skin thickness. The measured data were fed into a mathematical model, where the skin was modeled as an isotropic elastic membrane that was deformed spherically. Polynomial curve fitting was then used to deduce both the natural stress and Young's modulus of elasticity. Although the model used was not exact (since skin in reality is

anisotropic and has non-spherical deformation), the authors reported results that were of the same order of magnitude as those measured by Alexander and Cook (Alexander *et al*, 1977; Cook *et al*, 1975).

Our group repeated the Diridollou experiment on a volunteer subject using a cutometer as the suction device. Results of the same order of magnitude were also obtained. However, the results measured at repeated experiments at the same site were not reproducible. This was due to the curve fitting process, where a small change in the input suction height led to a large change at the output result. Therefore, it was deemed that the model used was too sensitive.

The natural tension obtained using this suction approach was also not directionally specific; the result was the average of the skin tension in all directions. This is inadequate because skin tension is anisotropic, and so the uniaxial tension (in the measured direction) should be determined instead so that the shrinkage in that direction can be estimated accordingly.

2.5.3. Modified extensometer

Emmanuelle measured the natural tension of elastomer and skin using a modified extensometer (Emmanuelle *et al*, 2007). Unlike a traditional 2-pad extensometer, the new design incorporated an additional follower pad behind the load cell pad (refer to Figure 2-9), which the authors claimed could allow *in vitro* force-displacement measurement to be accurately determined. The proposed method, which was based on analyzing the gradient change of the force-displacement data measured by the device, was found to estimate the natural tension of uniaxially pre-tensioned elastomer within

a precision of 15%. However, in experiments performed on human skin, the group reported that they were unable to obtain the similar gradient trend as seen in elastomer.
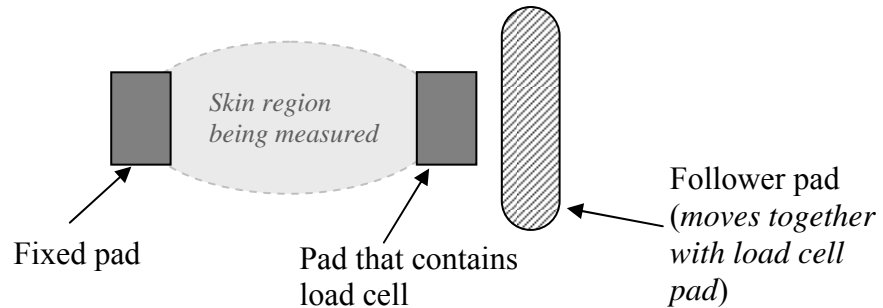
Figure 2-9: Pad arrangement of proposed extensometer design

It was clear from the device description that the follower tab protected the load cell from unwanted tensile forces *along* the measurement axis only. However, skin on the body is biaxially stretched and therefore, the follower tab was unable to protect the load cell from unwanted peripheral forces from directions other than the measurement axis. As a result, data trend similar to the uniaxially stretched elastomer was not observed at the skin experiments. This source of error was also identified by the authors. Hence, the proposed device was not suitable to estimate the natural tension of skin or any other biaxially stretched material *in vivo*.

The concept of using additional pads in an extensometer was also the basis of the device design in this thesis' work. It should be noted that our design was developed without prior knowledge of Emmanuelle's work, which was published online in March 2007; in fact, our work was mostly likely to be conceived earlier than theirs. Our work was submitted for patent application at the university in April 2005, and was also first publicly submitted to a conference (Proceedings of the 15th ICMMB, Singapore) in April 2006.

2.6.   <u>Summary</u>

Skin is a complex structure that has been shown to exhibit non-linear, direction- and time-dependent biomechanical behavior. Numerous groups have studied the shrinkage of skin flap qualitatively, but to the best of our knowledge, there is no work done to estimate flap shrinkage quantitatively. The literature survey also revealed that current non-invasive devices are inaccurate in measuring the uniaxial biomechanical properties of skin, due to complications in an *in vivo* setting. Therefore, it is the goal of this research to develop a new measurement device and methodology to aid the prediction of skin flap shrinkage.

CHAPTER 3
INSTRUMENTATION DESIGN

3.1.   <u>Introduction</u>

The extensometer measures the force-displacement property of skin directly, and works in similar principle to the standard *in vitro* test using the tensometer (e.g. the Instron tester). Among the various devices reviewed, the extensometer is one of the few that can measure the uniaxial properties, which is important since skin properties are anisotropic. Due to these advantages, the instrument that was developed in this research work was based on the extensometer's working principle.

The extensometer has been used both for studying the directional properties of skin (Alexander & Cook, 1977; Stark, 1977), and for clinical evaluation of healthy and diseased skin (Clark *et al*, 1987, 1996; Gunner *et al*, 1979a, 1979b). Evans and Siesennop were the first to design and build *in vivo* extensometers for measuring quasi-static properties of human skin (Evans & Siesennop, 1967). Their device consisted of two strain-gauged legs traveling along a slide, motor driven by a counter-cut lead screw. Later, several modified versions of this extensometer were developed by other researchers (Baker *et al*, 1988; Gunner *et al*, 1979a, 1979b; Larrabee *et al*, 1986; Manschot & Brakkee, 1986; Vescovo, 1998), where strain gauges were attached onto the pads to measure the force applied to the pads, and sensors were used to measure the pad displacement. Larrabee designed the first computer driven extensometer (with a stepper motor) where two strain gauges were connected to the motors via a pinion drive and thus the strain could be applied at a controlled predetermined rate (Larrabee *et al*, 1986).

All the designs described are capable of determining a qualitative measure of the uniaxial biomechanical properties, but the measured result differs from the *true* uniaxial properties significantly. This chapter discusses a new extensometer that was designed to solve the problem.

3.1.1. Existing design concept
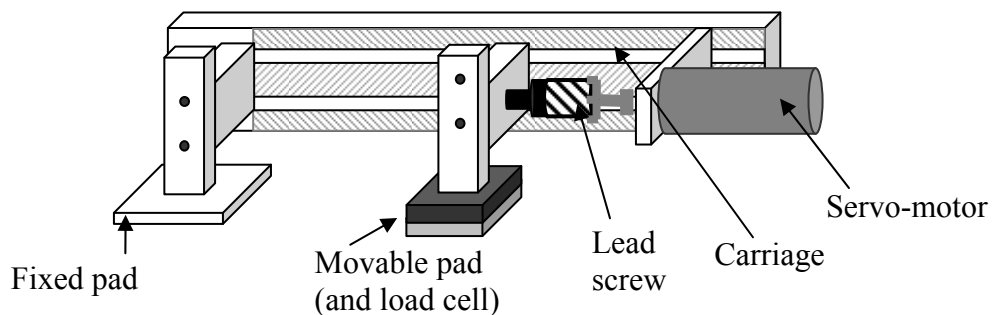
Figure 3-1: Schematic of a traditional "two-pad" extensometer design.

Figure 3-1 shows the 2-pad arrangement of a traditional extensometer. Two pads that are attached to the skin surface using adhesive tape deform the skin during a measurement. In an *in vitro* setting where a skin sample is harvested and isolated for measurement, only the skin between the grippers are stretched, and therefore the *true* uniaxial force-displacement data is obtained; Figure 3-2(a) shows the simplified tensor line representation of forces involved in an *in vitro* setting, where the stress field is uniform. However, obtaining such data using a 2-pad design *in vivo* is not possible. When displacement is applied to the skin, not only the skin tissue between the pads deform, but also the surrounding tissue around the pads. The latter inevitability contributes to the overall force detected by the force sensor. Therefore, as pictorially represented by the tensor lines in Figure 3-2(b) and (c), the measured force also includes force (F_p) contributed from directions other than the measurement axis, and so the result will differ significantly from the *true* uniaxial properties. Note that the

reader may also skip forward to Figure 3-14 to refer to the actual finite element analysis simulation images.
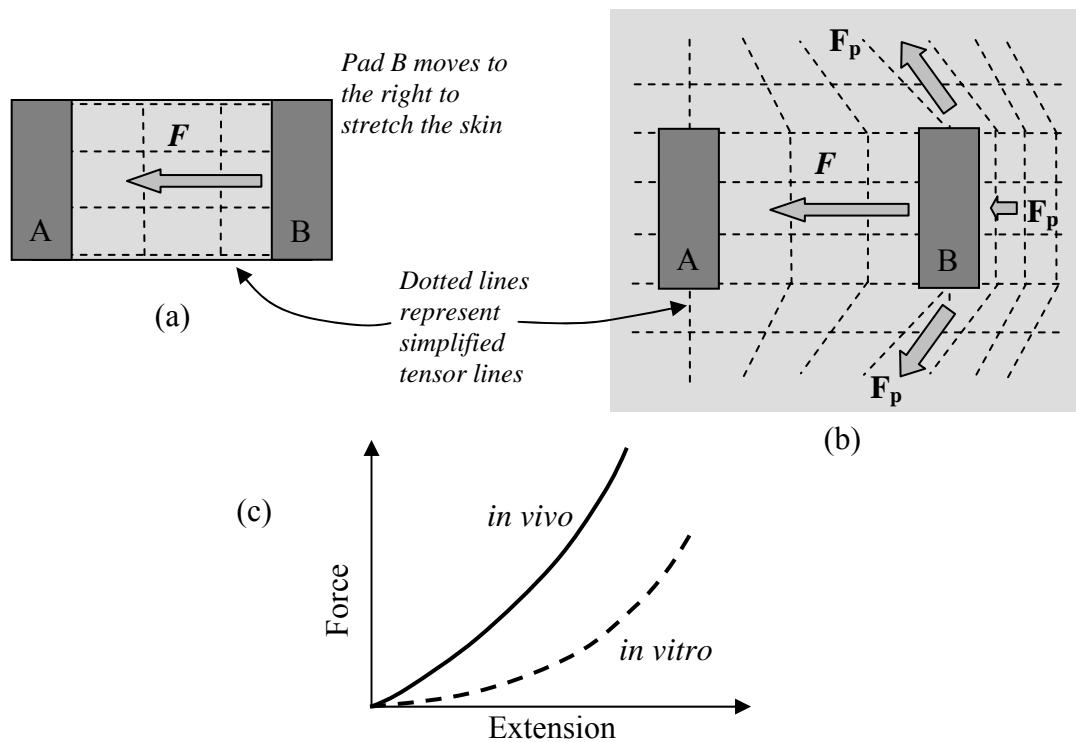
Figure 3-2: (a) *In vitro* setting – uniform stress field between pads A and B. (b) *In vivo* setting – stretching of surrounding skin contributes to peripheral forces F_p. (c) Comparative force-displacement data.

3.2.   **New design concept**

In order to improve the uniaxial measurement, a new extensometer was devised and the arrangement of the pads is shown in Figure 3-3. Here, a third pad (a C-shaped shield pad) partially envelopes Pad B which contains the load cell, thus effectively shielding out the peripheral forces, F_p, during measurement. Pad C achieves this by moving together with pad B, thus isolating the skin region between B and C so that the skin tension there remains constant as the skin at other parts deforms. In this way, the load cell is mostly subjected to the force F (along the measurement axis) between pads A and B, thus producing results closer to the *in vitro* properties.
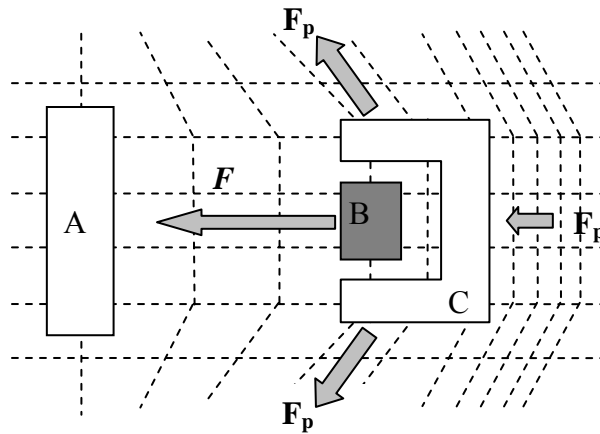
Figure 3-3: Configuration shows pad C shielding the load cell (at pad B) from peripheral forces F_p; pads B and C move as a single unit.

3.3. Method – Hardware

3.3.1. Constructed device

A schematic diagram of the constructed device is shown in Figure 3-4. This device, developed to conduct tests at a user-defined extension rate, consists of the 3 pads A, B and C mounted along a carriage. During measurement, the extensometer is attached to the skin at the pads using double-sided adhesive tape (3M® Brand). Pad A is fixed to the carriage body while B and C are free to slide on the carriage. The load cell, which has a flat profile, is attached by screws to pad B for force measurement, and pad C is used to shield the peripheral forces during the stretching from being detected by the load cell. Figure 3-5 shows the pad dimensions used.
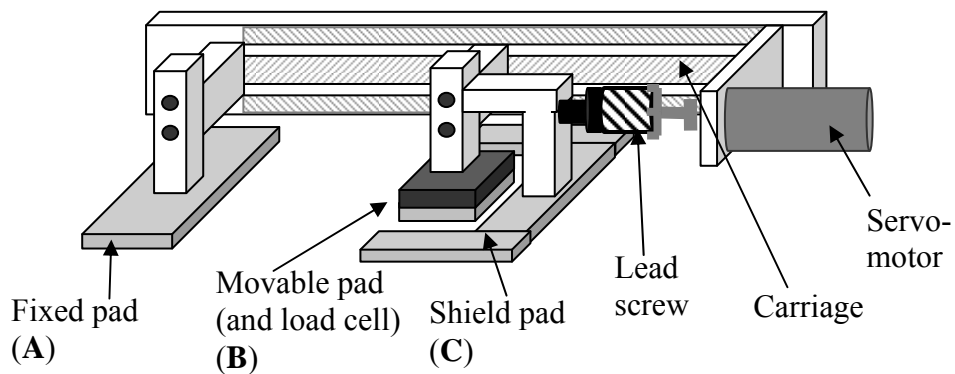
Figure 3-4: Schematic of new extensometer design
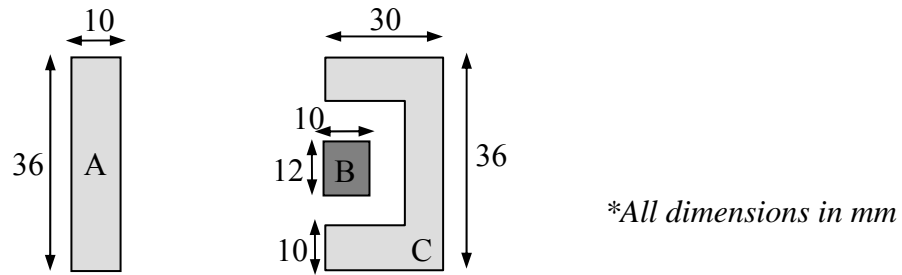
Figure 3-5: Pad dimensions

Pads B and C (attached together as a single unit) are connected via a lead screw to a servomotor which actuates the pads along the carriage. The displacement of the pads is logged from the servomotor encoder and the force is measured by the load cell, which has a resolution of 2mN. Pad B-C has a maximum velocity of 0.6mm/s.

3.3.2. Device attachment to skin

The device pads were attached using double-sided adhesive tape onto the skin surface, and it was essential to use tapes which have no slippage during measurement. After testing a variety of tapes, it was found that the tape from 3M® enabled skin measurements to be conducted up to a force of 9N (on a 12mm x 10mm clean surface area) with insignificant amount of slippage; tape slippage was determined by drawing reference lines on the skin at the edge of the pads before measurement, and then observing if those lines were shifted relative to the edge of the pads after measurement. It was also determined that the maximum force of 9N was more than sufficient to measure the biomechanical properties of skin in this research.

3.3.3. Instrumentation control

A computer, connected to a motor controller and driver, servomotor, load cell (strain gauge), strain gauge amplifier and data acquisition card, is used to automatically

control the movement of the pads and to log measurement data. Figure 3-6 shows the architecture of the control system.
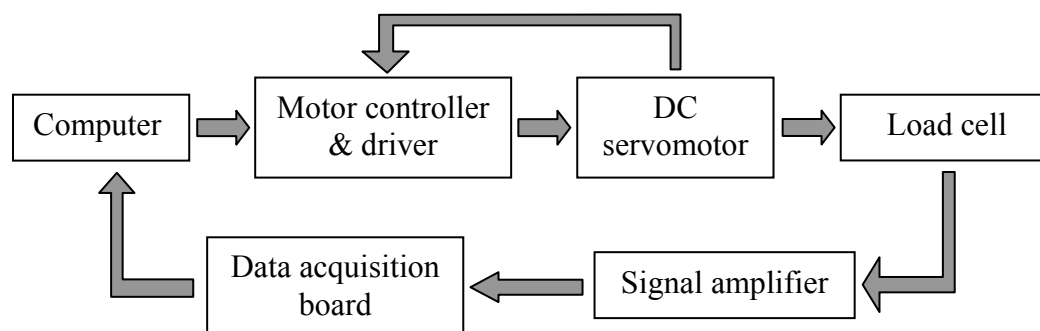
Figure 3-6: Overview of control system

The details of the components are listed in Table 3-1. The controls components are housed inside a small portable box, and it is connected to the computer conveniently using a USB cable.

Table 3-1: Details of device components

No.	Component	Brand and model
1.	Motor controller and driver	Faulhaber, model MCDC 2805
2.	DC servomotor	Faulhaber motor with gearbox; 200mNm torque, 180rpm speed
3.	Load cell	www.smdsensors.co.uk, model S270; flat load cell that measures force in a shear direction
4.	Signal amplifier	Newport Electronics, strain gauge signal conditioner, model iDRN-ST
5.	Data acquisition board	National Instrument, model NI-6015

The flexibility of modern control system enables various functions to be incorporated in the device. For example, a position controller was incorporated for force-displacement and force-relaxation measurements. In a force-relaxation measurement, which can be used to study viscoelasticity, the skin is stretched to a specified extension and then the force is monitored as the skin relaxes with time. In order to measure creep, which is another viscoelasticity property, a force controller was used. Here, the skin is stretched to a specified load and the extension needed to maintain

that load is monitored. Note that force-relaxation and creep measurements were not conducted as part of this research.

3.3.4. Articulated arm
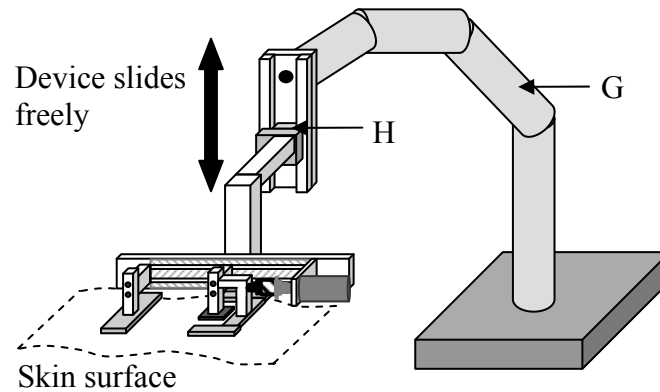
Figure 3-7: Schematic of the articulated arm, G; linear slide, H.

Figure 3-7 shows the articulated arm that was designed to hold the device rigidly onto the skin during measurement. Using a sturdy holding mechanism is part of the standardization protocol that is intended to eliminate handling inconsistency and variations in contact pressure of the device on the skin. This mechanism is also important because the magnitude of the forces measured is of the order of 0.1N, and hence sensitive to (external) handling unsteadiness. This arm has six degrees of freedom and thus enables the device to be easily placed in any position. It also has sufficient stiffness so that pad A remains stationary relative to the underlying skin tissue during measurement, and the only movement occurs at pads B and C. In order to standardize the placement pressure on the skin, a low friction vertical slide is used at the mount attachment so that the device always presses onto the skin with its own weight (2.45N).
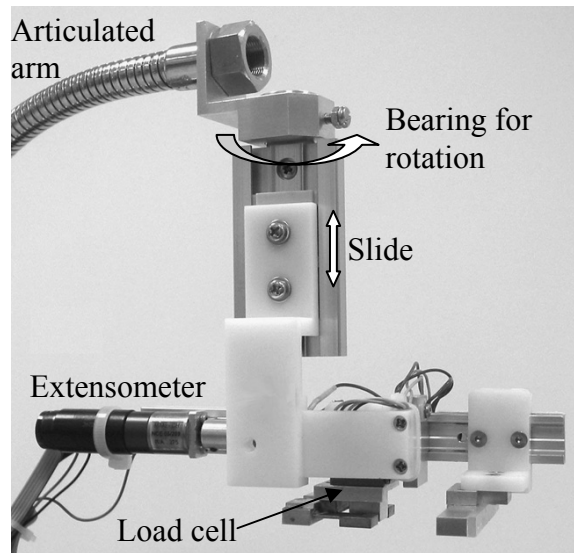
Figure 3-8: Photograph of new shield pad extensometer that is mounted on the articulated arm.

After calibrating the load cell, the measurement accuracy of the extensometer was compared against a universal tensometer (Instron, model no. 5440). The details of the load cell calibration process are described in the Appendix. Measurements of rubber strips (Theraband®) with different stiffness were made on both devices and compared. The obtained results showed high consistency and reproducibility between the devices. Subsequent data analysis indicated maximum standard deviation of only 5% and this was considered to be acceptable. Figure 3-8 shows the actual device with its articulated arm. A patent was also filed (refer to reference in page 135).

3.4.   Method – Modeling

3.4.1. Finite element modeling

A finite element simulation using Ansys 8.0 (Ansys, Inc) was used to determine the effectiveness of the shield pad. The analysis was simulated to determine force-extension in an *in vivo* setting using both the traditional 2-pad and the proposed shield pad arrangement; these results were then compared with those simulated for a 2-pad in an *in vitro* setting (refer to Figure 3-9).
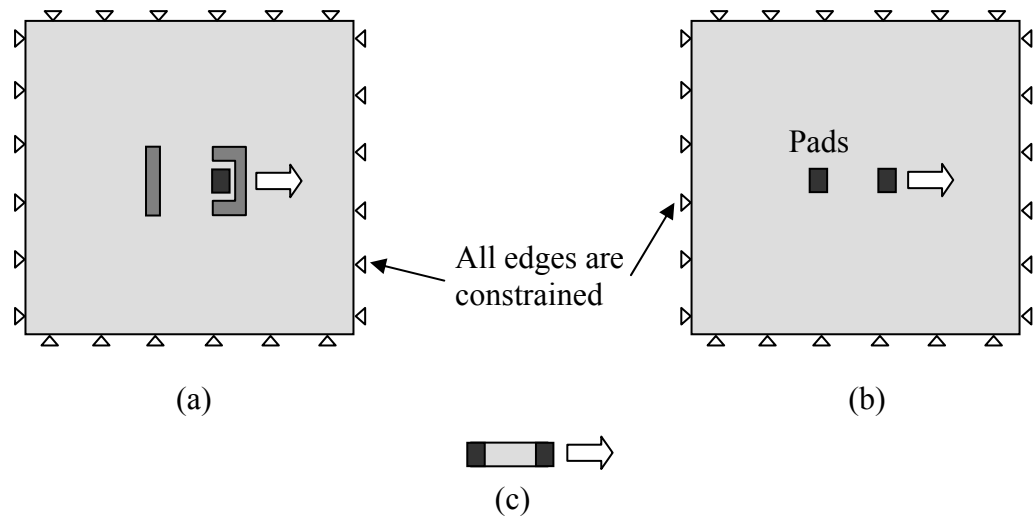
Figure 3-9: Simulation settings, showing (a) shield-pad and (b) traditional 2-pad arrangements on a square sheet constrained at all edges (*in vivo* setting); (c) 2-pad on a material strip (*in vitro* setting).

For the *in vivo* experiments, simulations were performed for pads placed at the centre of the square sheets (120mm x 120mm) which were constrained in space at all four edges. This scenario emulated that of skin covering a human body, since the material surrounding the pads would be stretched as the pads moved apart. For the *in vitro* experiment, the pads were tested on a strip of material that was as wide as the pads. The material property selected was a 2-dimensional, incompressible elastic shell, with a Young's modulus of 0.8 MPa. This value was selected because it is of the same order of magnitude as skin's elasticity. The dimensions of the shield pad arrangement were the same as that given in Figure 3-5; for the traditional 2-pad arrangement, the size of both pads were the same as that of the load-cell pad (B).

3.4.2. Modeling of residual peripheral forces

Due to the inherent boundary conditions, it is not possible for the shield pad to completely eliminate peripheral forces during measurement. Therefore, a small difference between the measured *in vivo* and *in vitro* data is still expected, and this difference shall be referred here as *residual* peripheral forces. A model to describe the

forces during measurement is proposed and illustrated in Figure 3-10. In this model, the forces inside the zone protected by the shield pad remain unchanged when skin is deformed during measurement. It is also assumed that the adhesion of the fixed pad to the skin holds the skin along its vertical axis immobile, thus causing skin fiber to deform as the left-hand-side pads move. As a result, the total force experienced by the load cell pad consists of all the forces radiating in the various directions from the load cell due to deformation of skin in these directions; this can also be thought of as stretched "spring fibers" radiating from the load cell pad to the vertical axis at the opposite fixed pad. The total residual peripheral forces are then given by the total force minus the uniaxial force along the measurement axis.
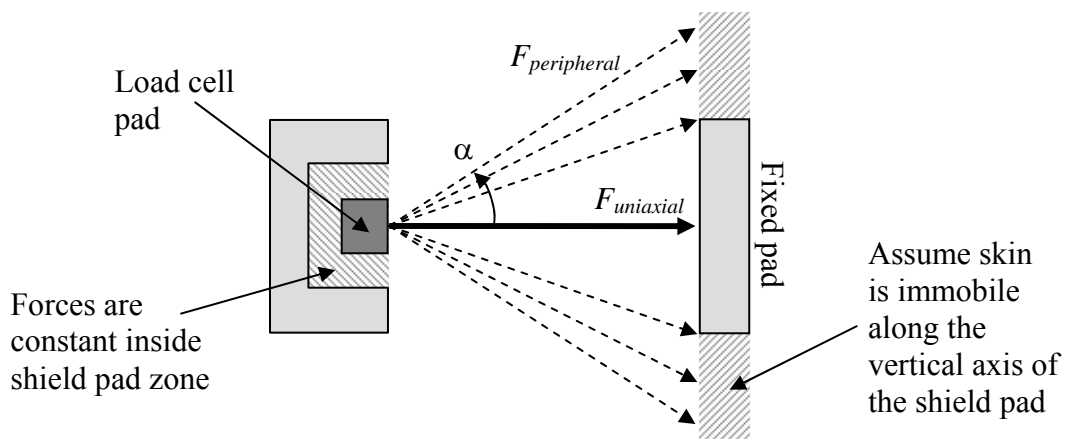
Figure 3-10: Forces experienced by the load cell due to stretched "spring fibers" radiating from the load cell pad to the fixed pad
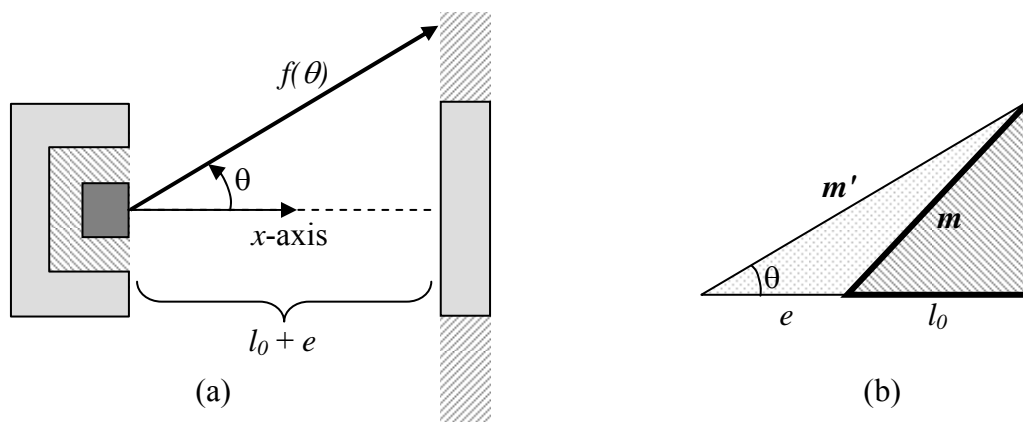
Figure 3-11: (a) Force due to "fiber" at angle θ stretched by extension e along the x-axis; (b) Length of fiber, m and m', before and after stretch.

Figure 3-11(a) illustrates the force due to a particular "fiber" at an angle θ, stretched by extension e from an original length l_0 (in the x-axis direction); figure (b) illustrates the length of the fiber being stretched from length m to m', as the load cell pad moves by extension e to the left. Using Hooke's Law, the force acting along the x-axis is then given by the following equation.

$$f_0(\theta) = k_{e,\theta}(m'-m)\cos\theta \qquad (\,3\text{-}1)$$

where f_0 = force acting along the x-axis,
$\quad$ e = extension along the x-axis,
$\quad$ θ = angle of fiber to the x-axis,
$\quad$ m = length of unstretched fiber,
$\quad$ m' = length of stretched fiber,
$\quad$ $k_{e,\theta}$ = spring constant of material at direction θ and extension e.

Note that only the forces along the x-axis are relevant in this model because the load cell only measures in this direction. Note also that the spring constant $k_{e,\theta}$ of skin is not a fixed constant but varies with orientation and strain, since skin properties are anisotropic and non-linear; for rubber, the spring constant is independent of θ and only varies with strain, since rubber is isotropic and non-linear. If $k_{e,\theta}$ of the material is known prior to the experiment, it can be substituted into the equation directly. However, if $k_{e,\theta}$ is unknown, it may also be estimated from the *in vivo* force-displacement data measured during the experiment. This is deemed to be a reasonable estimate of the actual $k_{e,\theta}$, since the shield-pad extensometer should already produce results close to the *true* uniaxial property.

Equation (3-1) can now be expanded to produce the following.

$$f_0(\theta) = k_{e,\theta}(e+l_0) - k_{e,\theta}\sqrt{l_0{}^2 + (e^2 + 2el_0)\sin^2\theta} \qquad (\,3\text{-}2)$$

where l_0 = original length along the x-axis.

Summing up the forces to cover a range of angles, the total force experienced by the load cell is then given by:

$$F_{total} = \int_{-\alpha}^{\alpha} f_0(\theta)d\theta \qquad\qquad (3\text{-}3)$$

where α = maximum angle (range) of the forces in one quadrant, with respect to the x-axis. It was later determined empirically that 45° produced the best results, and the details of this analysis are given in the Appendix. The angle of 45° is also reasonable, since it is unlikely that the range will cover as far as the entire 90°.

As the residual peripheral forces $F_{peripheral}$ are the sum of forces in all directions *except* along the measurement axis (i.e. the x-axis), it is simply given as:

$$F_{peripheral} = F_{total} - k_{e,0}e$$

$$F_{peripheral} = k_{e,\theta} \int_{-\pi/4}^{\pi/4} \left[(e + l_0) - \sqrt{l_0^2 + (e^2 + 2el_0)\sin^2\theta} \right] d\theta - k_{e,0}e \qquad (3\text{-}4)$$

where $k_{e,0} = k_{e,\theta}$ at $\theta = 0°$, i.e. along the x-axis.

The accuracy of this model was verified with mechanical experiments, which are described in section 3.6.3. During data analysis, $F_{peripheral}$ would be subtracted from the measurement data to test if the result is brought even closer to the *true* uniaxial property. The value of $F_{peripheral}$ was computed numerically (in MATLAB®), since the integral in the equation did not seem to have a closed solution.

3.5. <u>Method – Mechanical testing</u>

Mechanical tests were conducted to determine experimentally the effectiveness of the new device in measuring the *true* uniaxial properties of materials.

3.5.1. Materials

Two rubber sheets (Theraband®) with different stiffness were purchased from a hospital pharmacy. These two grades of Theraband® (yellow and gray) have average stiffness values of 0.8MPa and 2.9MPa at 50% strain respectively; these stiffness values were determined by tensile measurements on an Instron machine. The yellow Theraband® has stiffness values closer to that of the elastic deformation region of skin. Commercial double sided tape (3M) was purchased from a local supplier and used to attach the extensometer pads to the test surfaces.

Pig models have frequently been used to emulate human models in the study of skin biomechanics due to the similarity of skin structure (Larrabee *et al*, 1986). Two piglets (6 months old; *genus: Sus; species: Duroc & Yorkshire*) supplied by the Singapore National University Hospital's animal holding unit were used in the experiment (*animal ethical clearance number: 006/06; clearing authority: Institution of Animal Care and Use Committee, National University of Singapore*).

3.5.2. *In vitro* experiment: Rubber strip

Using a universal tensometer (Instron, model no. 5440), the force-extension measurements of the rubber (Theraband®) strips were obtained. In order to avoid premature failure of the test sample at the grippers during measurement, a dumbbell-shaped specimen of test size 25(L) x 12(W) mm was stretched at a speed of 0.6mm/s

and the resultant force-extension data was recorded. This procedure was repeated three times.

3.5.3. *In vivo* **experiment: Rubber sheet**

The force-extension experiments using the extensometer were conducted on large Theraband® sheets (both yellow and gray) using both the traditional 2-pad and the proposed shield pad arrangement. The experimental settings were the same as what were used in the earlier measurements on the rubber strips. The measurements were performed at the centre of the square sheets (120mm x 120mm) which were attached by double-sided tape onto a fixed frame (on all 4 sides) to emulate skin covering a human body (refer to Figure 3-12). The extensometer was held rigid, such that the position of pad A was fixed relative to the frame. Since the rubber edges were constrained by the frame, the rubber surrounding the pads was stretched as the pads moved. This set of experiments were compared with the *in vitro* measurements described earlier to evaluate how effective the shield pad is in removing peripheral forces during stretching.

Outlines of
extensometer
pads

Rubber sheet
taped onto
square frame
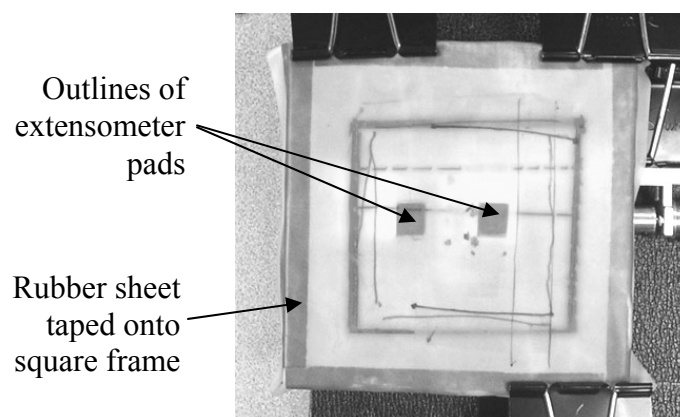
Figure 3-12: Picture of experiment setup, in which a rubber sheet was taped to a frame to emulate skin on a body; the extensometer was held fixed.

3.5.4. *In vivo* experiment: Pig skin

All handling and experimentation involving animals were done in a humane, ethical manner. The pigs were humanely killed at the university animal facility (according to strict ethics regulations) and the hair at the planned test sites was shaved-off to ensure maximum adhesion between skin and device pads. *In vivo* extensometer measurements using both the 2-pad and shield pad arrangements were carried out on abdomen, upper thigh and upper shoulder skin surfaces. The measurements were performed in the compressive mode, where the pads move towards each other instead of moving apart. The reasons for compressive mode measurement are discussed in the discussion section. The initial separation between the fixed and movable pads was set at 25mm.

Unlike the rubber experiments, pig skin was not harvested in order to obtain the *in vitro* measurements to compare against the *in vivo* ones. Instead, an island of skin area was isolated from the surrounding tissue (refer to Figure 3-13) and *in vivo* compressive mode measurements were taken there. Isolating the skin area removed peripheral forces during measurement, thus emulating an *in vitro* setting. It was important that the skin remained attached to the body (via the fascia) because this was the state that the *in vivo* measurements were taken. Thus, this ensured minimum variations at the underlying skin section among the three different measurement configurations. Furthermore, it should be noted that the test dimensions of the skin in all three configurations were similar, thus enabling direct and effective comparison.
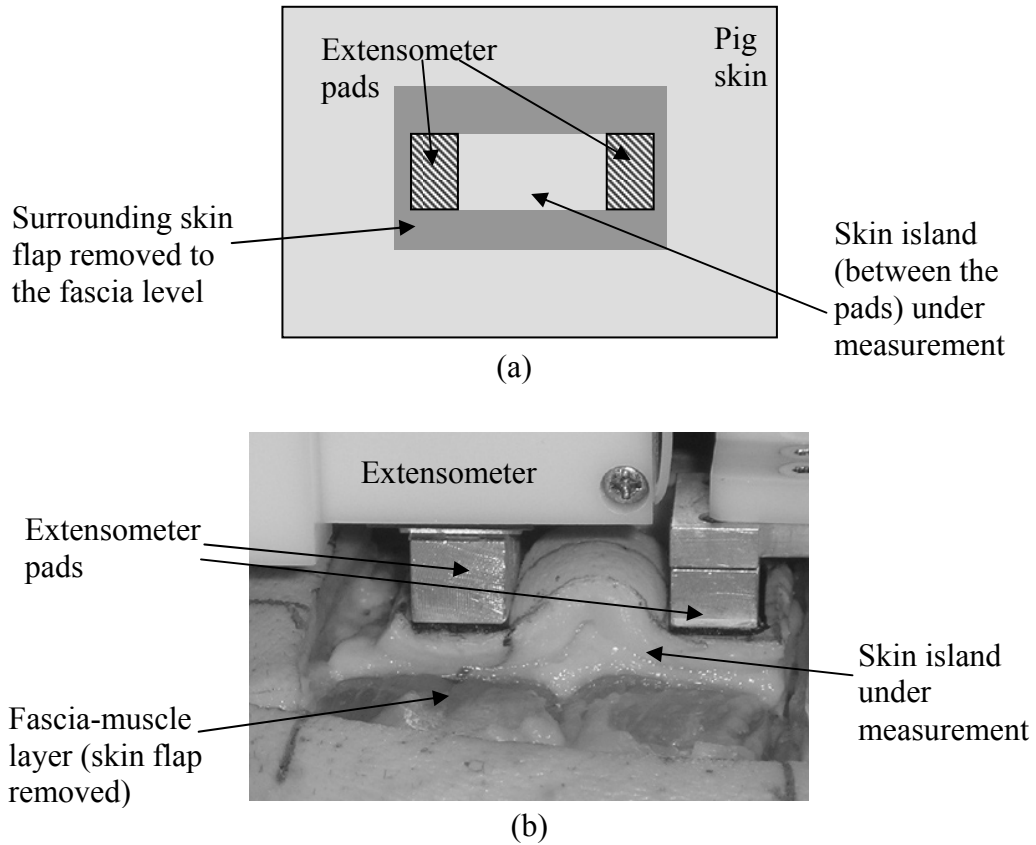
Figure 3-13: (a) Schematics showing skin flap between the pads isolated to remove influence of peripheral forces during measurement, (b) picture of actual setup.

3.6. Results

3.6.1. Finite element analysis

The finite element simulated results for measurement representing *in vivo* 2-pad and shield pad arrangements are given in Figure 3-14 (a) and (b) respectively. In the shield pad arrangement, the load cell that is located at pad B is protected from the generated peripheral forces (both compressive and extensive forces) due to the deformation of surrounding materials. Therefore, the force experienced by the load cell will have minimal contribution from the forces of the surrounding tissues.

(a)   (b)
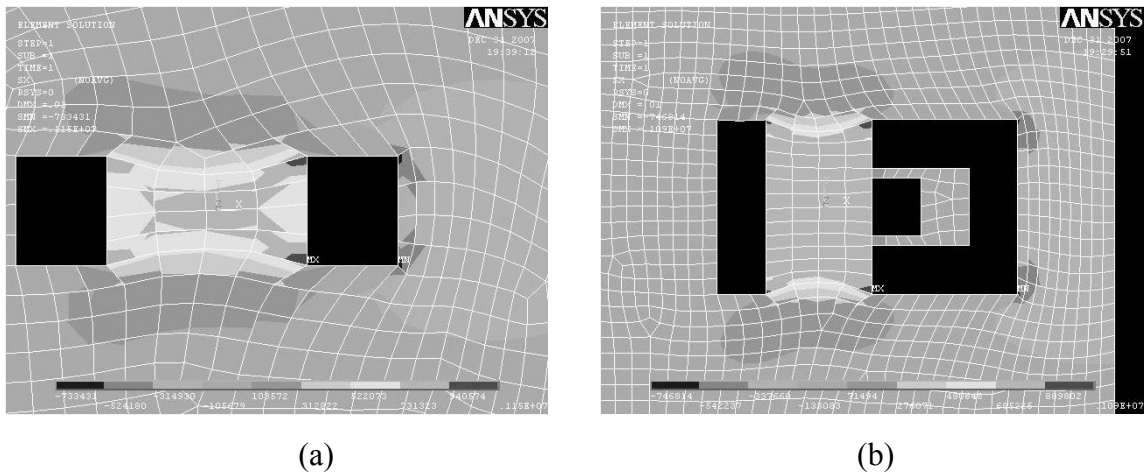
Figure 3-14: FEM results of (a) traditional 2-pad and (b) shield pad arrangement. Shades represent stresses along the principle (horizontal) direction of testing.

Table 3-2 compares simulated results of stress in different settings when a strain of 0.42 is applied. In simulation, the stresses on all the nodes surrounding the pad labeled B were taken as the overall stress that was experienced by the load cell and thus added up. The percentage error of simulated stress values compared to the *in vitro* value was computed. It can be clearly seen that *in vivo* shield pad arrangement produces result that is much closer to the *in vitro* result.

Table 3-2: FEM simulated stress at a strain of 0.42, and percentage difference between *in vivo* and *in vitro* values

Method of simulation	Stress (MPa) at 0.42 strain	Difference with *in vitro* value
In vitro arrangement	0.34	-
Shield pad arrangement	0.39	13.7%
Traditional 2-pad arrangement	0.66	91.0%

3.6.2. Mechanical testing – Rubber

Experiments were conducted to test the effectiveness of the shield pad on constrained rubber sheets. Force-strain data of the yellow and grey Theraband® are shown in Figure 3-15 and Figure 3-16 respectively. Both produced the same trend, where it can be seen that the shield-pad data are significantly closer to the *in vitro* data, but the data from the traditional 2-pad diverge from the *in vitro* data by more than 100%.
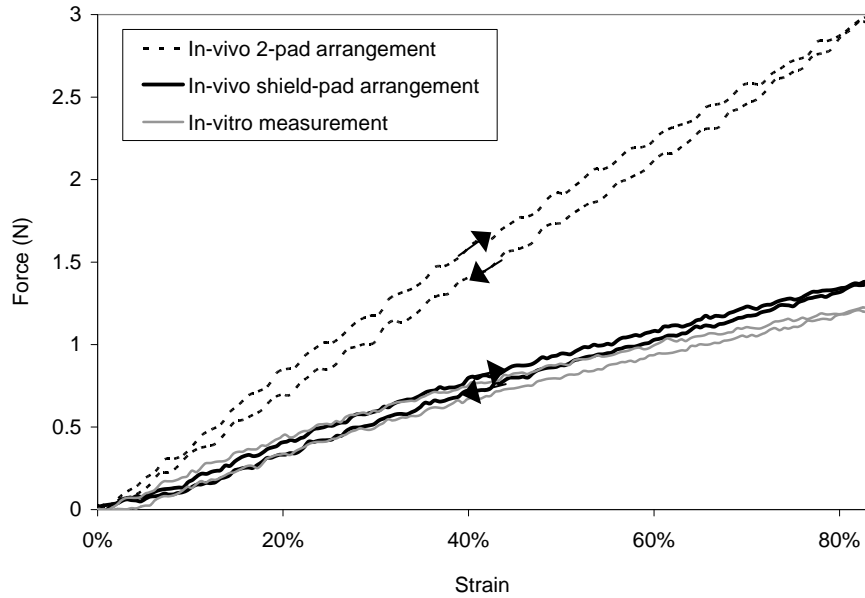
Figure 3-15: Tensile test data of yellow Theraband® for *in vivo* 2-pad, *in vivo* shield-pad, and *in vitro* configurations.
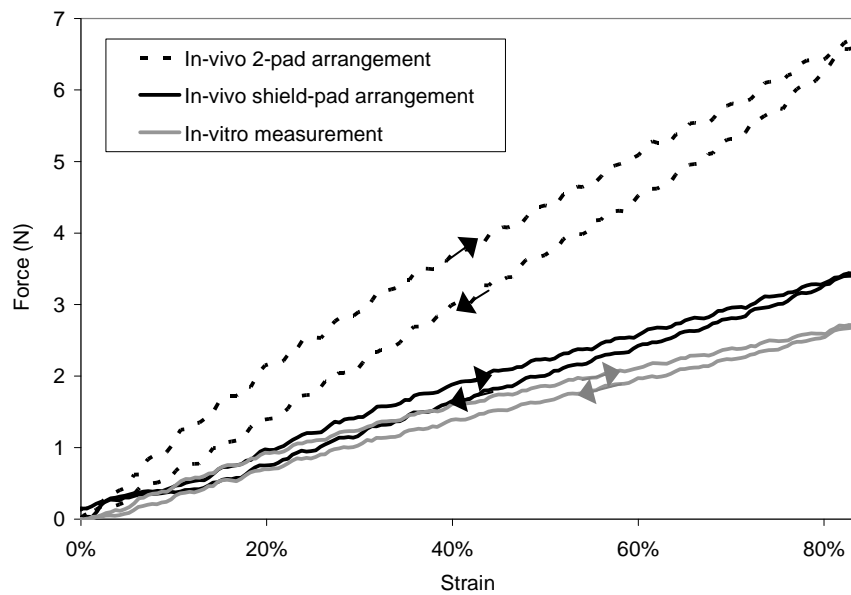
Figure 3-16: Tensile test data of grey Theraband® for *in vivo* 2-pad, *in vivo* shield-pad, and *in vitro* configurations.

3.6.3. Modeling of residual peripheral forces - Rubber

To test the accuracy of the model described in Section 3.4.2, the residual peripheral forces $F_{peripheral}$ given by equation (3-4) were subtracted from the *in vivo* shield-pad data to compare against the *in vitro* data of the rubber sheet experiment; ideally, the result should match closely with the *in vitro* data. The value of the spring constant $k_{e,\theta}$

was computed from the *in vitro* force-displacement data by using the mean gradients of the loading and unloading cycles at the specified displacements *e*. The results for the yellow and grey Theraband® are shown in Figure 3-17 and Figure 3-18, where the (1) shield-pad data, (2) $F_{peripheral}$ compensated data, and (3) *in vitro* data are compared.
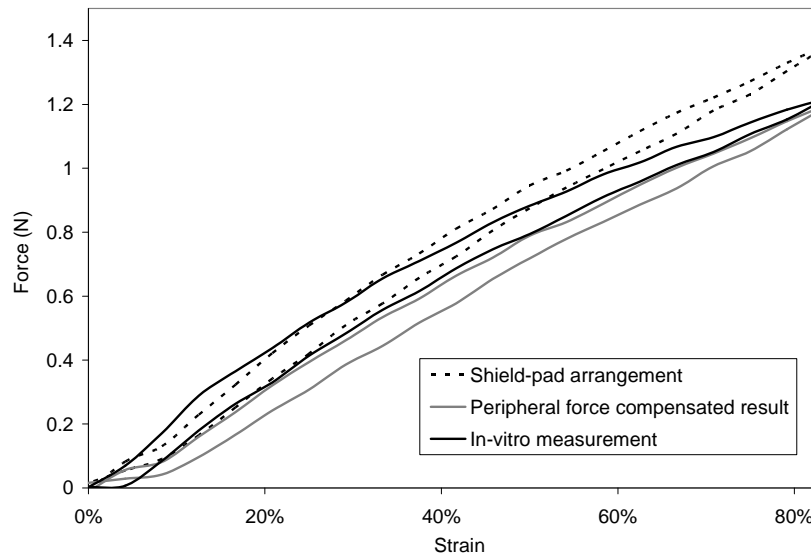
Figure 3-17: Comparison of $F_{peripheral}$ compensated result for yellow Theraband®.
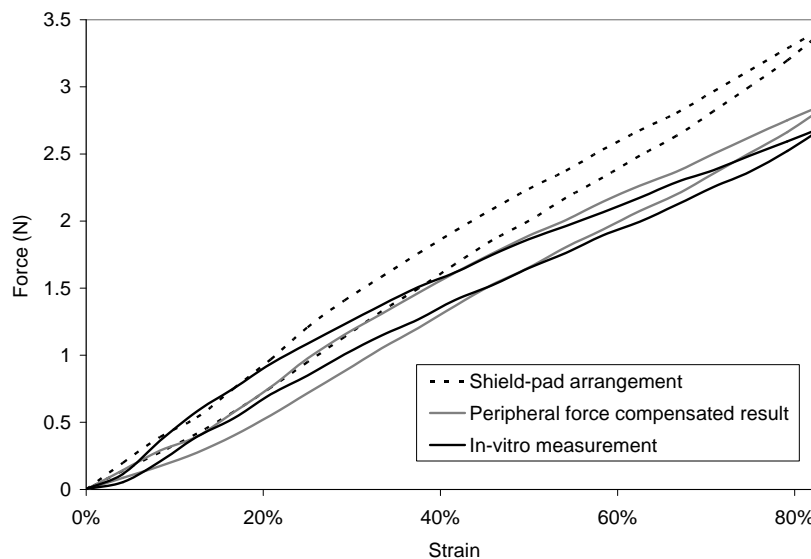
Figure 3-18: Comparison of $F_{peripheral}$ compensated result for grey Theraband®.

It was observed that the shield-pad data compensated for $F_{peripheral}$ were generally closer to the *in vitro* data, which is the desired outcome. It was also observed from the plots that the difference with the *in vitro* data was relatively larger in the beginning,

but this difference became smaller as the displacement increased. It was also determined empirically that using a coverage angle of ±45° for the residual peripheral forces (refer to variable α in equation (3-3)) produces better results than other angles. The details of this analysis are given in the Appendix.

A similar test for pig skin did not produce satisfactory results, as it was observed that the shield-pad data (compensated for $F_{peripheral}$) generally deviated away from the *in vitro* data, instead of moving towards it. It was found that this was attributed to complications in applying the appropriate $k_{e,\theta}$ values in the model's formula. More details will be described at the Discussion section.

3.6.4. Mechanical testing – Pig skin

The results from the *in vivo* pig experiment have the same outcome, where the shield pad data is significantly closer to the data in which the skin sides are removed ("*in vitro*" setting emulated). The typical results are given in Figure 3-19 and Figure 3-20.
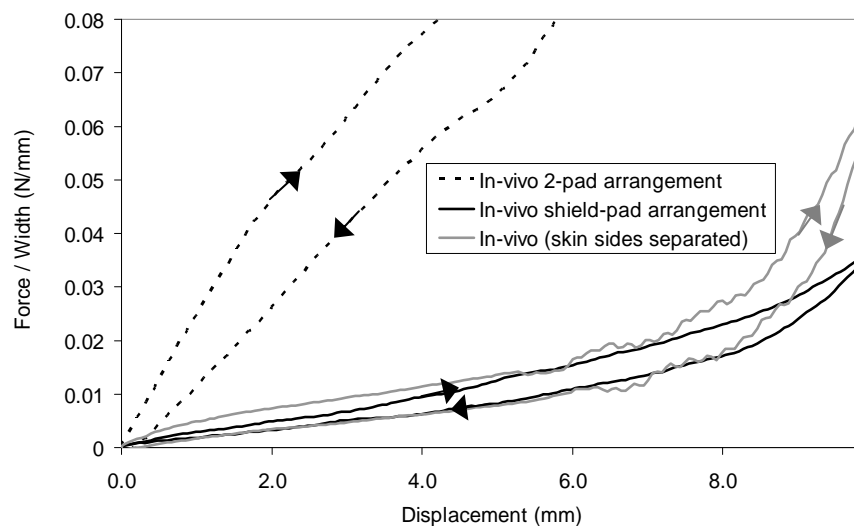
Figure 3-19: Tensile test data of pig abdomen region for *in vivo* 2-pad, *in vivo* shield-pad, and *in vivo* 2-pad of isolated skin island configurations. Note that for the plots' vertical axes, the force is normalized against the width of the load cell pad because the pad widths used for the 3 experiments differ slightly.
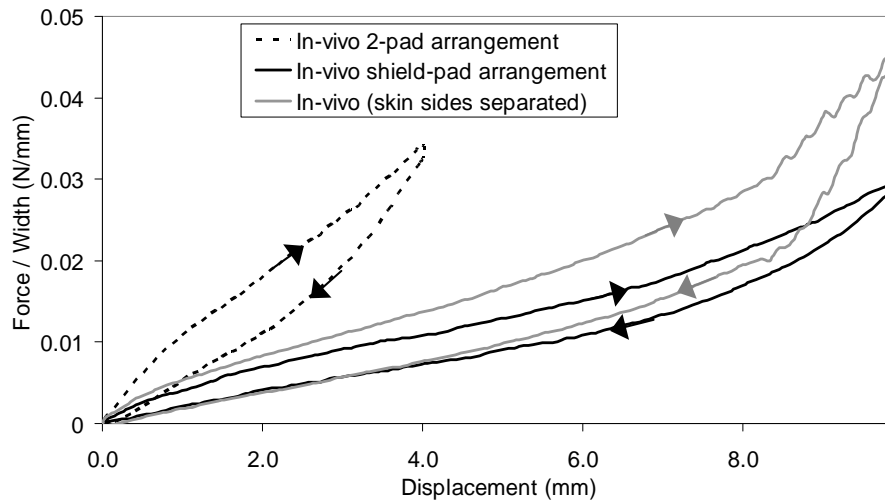
Figure 3-20: Tensile test data of pig shoulder region for *in vivo* 2-pad, *in vivo* shield-pad, and *in vivo* 2-pad of isolated skin island configurations.

3.6.5. Device contact pressure

It was observed during the initial experiments that contact pressure of the device on the skin marginally influenced the obtained reading. For example, the contact pressure was increased by placing a 2N weight on the top of the device before measurement so that the pads pressed harder onto the skin. In this setting, the produced data was found to differ by about 10% compared to data obtained with no extra weight. Furthermore, it was observed that this difference increased further as the pressure was increased, thus suggesting that the measurement was sensitive to the contact pressure. Due to this sensitivity, an articulated arm with a vertical slide attachment was used to hold the extensometer onto the body so that the device rests on the skin with its own weight, as seen in Figure 3-7.

3.7. Discussion

3.7.1. Effectiveness of shield pad design

Data measured in an *in vitro* setting may be considered as the true biomechanical uniaxial properties of the skin because the stress field in the test material is uniform. The FEM and mechanical tests showed that the proposed shield-pad data is significantly closer to the *in vitro* data, but the data from the traditional 2-pad diverges significantly. Therefore, it is deemed that the new design is capable of measuring the true properties effectively.

It can be observed that the differences between the shield-pad result and *in vitro* result is greater for the grey than yellow Theraband®. This is expected because the grey Theraband® is stiffer than the yellow one and so the magnitude of the peripheral forces, which cannot be completely removed by the shield pad, is higher.

It should be noted that the experiments were carried out in the extensive mode for rubber sheets and in the compressive mode for pig skin. In the extensive mode, the pads moved apart at the loading cycle, and then moved back together at the subsequent unloading cycle. On the other hand, in the compressive mode, the pads were first moved towards each other at the loading cycle, and then back apart at the subsequent unloading cycle. The compressive mode measurement is conducted for skin because the skin at rest on the body is already in a stretched state with internal tension. Therefore, the biomechanical properties will be measured for the skin from the initial pre-tensioned state, to a relaxed tension-free state, and then to a wrinkled/compressed state. Since the purpose of this research is to eventually estimate the skin deformation upon harvest (where the skin is tension-free), it is therefore more

relevant to measure in the compressive mode. In fact, a subsequent chapter describes a new method to use the biomechanical behavior in the compressive direction to estimate flap deformation upon harvest (also published at Lim *et al.*, 2006).

When calculating the mechanical stress involved during measurement, the width of the skin tested must be known. In an *in vitro* measurement, the width of the skin tested is simply the width of the sample itself since the stress field is uniform. Manschot had suggested that in an *in vivo* extensometer measurement (using the traditional 2-pad extensometer), the effective width of the skin can be approximated by the width of the pads itself (Manschot *et al*, 1986). However, this cannot be the case since the adjoining skin around the pads is inevitably deformed during measurement, which can also be clearly seen in the simulated FEM images in Figure 3-14. In the experiments conducted with the new device, it is evident that the *in vivo* measurements showed significant closeness with the *in vitro* measurements (in which the width of the *in vitro* samples was the same as the width of pad B). Thus, it can be concluded that in the new device, the effective width of the skin measured *in vivo* can be approximated by the width of the pad itself, thus enabling the stress involved during measurement to be calculated directly and conveniently.

3.7.2. Accuracy of residual peripheral force modeling

The model of the residual peripheral forces has been shown to be effective in bringing the shield-pad data closer to the *in vitro* data in the rubber sheet experiments. The data correction was not exact, which suggested that this simple model still did not completely describe the residual peripheral forces; this may also be due to experimental or handling error during measurement. Nevertheless, the model

approximated the forces well, thus producing results even closer to the *true* uniaxial property. It was also determined from the model that the coverage cone of the residual peripheral forces was approximately ±45°, which was an intuitively reasonable value.

It was observed from the data plots (refer to Figure 3-17 and Figure 3-18) that the difference with the *in vitro* data was relatively larger in the beginning, but this difference became smaller as the displacement increased. The reason may be due to small setup errors in the experiment, since the measured materials being handled were small in size. At the initial displacements when the forces involved were small, the load cell reading was relatively more influenced by external factors compared to later displacements when the forces involved were larger.

The spring constant $k_{e,\theta}$ (refer to equation (3-4)) of a specific material can be determined *in vitro* one-time and treated as a constant to be reused in the future. For synthetic materials that are isotropic, such as the rubber sheets, $k_{e,\theta}$ can be easily measured and reused. However, if $k_{e,\theta}$ is unknown, it can also be reasonably estimated from the *in vivo* force-displacement data measured during experiment since the shield pad extensometer would already produce data close to the *true* uniaxial property. On the other hand, obtaining $k_{e,\theta}$ *in vivo* is challenging for biological materials that are anisotropic and non-linear, such as skin on the body. The reason is that $k_{e,\theta}$ varies with direction, strain and skin thickness. Direction variation adds complexity because the $k_{e,\theta}$ values along and around the measurement axis must be substituted correctly (according to θ), and this is difficult. Skin stiffness also varies considerably according to location because it depends on skin thickness, which is non-uniform throughout the body and not easily determined non-invasively. Thus, $k_{e,\theta}$ cannot be pre-determined

and reused for all skin. Last but not least, skin is under a natural tension on the body and the natural length may be unknown; thus, the exact strain e may also be unknown. Therefore, due to some of these complications, the validation test for pig skin did not produce satisfactory results.

3.7.3. Standardization of measurement

It was found during experiments that contact pressure of the device on the skin should be standardized during measurement. As the forces measured were small (generally around 1N magnitude), the load cell used was very sensitive such that forces from directions other than the specified measurement axis may be registered marginally. Since downward pressure created vertical forces which would affect the reading, this variable should be kept constant by standardizing the contact pressure. The design solution currently employed was to use a vertical slide attachment at the articulated arm so that the extensometer always presses onto the skin with 2.45N (i.e. its own weight). However, this design has the disadvantage that measurements must be done with the device at a horizontal position. For future improvement, a pressure transducer can replace the slide attachment to ensure a constant pressure. Ideally, the extensometer should just sit on the skin surface with zero pressure.

In real measurements, standardization of the measurement parameters and procedure is essential in order to achieve measurement consistency and reproducibility, and to ensure that results acquired can be compared across different measurement sessions. While there is currently no internationally adopted standard, this issue must be recognized when conducting research on skin measurement. Therefore, a standardizing protocol was used in this study, which included standardizing the (1)

pad dimensions, (2) distance between the pads, (3) strain rate, (4) device contact pressure on the skin, and (5) means of holding the device during measurement. This standardization protocol, coupled with the new shield pad design, would ensure that the results obtained are consistent, reproducible and more accurate.

3.8. <u>Summary</u>

It can be concluded that by eliminating the peripheral forces during an *in vivo* skin measurement, one can obtain considerably reliable biomechanical properties of skin that are significantly closer to the actual *in vitro* properties. Thus, an extensometer with an additional third pad, shielding the pad containing the force sensor, was proposed. Experimental results indicated such arrangement was effective. A model was also developed to model peripheral forces during measurement, and has been shown to be reasonably accurate in calculating the peripheral forces for isotropic synthetic materials, such as rubber sheet.

Finally, it can be summarized that a measurement standardization protocol that consisted of the device design and measurement parameters should be used. Compared to a traditional design of 2-pad arrangement, this new system is standardized to obtain accurate, reliable and consistent results.

CHAPTER 4
SKIN MEASUREMENT PRINCIPLES

4.1. Introduction

The *in vivo* non-invasive measurement of skin properties is challenging due to many factors. Firstly, skin is a complex layered structure that has non-linear, directional dependent, elastic and viscoelastic biomechanical properties. Furthermore, skin on the body is not isolated (like an *in vitro* setting), but is connected both directly and indirectly to other tissues and structures, such as the muscle and the joints; the movement and position of the joints will influence the skin tension around them. Last but not least, in a non-invasive setting, only the top dermal layer of the skin can be accessed for measurement, and so it is uncertain if the measured data can represent the properties of the entire flap. This chapter examines these issues individually, and establishes the principles and assumptions of the skin measurement in this research work. In addition, this chapter also discusses in detail the standardization protocol used in this study, as well as the use of the pig model as a human surrogate in the study of skin biomechanics.

4.2. Non-invasive skin measurement

As discussed in the literature review, at sites such as the dorsal or volar region, the skin flap is not anchored to the underlying muscle. There, the flap slides easily over the fascia that separates it from the muscle. This is schematically represented in Figure 4-1, showing simplified anatomical cross-section of skin flap, where the flap is

modeled as 2 layers of skin (dermal) and fat, fascia is modeled as a slippery tissue layer, and muscle is modeled as the base on which the flap slides.
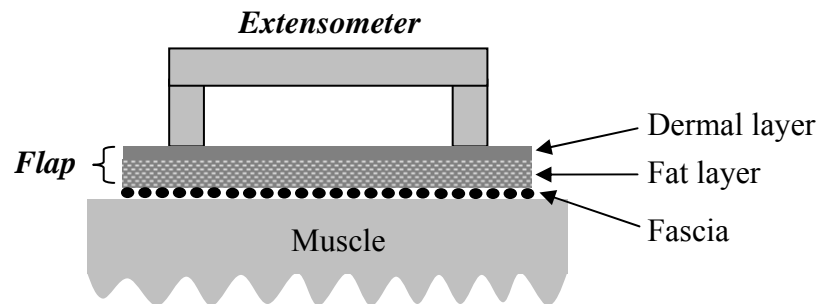
Figure 4-1: Schematic representation of skin flap measurement *in vivo*

The extensometer pads are attached to the skin surface (upper dermal layer) using double-sided adhesive tape, and the force during pad displacement is measured. Skin flap consists not only of the dermal layer, but also of the underlying fat layer. Therefore, the surface measurement may not completely measure the biomechanical properties of the entire flap.

However, one can substantiate that surface measurement would represent the biomechanical properties of the entire flap in terms of the relative stiffness value of each layer. The dermal layer stiffness is reported to be much greater than that of the fat layer. In one study using suction measurements and numerical analysis (Hendriks *et al.*, 2003), the Young's Modulus of the elastic region of dermis and fat were estimated to be 56.4 KPa and 0.12 KPa respectively; indicating stiffness difference of 470 times. In a separate modeling study of buttock tissue (Sun, 2005), the Young's Modulus of dermal and fat tissues were reported to be 0.85 MPa and 0.01 MPa respectively, which has a stiffness difference of 85 times. In yet another study using suction, it was reported that the resistance of the applied vertical stress was essentially due to the dermis rather than the subcutaneous fat, although the authors did not quantify the relative contributions (Diridollou *et al*, 1998). Therefore, one can infer

from these studies that the dermal layer has the prevailing stiffness. Since the extensometer pads are attached directly to this layer, it is reasonable to assume that this dominating property of dermal tissue would be measured.

To prove further that the fat layer has indeed relatively small influence on the shrinkage, 2 skin samples were harvested during a pig experiment. These samples were harvested from the same site on the animal and adjacent to each other to ensure that their biomechanical properties were similar. In one sample, the fat layer was immediately removed. Upon comparing both samples, it was observed that their lengths were approximately the same (refer to Figure 4-2 (a)). This demonstrated that the removal of fat layer from one sample has little effect on the dimension of the stiffer dermal layer. In addition, figure (b) shows a sample with its skin and fat layers separated. In this sample, it was observed that the fat layer shrunk (from both ends) by approximately 10% after separation, while the skin layer remained unchanged. Hence, these demonstrations revealed that the dermal layer has the prevailing stiffness, and the fat layer has relatively small influence on the total flap shrinkage.

(a)   (b)
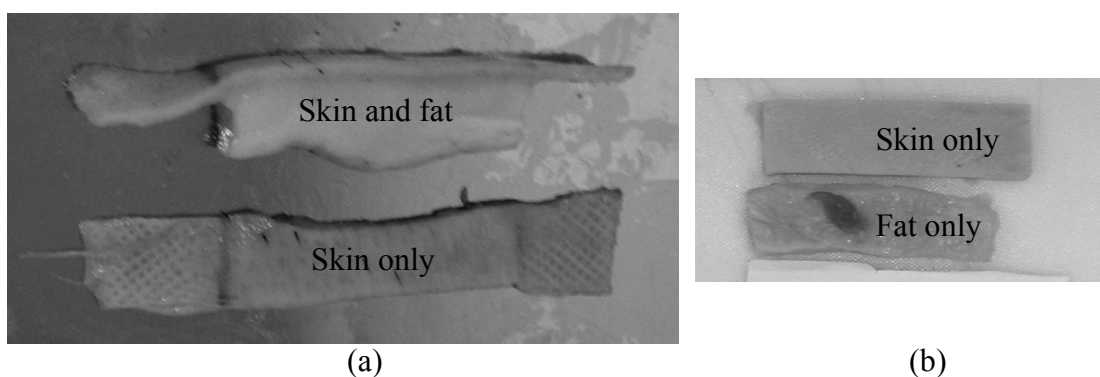
Figure 4-2: (a) Picture of adjacent skin samples, showing skin-fat and skin-only having equal length. (b) Picture of a sample with skin and fat separated.

4.2.1. Deformation uniformity of skin thickness

Having established that measuring the dermal layer is sufficient to represent the entire flap, another concern is the deformation uniformity of the dermal layer during pad displacement. A typical value for skin thickness is 1.2mm. The increase in length of the dermal layer all over its thickness may differ from the pad displacement. In fact, the change in length in the deeper layers of the dermis is less as compared to that at the surface (refer to Figure 4-3), such that the stress across thickness is not homogenous. However, due to the small dermis thickness compared with the other dimensions (width and length), the stress and deformation heterogeneity can be deemed to be negligible.
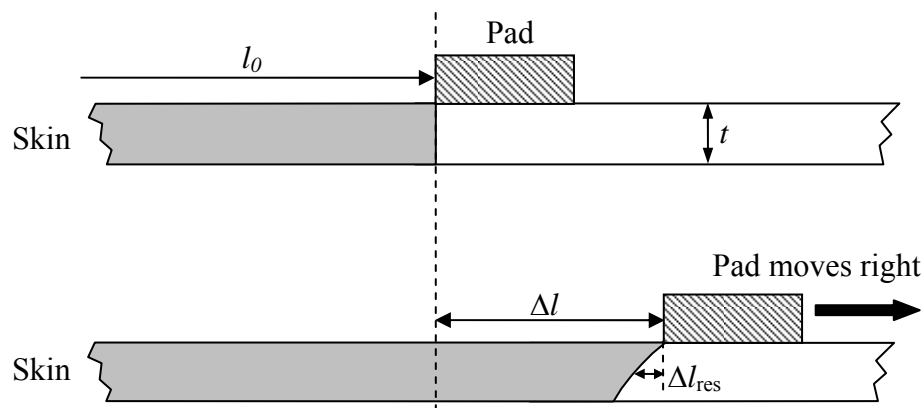
Figure 4-3: Schematic representation of the cross-section of dermal layer during pad displacement, (a) initial separation, (b) strained situation.

The issue of deformation uniformity was also studied by Manschot for high uniaxial load (Manschot *et al*, 1986), in which his group described the correction for the lag in deformation of the lower layer of the dermis as the residual deformation Δl_{res}. It was found that Δl_{res} depended linearly on the stress applied and skin thickness (t), but was independent of the width of the pads; the relationship is given by equation (4-1). This equation can be further simplified and converted to residual strain $\Delta \varepsilon_{res}$, as given in equation (4-2).

$$\Delta l_{res} = 2.3 \times 10^{-7} \times t \times \sigma \qquad (4\text{-}1)$$

where Δl_{res} = residual deformation (mm),
$\quad t$ = skin thickness (mm),
$\quad \sigma$ = stress (Nm^{-2}).

$$\Delta \varepsilon_{res} = \frac{2.3 \times 10^{-7} \times F}{w \times l_0} \text{ given that } \Delta \varepsilon_{res} = \frac{\Delta l_{res}}{l_0}, \ \sigma = \frac{F}{w \times t} \qquad (4\text{-}2)$$

where $\Delta \varepsilon_{res}$ = residual strain,
$\quad l_0$ = initial pad separation,
$\quad F$ = force measured,
$\quad w$ = width of load cell pad.

To compute the *effective* strain of the extensometer pad, $\Delta \varepsilon_{res}$ was to be subtracted to the strain imposed by the device pad. In this research work, the pad width w used was 12mm, and the minimum value of l_0 was 15mm. Calculating based on a force F of 10N, which is typically the maximum value encountered during experiments, the amount of residual strain $\Delta \varepsilon_{res}$ to compensate is only 1.28%. This value is almost negligible, and therefore, one can safely assume stress and deformation homogeneity across the skin thickness.

4.3.   Preconditioning of skin

Preconditioning of the skin using the extensometer is needed before acquiring measurements to ensure reproducible force-displacement curves at successive cycles (Fung, 1986). Figure 4-4 shows four consecutive stretching loops of a typical force-strain data measured using the new shield-pad extensometer; the typical J-shaped profile is observed. Figure 4-5 shows four consecutive force-strain loops of skin measured in the compressive direction (i.e., extensometer pads on the skin surface travel towards each other initially).
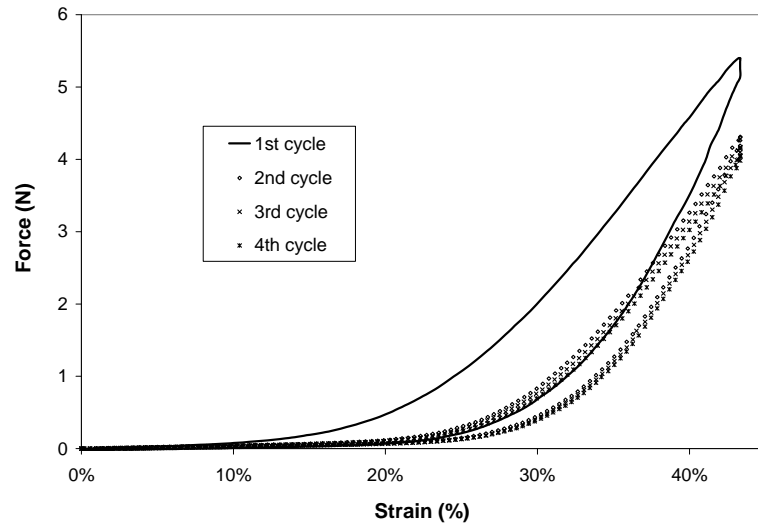
Figure 4-4: Preconditioning of a skin tissue in *extensive* direction, with the first cycle showing marked variation with the subsequent cycles.
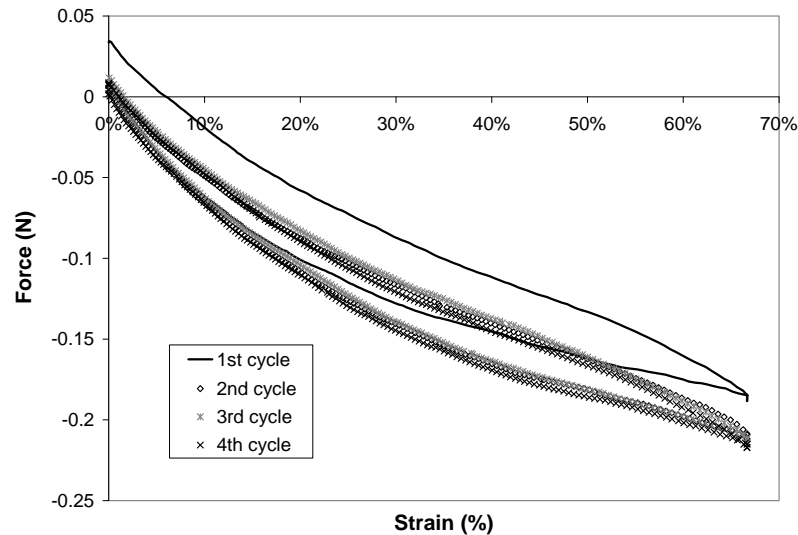
Figure 4-5: Preconditioning of a skin tissue in *compressive* direction, with the first cycle showing marked variation with the subsequent cycles.

In both measurements, the successive cycles converge after the first cycle. Therefore, it can be seen from the graphs that it is necessary to perform the loading and unloading cycle at least once, before the relationship becomes repeatable. This may be due to some interaction of dermis with underlying fascia. Such behavior is reported to occur in biological materials (Fung, 1996). From this observation and the literature

evidence, it should be emphasized that all experimental sites must be pre-conditioned by at least two repeated cycling before any data gathering.

4.4. <u>Viscoelasticity</u>

The dermal layer provides the mechanical strength of skin. Its principal components include: elastin, collagen, water, ground substances and mesodermal cells (Sanders *et al.*, 1995). Elastin is a fibrous protein which forms a mesh-like network between collagenous fibres; it gives mechanical integrity at low loads (Daly, 1969). Collagen, on the other hand, is the principal load-bearing component and gives mechanical integrity at high load levels. Under normal physiological conditions on the body, skin is stretched by *small loads* and so elastin may be regarded as the main load bearing component (Gibson 1965). Elastin networks display elastic material behavior and do not undergo stress-relaxation to dissipate internal tension. When tension is released (i.e., during skin flap harvest), the stored energy is generally used for immediate shrinkage. The subsequent shrinkage due to viscoelasticity, also known as hysteresis, is negligible in comparison to that initial immediate shrinkage.

The model used in this research work to study skin shrinkage involved only small loads under normal physiological conditions; high bearing loads were not involved. As is described in subsequent chapters, data analysis is generally based on the force-strain data in the compressive direction, and so the skin is not stretched at all. Therefore, to simplify modeling in this work, it is assumed that skin is an elastic material and its viscoelastic behavior can be ignored.

As a note of interest, one can refer to the hysteresis in the force-strain data in Figure 4-5 to get an estimate for the relative influence of viscoelasticity between high and low load conditions. Hysteresis, which is a measure of viscoelasticity, is calculated as the area between the loading and unloading cycles. In figure (a), the hysteresis for the extensive force-strain data (high load condition) is significantly higher than the hysteresis for the compressive data (low load condition). Thus, the compressive measurement, involving low loads, has relatively minimal viscoelastic contribution.

4.4.1. The effect of measurement strain rate

Skin is a viscoelastic material and therefore the force-displacement profiles is expected to show time and strain rate dependencies, and such behavior is seen in both *in vivo* and *in vitro* extensive force-extension data. In order to test strain rate dependency, a set of measurements was carried-out at various strain rates (0.005, 0.01, 0.015, 0.02 and 0.024 s^{-1}). The data for extensometer measurements done in the compressive direction is presented in Figure 4-6. As the current device had the maximum velocity of 0.6mm/s (0.024 s^{-1}), it was chosen as the upper limit.
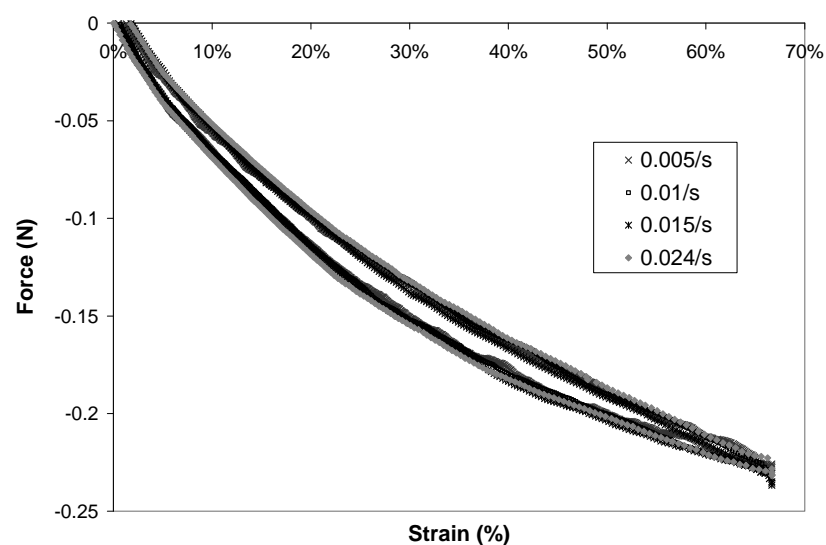
Figure 4-6: Force-strain behavior *in vivo* at different strain rates; tests are performed in the compressive direction.

The data in Figure 4-6 shows that, within the studied strain rates and displacement limit, there is little pronounced variation with applied strain rate. This observation was similarly seen for data measured in the extensometer extensive direction (which is not shown here). Furthermore, this observation was also reported in other human tissues, such as liver, where the tensile behavior is similar across a range of low strain rates from 0.003 to 0.606 s^{-1} (Chui *et al*, 2004). From these results, one can say that the tensile behavior is relatively independent of the measurement strain rate at low levels. Thus, the operating speed of the extensometer was standardized at the maximum velocity of 0.6mm/s.

4.5. <u>Standardization of measurement</u>

The earlier chapters discuss the importance of measurement standardization with regards to the device. A standardization protocol was proposed (refer to Section 3.7.3), which was necessary in order to achieve measurement consistency and reproducibility, and to ensure that results acquired can be compared across different measurement sessions. Aside from the hardware design and measurement parameters, the standardization of the measured object is also important (Serup *et al*, 2006); the measured object refers either to human, animal or synthetic material. The factors that are important for standardization are summarized in Table 4-1.

It is known that the position of limbs, which affects external skin tension, will have marked influence on shrinkage of adjoining skin zone (Langer, 1978 B). It is also reported that the force-extension property of *in vivo* human skin are dependent on both internal and external skin tensions (Thacker *et al*, 1977). Joint movement places much larger forces on to the neighboring skin areas (Thacker, 1977) than the skin's internal

tension. It should also be noted that the joint movements not only stretches skin, but in some directions and positions, skin may even be compressed. Therefore, it should be stressed that at certain position of joints, it is also probable that when a skin flap is excised/harvested, it may elongate in some directions. In order to avoid these scenarios and to reduce the influence of the external tension, studied sites were standardized by choosing them away from the joint areas, and joints were placed in relaxed position.

Table 4-1: Standardization protocol

Category	Factors to standardize
Hardware design	• Dimensions of the pads • Initial distance between the device pads • Means of holding the device during measurement
Measurement parameters	• Measurement strain rate • Contact pressure of device on the skin
Test preparation	Positioning of the body region, in particular with respect to the positions of adjacent large joints, including supination/pronation
	Careful selection and marking of the site to be measured
	Measurement direction with respect to the Langer's line, since skin properties are sensitive to orientation
	Surround skin is fixed and remains fixed during measurement
Measurement processes	Preconditioning of the skin by at least two repeated cycling before data gathering
	Avoid repeated measurements in the same site, at least for one hour; the initial recording will temporarily modify the viscoelastic behavior within that site

4.6. <u>Clinical trial on animal</u>

Animal studies are often used as a precursor to the human clinical trial. In the study of skin biomechanics, pig models have frequently been used to emulate human models due to the similarity of skin structure. Larrabee (Larrabee *et al*, 1986) showed that piglet may be the best animal for *in vivo* skin testing, since its skin bears a close

resemblance to human skin histologically; the elastin content of the piglet dermis is closest to that of human, piglet has low hair density, and the skin thickness is approximately the same as human skin. Still, results obtained from animal experiments cannot be applied completely to the human patient (Kenedi *et al*, 1975).

This research study used freshly slaughtered pigs for all experiments (3 to 6 months old; *genus: Sus; species: Duroc & Yorkshire; animal ethical clearance number: 006/06; clearing authority: Institution of Animal Care and Use Committee, National University of Singapore*). All handling and experimentation involving animals were done in a humane, ethical manner, and according to strict ethics regulations.

The experiments were usually conducted after the animals were dead for approximately 2 hours. The extent to which the postmortem skin tissues maintain the biomechanical properties of living tissues governs the degree to which the cadaver response represents the human response. Studies of biomechanical property differences show that postmortem skin (Foutz *et al*, 1992) is similar in terms of strength, ultimate strength, and loading response to their live comparisons. The histological post-mortem changes are also minimal (Kovarik *et al*, 2005), especially within the first few hours. Most of the tissue stiffening occurs at the muscle (rigor mortis) (Van Ee *et al*, 2000), and this does not directly affect skin stiffness and shrinkage.

4.6.1. Invasive determination of Langer's line

In this study, the direction of the Langer's line was often needed in the animal experiments. At each test site, the Langer's direction was initially estimated by

looking for wrinkle crease lines on the skin and using tension line maps found from literature (Rose, 1976). The direction was then verified by punching 3mm circular holes near the test site and speculating on the tension lines (Rose, 1976). When a circle is pierced on to a skin, it is subjected to radial forces and greater deformation will occur in the direction of maximum tension. Thus the major axis of the wound was taken as the direction of Langer's lines. Since punctured holes may affect tension measurements at the immediate regions, the invasive technique was done sufficiently far away (at least 50mm distance) from the intended measurement area.

4.7. <u>Summary</u>

The dermal layer of the skin has been shown in literature and experimental studies to have prevailing stiffness over the fat layer. This evidence supported the assumption that the extensometer's measured data can sufficiently represent the properties of the entire flap. In addition, in order to simplify modeling, it was assumed that skin is elastic, and its viscoelasticity can be ignored. During measurement, the preconditioning of skin, as well as the standardization of the device and measured object parameters are important to ensure measurement consistency, reproducibility and comparison possibility.

CHAPTER 5
PREDICTION OF LANGER'S LINE

5.1. <u>Introduction</u>

The direction of Langer's lines, or lines of tension, is an important parameter to determine in the study of skin biomechanics. As discussed in the literature review in Section 2.3, the biomechanical and shrinkage properties show symmetry along and perpendicular to the Langer's line. Thus, the skin may be treated as an orthotropic material, such as in Finite Element Modeling (FEM). Even though the general direction of Langer's line is well documented in literature, this direction slightly differs between individuals and the precise direction can only be determined by invasive penetration techniques. Non-invasive determination of Langer's line is of importance to this work. Firstly, skin flap shrinkage often shows symmetry along this line and therefore to model the subject and location specific flap shrinkage, one needs to measure the material properties along and perpendicular to the Langer's line. A detail account of the FEM work is published in a parallel study to this thesis work (Jeyapalina and Lim, 2005). In a nut shell, skin was modeled in the FEM as an orthotropic material, and the Langer's line is simply the principal stress axis in the model; when taking measurements for the FEM, the material properties must be measured along and perpendicular to the principal axis.

This chapter discusses and establishes the relationship between the Langer's line and properties such as the orientation of skin's collagen fibers network, force-extension data, and terminal stiffness. In addition, this chapter describes an *in vivo* non-invasive method to predict the direction of the Langer's line using the extensometer.

5.2. Method – Imaging and mechanical testing

It has been shown that fibers predominantly align themselves along the Langer's line (Cox, 1941). To study this relationship at the microscopic level, scanning electron microscopy (SEM) of skin tissue cross-sections was performed. It is well known that the tensile property of skin has dependency on the Langer's line direction (Gibson *et al*, 1969; Lanir, 1974; Stark, 1977). To investigate this further, *in vitro* and *in vivo* mechanical tests were conducted to determine the relationship between the force-displacement behavior of skin and the direction of Langer's line of test site.

5.2.1. Materials

SEM imaging and *in vivo* mechanical tests were undertaken on pig model due to the similarity of skin structure to human model. Prior to the experiment, one piglet was freshly slaughtered at the animal facility according to strict university ethics regulations. For *in vivo* tests on humans, measurements were carried out on the upper leg (inner thigh) of four healthy volunteers (two males and two females), aged from 22-32 years. Finally, for *in vitro* mechanical tests, soft leather sheet samples (obtained from the University of Northampton, UK) were used.

5.2.2. Scanning electron microscopy

Prior to SEM imaging, a skin flap was harvested from the shoulder of the pig after determining the direction of the Langer's line invasively (refer to technique described in Section 4.6.1). The fat layer was then removed and the skin was acetone washed several times in order to prevent fiber sticking following the dehydration. Skin sections were cut in two planes, along and perpendicular to the Langer's lines. Cross-

sectional areas were examined using a Hitachi S3000 Variable Pressure Scanning Electron Microscope.

5.2.3. *In vitro* experiment: Leather

As seen in Figure 5-1, samples of soft leather were cut in 12 directions of 30° intervals with respect to the backbone of the animal. The *in vitro* force-extension profiles of dumbbell shaped samples were examined by uniaxial measurements using a universal tensometer (Instron, model no. 1122) at an extension rate of 10mm/min. The effective test dimension was 20 mm x 4.5 mm.
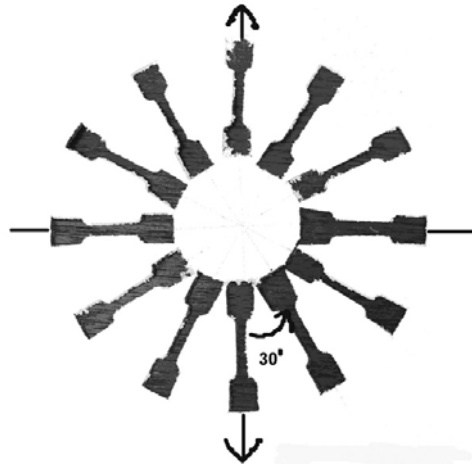
Figure 5-1: *In vitro* measurements on samples cut out from a soft leather sheet; 12 test directions are shown at 30° interval.

5.2.4. *In vivo* experiment: Human skin

The *in vivo* force-extension behavior of skin was measured with the extensometer on all four subjects. Tests were performed in 12 directions with respect to the long body axis. The first axis was taken as 0° and subsequent axes were at 30° intervals anticlockwise from it (refer to Figure 5-2). At each test site, measurements were carried out by attaching the pads to the skin surface using double-sided adhesive tapes, where the width of the gap between the fixed and movable pads was 12mm. The pads separation was then extended by 10mm (or to a load of 9N) at a rate of 0.6 mm/s, and

the force-extension data was recorded. Experimental sites were preconditioned by two successive loading-unloading cycles, and data from the third cycle was taken as the actual measurement. Necessity for such preconditioning was explained in Section 4.3.

It was reported that the force-extension property on the body is dependent on both internal and external skin tensions (Thacker *et al*, 1977). Therefore, to eliminate the external tension introduced by the joint positions, the legs were kept straight so that the area under investigation was in a lax state throughout the measurements.
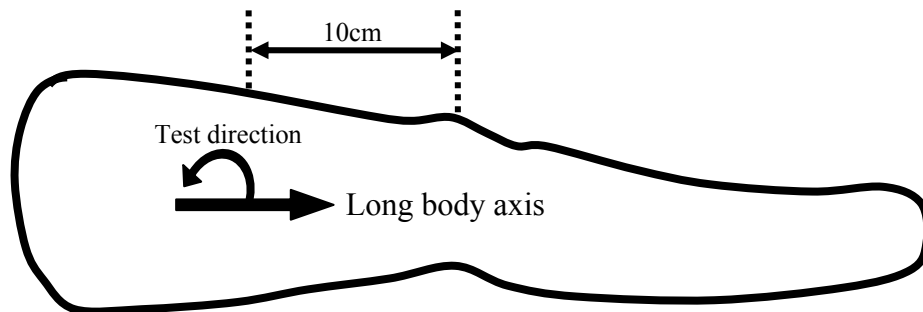
Figure 5-2: *In vivo* measurements on the leg; test directions are shown.

5.2.5. *In vivo* experiment: Pig skin

Animal hair was shaved off to ensure maximum adhesion between skin and device pads. Three specific test sites (abdomen, upper thigh and upper shoulder) were chosen to cover a variety of anatomical regions. At each site, a 100mm circle was marked on the skin and extensometer measurements were conducted at the center in three different directions (or axes). The first measurement axis was taken as 0°, and this direction was chosen based on wrinkle crease lines as well as the literature reference to the Langer's line of the test site (Rose, 1976). The subsequent measurement axes were taken at 60° interval anticlockwise from the first axis (refer to Figure 5-3). The extensometer's measurement setting was the same as the human tests described earlier.
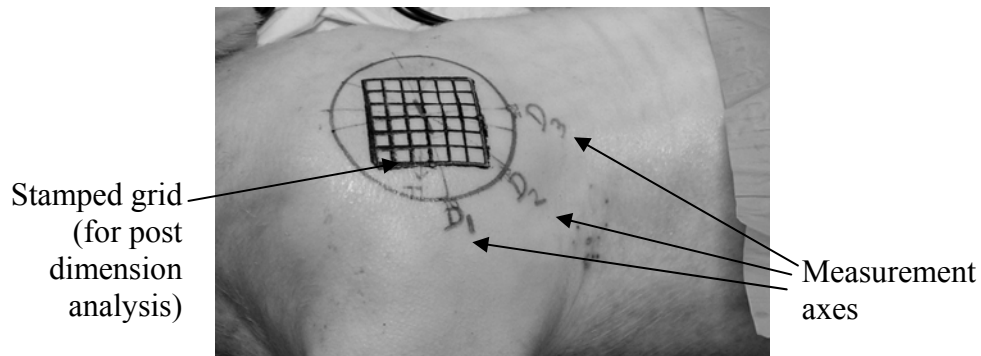
Figure 5-3: Photograph of a test site showing three axes of measurement. *NB: axes angles shown here are at 45° interval, instead of the 60° used in actual experiment.*

After each set of measurements, the skin flap (dermis-fat layers) was excised along the 100mm marked circle and to the fascia-subcutaneous junction. The harvested flap was then placed in a tray that contained a thin layer of saline solution to stop the evaporation of water, and to prevent the further associated shrinkage. The saline also prevented the underlying fat layer from sticking to the tray surface (which otherwise would affect the shrinkage). Then, the direction of major axis of the shrunken elliptical flap was determined by Vernier caliper measurements across the span in all orientations, and also verified by image analysis after capturing an orthogonal picture. The major axis was taken as the direction of the actual Langer's line (Reihsner *et al*, 1995), and the result was recorded with respect to the first measurement axis.

5.3. Results and Discussion

5.3.1. Scanning electronic microscopy

As discussed earlier, several researchers have reported that loading in the high stiffness region is primarily due to stretching of collagen fibers (Daly, 1982). Furthermore, Cox has indicated that fiber alignment along and perpendicular to the Langer's line is different (Cox, 1941). In order to validate the preferential alignment of collagen fibers within the dermis, skin cross-sections were cut parallel and

perpendicular to the Langer's line of a pig shoulder skin and were analyzed using the SEM. The SEM micrographs are shown in Figure 5-4.

(a)   (b)
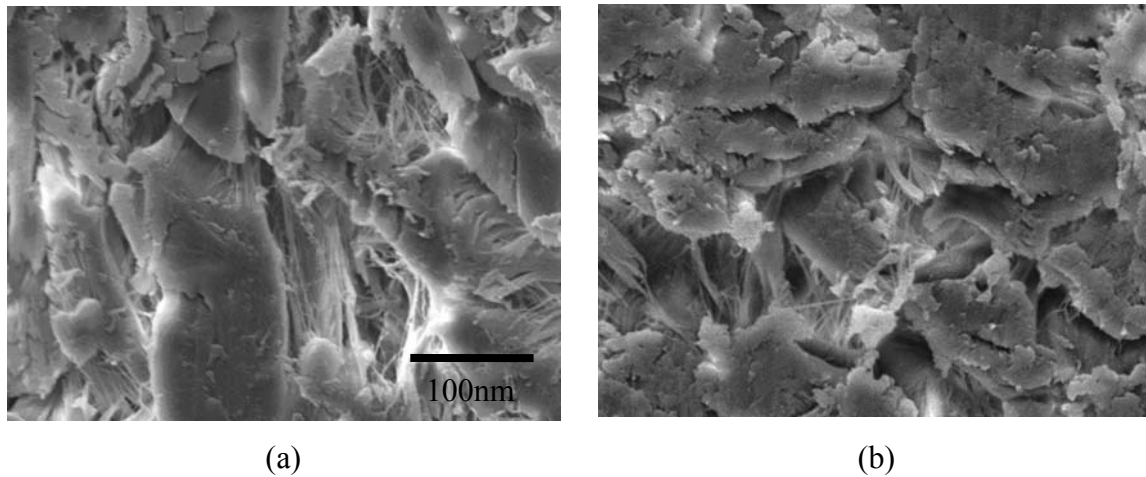
Figure 5-4: SEM micrographs of pig skin section (a) cut parallel to the Langer's line, (b) cut at right angle to Langer's line.

In sections cut along the parallel, most of the collagenous bundles of the reticular (dermal) layer were severed at an angle, an indication of some degree of fiber alignment along the Langer's line. In sections cut perpendicular to the line, the bundles were severed at a right angle, indicating fibers are running transversely. The initial interpretation of this result is that collagen network is not quite random but biased in one direction. This undoubtedly concludes that the collagen fibers of reticular dermis show high degree alignment to the Langer's line (maximum tension line) than perpendicular to it. This observation implies that by studying the high stiffness region of the stress-strain curve, it is possible to ascertain structural information of collagen network and consequently the direction of the Langer's line.

5.3.2. Human skin and leather experiments

Figure 5-5 shows a typical direction-dependent force-strain data on pre-conditioned human skin. As expected, these curves show differing behavior with respect to test direction; this trend is similar to those reported in the literature (Gibson *et al*, 1969;

Stark, 1977; Lanir, 1974). It is clear that the curve near the Langer's line is the shortest, while perpendicular to the Langer's line gives the longest *toe* region or limit strain value; for this particular data set, the Langer's line is approximately 120° anti-clockwise to the long axis of body (refer to the Langer's line map in Figure 5-6). Another obvious feature of this result is that the terminal stiffness (computed from the gradient of the linear third phase) of the curves shows a clear and distinct periodic trend.
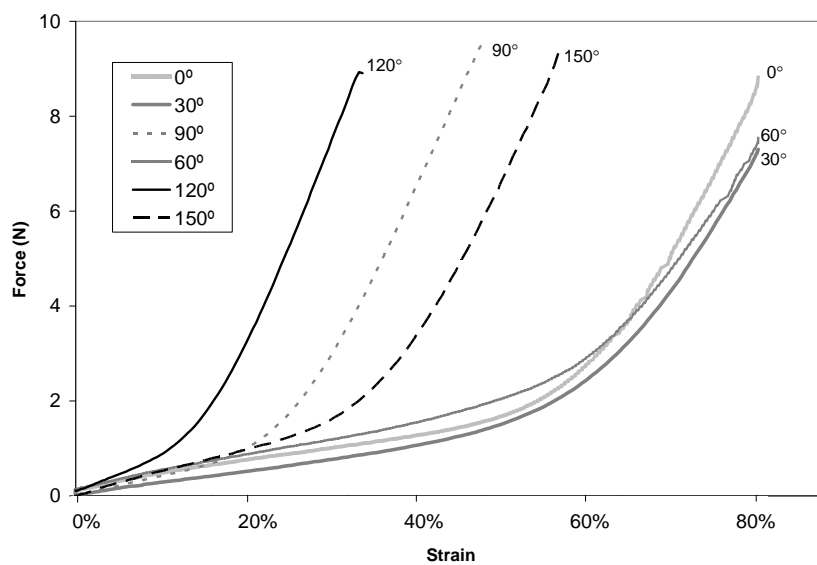
Figure 5-5: *In vivo* force-extension curves of skin; showing least extensible direction at 120° and highly extensible direction at 30°.
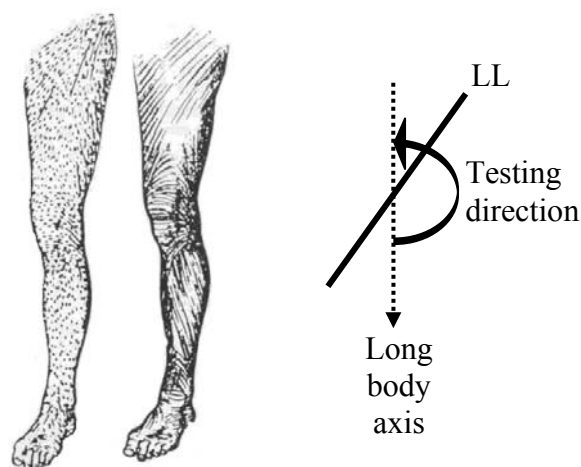
Figure 5-6: Diagrammatic representation of Langer's line of left leg (reprinted from Reihsner *et al*, 1995); LL- Langer's line direction.

A similar trend (refer to Figure 5-7) is observed for *in vitro* tensile experiments of soft leather representing the skin tissue. Thus, it can be said that skin, either in the presence or in the absence of natural tension, behaves in a similar way showing directionally varying mechanical properties. Therefore, the observed directional behavior of the force-strain curves can only be attributed to the fiber structure itself. This conclusion further supported the findings from the SEM imaging.
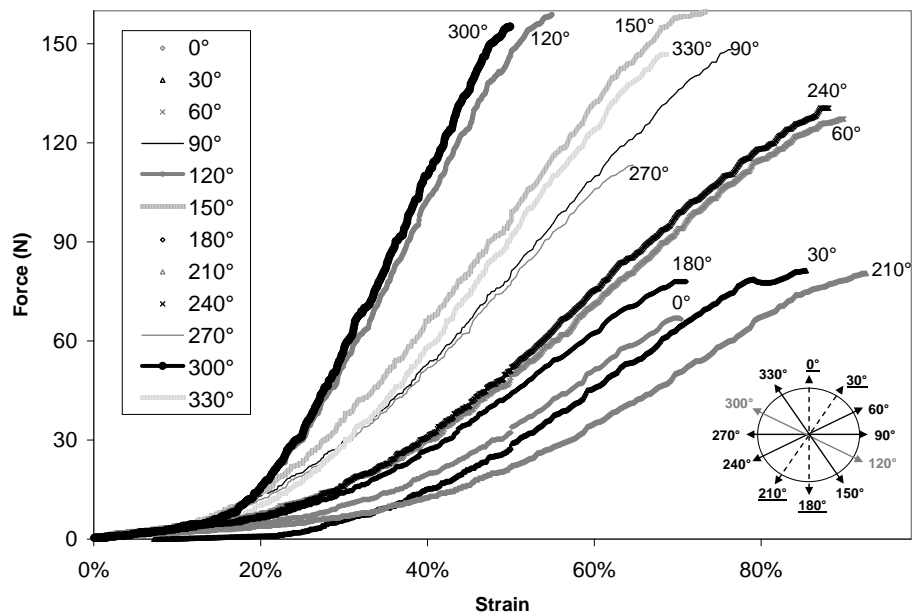
Figure 5-7: *In vitro* force-extension curves of leather; axis of back bone was taken as 0° direction and samples were taken at 30° intervals.

Stark characterized the stress-strain curves in terms of limit strain and stiffness of terminal region (refer back to Figure 2-6), and reported a correlation between these parameters and testing direction (Stark, 1977). He also found that Langer's lines correlate well with the direction of minimum limit strain and maximum terminal stiffness. Our data further supports this relationship.

When the terminal stiffness was plotted with respect to the testing direction, it was observed to be periodic and the data points always form an ellipse (refer Figure 5-8); an example of how terminal stiffness was calculated is shown in the Appendix. This is

unlike the observation of Stark, where the data points did not always conform to a regular geometrical form (refer to example in Figure 2-7). This observation may be due to the limitation of the extensometer or experimental setup, where for some instances the skin may not have been stretched beyond the 2nd phase in their experiments; hence, the terminal stiffness value of the 3rd phase may have been computed with error. Thus, the results presented in Figure 5-8 clearly show that the direction of the major axis of ellipse reflects the direction of Langer's line, and that the directions and magnitudes of major axes of ellipses differ slightly between experimental subjects.
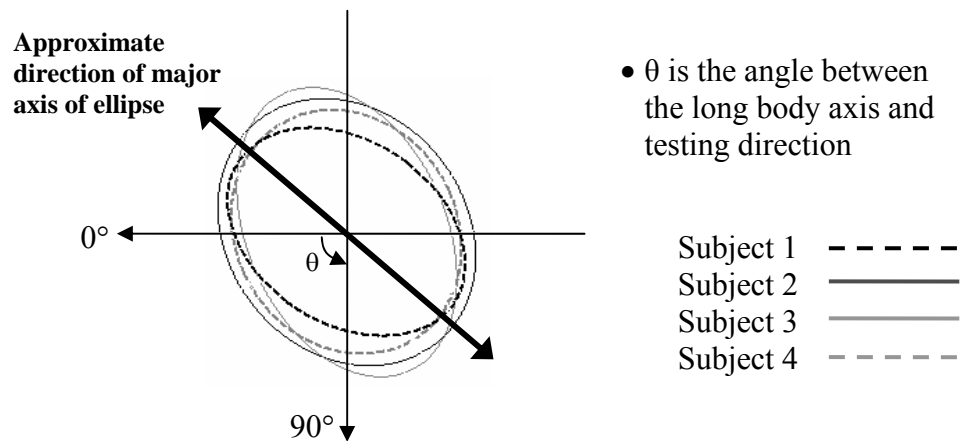
Figure 5-8: Polar plots of terminal stiffness from force-strain curves of four volunteers. The major axes of resultant ellipses indicate the direction of Langer's line, found to be 120° to 135° anti-clockwise from long body axis.

It is obvious from the results that force-extension properties of skin are not completely random but shows some degree of symmetry. The literature (refer to Section 2.3) also reports similar observations, that the biomechanical behavior shows symmetry along and perpendicular to the Langer's line. Thus, one can conclude that skin can be treated as an orthotropic material. It was further established from this trial that terminal stiffness (in a polar plot) can be approximated to follow an elliptical model. There is an important advantage of using the terminal stiffness instead of limit strain to infer the direction of the Langer's line. As described at the SEM images in Figure 5-4, the

high stiffness region of the force-extension curve (i.e. the terminal stiffness) is related to the orientation of the collagen network, which is a material constant. On the other hand, the limit strain is not related to a material constant, and may vary according to factors such as the external tension, which is affected by limbs position (Thacker *et al*, 1977). Therefore, using the terminal stiffness to predict the Langer's line direction is more reliable.

5.3.3. Method of predicting Langer's line direction

At present, Langer's lines are predicted in practice by invasive penetration techniques. The results presented here emphatically demonstrated that the direction of a local Langer's line can be determined by multiple *in vivo* force-extension tests in different orientations. However, to obtain a complete set of force-extension curves (e.g. 12 directions with triplicates in each direction for skin pre-conditioning) is very time consuming. To minimize the number of tests needed, only three data points are sufficient, since it was established earlier that an ellipse can be fitted over these points (refer to Figure 5-9).
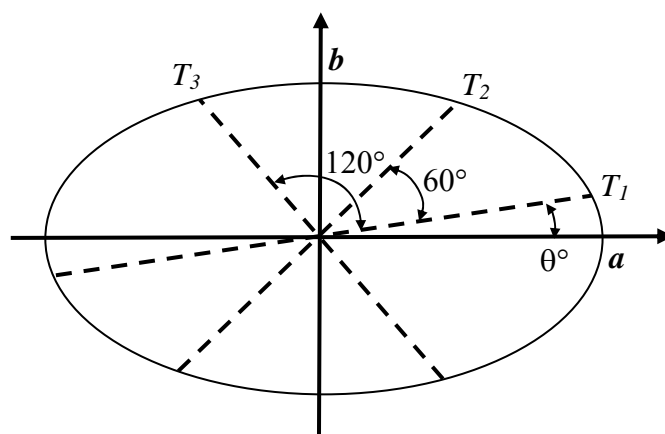
Figure 5-9: An illustration of three data points (T_1, T_2 and T_3) on the ellipse, where they are separated by 60°.

The equation of an ellipse in polar coordinates is given by:

$$\frac{T_i^2 \cos^2 \theta}{a^2} + \frac{T_i^2 \sin^2 \theta}{b^2} = 1 \qquad (5\text{-}1)$$

where T_i = terminal stiffness value of a force-extension curve,
  a = major axis,
  b = minor axis,
  θ = angle between point T_i and the major axis.

By choosing a 60° sampling interval, one ensures that the three data points of terminal stiffness (T_1, T_2 and T_3) will cover more than one quadrant of an ellipse for maximum fitting accuracy. The set of equations in (5-2) can then be obtained by substituting the data points into equation (5-1). A numerical solution can be found that will yield the values of the unknowns a, b and θ.

$$T_1^2 a^2 \sin^2 \theta + T_1^2 b^2 \cos^2 \theta = a^2 b^2$$
$$T_2^2 a^2 \sin^2\left(\theta + \frac{\pi}{3}\right) + T_2^2 b^2 \cos^2\left(\theta + \frac{\pi}{3}\right) = a^2 b^2 \qquad (5\text{-}2)$$
$$T_3^2 a^2 \sin^2\left(\theta + \frac{2\pi}{3}\right) + T_3^2 b^2 \cos^2\left(\theta + \frac{2\pi}{3}\right) = a^2 b^2$$

where T_1, T_2, T_3 = data points (terminal stiffness) at 60° interval,
  θ = angle between data point T_1 and the major axis.

A software program based on the set of equations in (5-2) was developed to allow a user to compute the Langer's line direction based on three terminal stiffness inputs. It should be noted that the set of three equations should be reduced to two (by using simultaneous equations method), because this simplification will enable a numerical solution to be computed with higher accuracy and speed.

5.3.4. Pig skin experiment

The purpose of conducting the pig skin experiment was to test the accuracy of the Langer's line prediction method described in the previous section. At each test site,

the experiment conducted force-extension measurements at three directions at 60°

interval. Three terminal stiffness values were then computed from the data and input

into the software program developed based on equation (5-2); an example of how

terminal stiffness was calculated is shown in the Appendix. The program calculated

the direction of the Langer's line, which was then compared with the actual direction

that was determined invasively. The results for the various test sites are summarized in

Table 5-1. From this table, it can be seen that the Langer's directions were estimated

within 4° from the actual direction, thus demonstrating the high accuracy of the

proposed method. It should be emphasized here that this method allows one to find the

actual directions of Langer's line without the need for the invasive penetration

techniques.

Table 5-1: Results of the Langer's line (LL) direction estimated non-invasively

Location	Thigh			Shoulder			Abdomen		
Measurement axis	Dir1	Dir2	Dir3	Dir1	Dir2	Dir3	Dir1	Dir2	Dir3
Terminal stiffness (N/mm)	2.97	2.39	2.81	2.99	2.47	2.74	2.77	2.37	2.65
Estimated LL angle (from Dir1 axis)	24°			18°			23°		
Actual LL angle (from Dir1 axis)	20°			21°			25°		
Error	4°			3°			2°		

5.4. **Summary**

This chapter has demonstrated the importance of directional variations in relation to

the structural make up of skin. It can be concluded that there is a strong correlation

between skin stiffness and Langer's lines, and that terminal stiffness can be

approximated to follow an ellipse. It was also established that by measuring the force-

extension data of skin in three different orientations, one can estimate the direction of

the Langer's line by use of an elliptical model. In verification experiments on animals,

the precision was found to be within 4° of the actual direction, thus indicating that this non-invasive method was accurate in predicting the Langer's line direction. As this is a non-invasive technique, it can be employed in clinical studies of skin. It should be emphasized that in order to use this technique, one has to stretch the skin up to its third phase to calculate the terminal stiffness; otherwise obtained result is inaccurate.

CHAPTER 6
PREDICTION OF SKIN FLAP SHRINKAGE

6.1. <u>Introduction</u>

Numerous groups have studied the extent of flap shrinkage after harvest. Barrett-Brown and Cannon's groups stated that an allowance of an excess of at least one-third in the flap size is necessary to compensate for shrinkage (Barrett-Brown *et al*, 1945; Cannon *et al*, 1947). Coakley *et al* stated that an allowance of 25% should be made for shrinkage when using forearm defects to resurface the leg (Coakley *et al*, 1950). Last but not least, Blocker and Mithoefer (Blocker *et al*, 1950) reported a 30% allowance when harvesting direct flaps. Apart from these clinical impressions, skin flap shrinkage does not appear to have been studied experimentally and quantitatively.

In an earlier chapter, a shield-pad extensometer has been shown to be effective in measuring the *true* uniaxial biomechanical properties of skin. The next objective is to develop a methodology using this device capability to predict flap shrinkage, as well as the natural tension and Young's modulus of elasticity. This chapter reports this new methodology and the validation experiments on rubber sheets and animal skin.

6.2. <u>Proposed model and hypothesis</u>

6.2.1. Predicting natural length

Since the skin on one's body is generally pre-stretched within its linear force-displacement region (first phase; refer to Figure 2-5), it is hypothesised that by removing the natural pre-tension of skin in a controlled manner, one can find a

deflection point in the force measurement that corresponds to its un-stretched natural length. This proposed method relies on the custom-built extensometer to find the force-displacement behaviour of skin flap in compressive direction, i.e. the extensometer pads on the skin surface travel towards each other during measurements. The compressive mode of measurement is used so that the skin property would be measured as it passes through the natural length when the pads move together.

Theoretically, a linear force-displacement data set is expected when the extensometer's pads movement causes the elastically-strain skin between them to return to its natural length. Beyond this point, the skin forms wrinkles or buckles-up as it is not capable of supporting negative forces (Danielson *et al*, 1975; Lanir, 1987). Thus, the obtained data may be expected to respond in three unique ways as schematically shown in Figure 6-1.
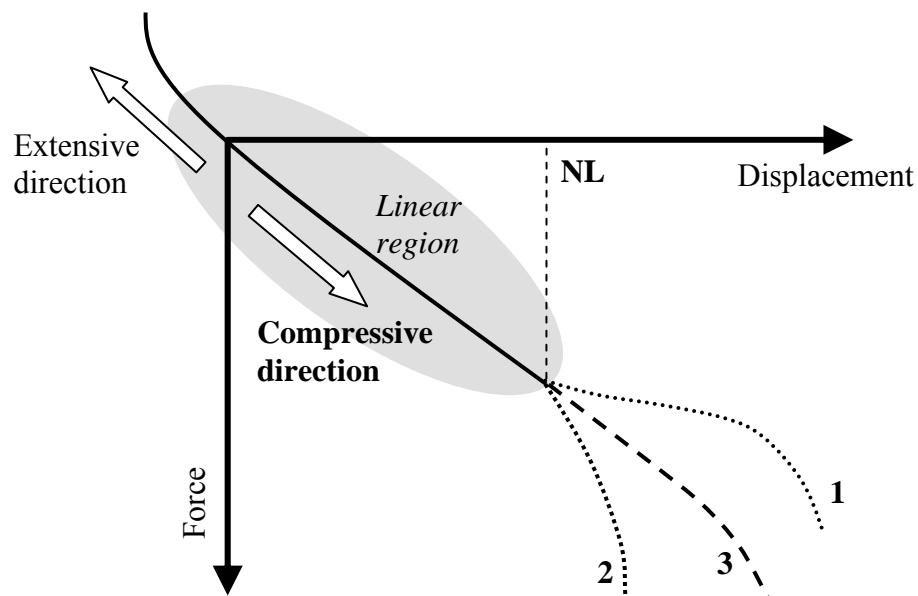
Figure 6-1: Theoretical prediction of skin flap behavior under an applied compressive displacement; illustrating the linear elastic and possible deflection behaviors beyond the natural length (NL).

In case 1, the skin will wrinkle and relax, so the rate of (absolute) force increase will level off. This continues until at a much further stage when the skin folds begin to

squeeze together, causing the force to increase rapidly as it takes relatively greater force to compress further. In case 2, the force will increase rapidly almost immediately as the skin folds and presses together just beyond the natural length. In case 3, the force continues to increase at the same rate until the skin folds press together, after which the force will rapidly increase. If a skin behaves like in cases 1 and 2, then there is a change in the direction of the initial straight line. Here, the natural length of the test site is proposed to be at the position where this gradient change occurs. Therefore, this method will allow the natural length to be estimated non-invasively. However, in case 3, the gradient change occurs at a later position and the natural length may be over-estimated. It is shown later in the result section that the shrinkage is significantly over-estimated in only 2% of the tested sites during the validation experiments on pigs.

It should be stressed that the described hypothesis is only valid if the extensometer can measure the *true* uniaxial biomechanical properties. Existing extensometers with two pads are unable to measure these uniaxial properties due to their inability to isolate and detect forces in the test direction only (a result of unwanted force contributed from deformation of skin around the pads). Therefore, the new shield-pad extensometer must be used. In addition, the natural length estimated would apply for shrinkage along the device's measurement direction only. As skin is biaxially stretched over the body's bony framework, in most cases, it shrinks in a non-uniform manner, and so the natural length measured in various directions may be different. Finally, it should be noted that in this model, skin is considered to be an elastic material, as discussed in Section 4.4; viscoelastic property is ignored.

6.2.2. Predicting natural tension and elastic modulus

As the extensometer measures close to the *true* uniaxial properties, it is then possible to deduce the natural tension and Young's modulus of elasticity directly from the compressive force-displacement data, after the natural length has been determined. Figure 6-2 illustrates hypothetically the forces experienced by the load cell pad of the shield-pad extensometer in 2-dimensional space. In figure (a), the pads A and B-C are at the initial separation, and so the load cell measures zero force because the forces on its left and right sides are balanced; each force is equal to the natural tension T_N. In figure (b), the pads B-C are moved to a position where the skin between pads A and B-C reaches the natural length. Here, the force to the left of the load cell is zero, while the force on its right is maintained at T_N due to the shield pad. Hence, the net force measured by the load cell is then equal to the natural tension T_N.
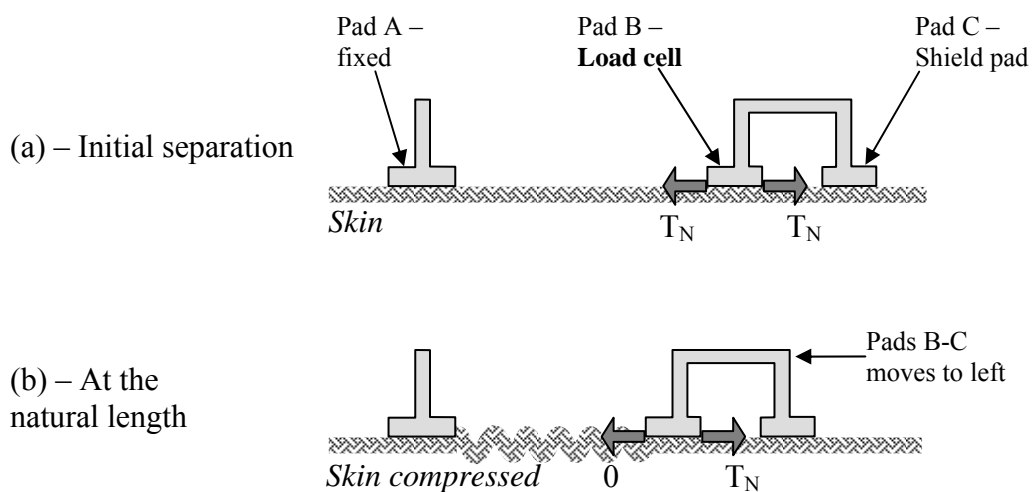
Figure 6-2: Schematic representation of forces measured by load cell (a) at the initial separation, (b) when skin in between the pads reaches the natural length.

Figure 6-3 illustrates a compressive force-displacement data. The natural tension is simply the force that corresponds to the natural length. The elastic modulus is given by the gradient of the data's linear portion (provided the skin thickness is known); skin thickness can be determined non-invasively using ultrasonic echography.
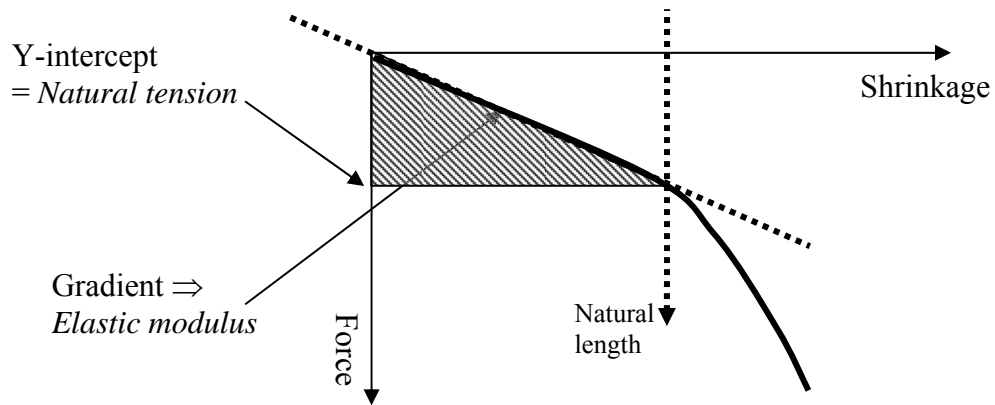
Figure 6-3: Deducing the natural tension and elastic modulus from the compressive force-displacement data (after determining the natural length).

6.2.3. Algorithm for data analysis

To determine the natural length from the measured data, instrumentation noise needs to be filtered out to obtain a smooth curve prior to identification of the linear segment near the origin. There are several methods to identify this linear segment. One such method is to spot this linear segment visually, but it is tedious and open to subjective interpretations. Hence, a computer algorithm was developed to analyze the data automatically and in a standard manner. A straightforward method based on gradient analysis is summarized in the flow chart in Figure 6-4.
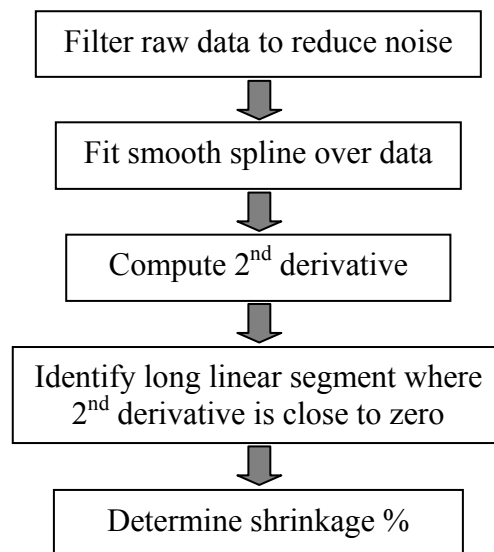
Figure 6-4: Flow chart of gradient analysis method to determine flap shrinkage

Noise filtering

The signals from the extensometer's force sensor were noticeably noisy, which needed filtering. It was found that the moving average was an appropriate filter (refer to equation (6-1)). The width of the filter was kept relatively small to preserve the shape profile but at the same time effectively reducing most of the noise. It was determined empirically that filter size of 25, which covered approximately 7% of the data size, was suitable.

$$f(x) = \frac{1}{N} \sum_{k=-\frac{N-1}{2}}^{\frac{N-1}{2}} g(x+k) \qquad\qquad (\,6\text{-}1)$$

where $f(x)$ = filtered data,
$g(x)$ = raw data,
N = size of filter.

Data smoothing

Even after this filtering, small local fluctuations were obvious (since the filter size was relatively small). As the second order derivative would be computed as part of the analysis, these fluctuations would amplify noise issues. Hence, a smooth curve that conformed tightly to the shape of the data need to be fitted before computing the derivative. The curve fit was achieved by interpolating a cubic smoothing spline over the data points (using the function *CSAPS* in the MATLAB® spline toolbox; refer to *www.mathworks.com* for details on the *CSAPS* mathematical formulation). The *CSAPS* function allows a smoothing parameter, p, to be specified, where $p = 0.0$ is the least-squares straight line fit, while $p = 1.0$ is the natural cubic spline that fits through *all* the data points with no smoothing. It was found empirically that $p = 0.9$ was sufficient to fit a spline that conformed to the data tightly, while providing enough smoothing to eliminate the local fluctuations.

Identifying linear segment of force-displacement curve

For a given function $f(x)$, a linear range will have a constant $f'(x)$ (1st derivative) and zero $f''(x)$ (2nd derivative). Therefore, the linear segment can simply be found by locating a continuous range where the 2nd derivative is zero. For real data sets, the 2nd derivative may not be exactly zero, but is close to it. The 2nd derivative was obtained using finite difference approximation, and is given by equation (6-2). It was found empirically from the data that $|f''(x)| < 0.004$ N/mm^2 conformed closely to a straight line. At this $|f''(x)|$ threshold value, the R-squared value for a linear fit over the data has a minimum value of 0.995, which indicated a strong linear correlation. Therefore, a continuous range of data below this $|f''(x)|$ threshold value will give a straight line.

$$f''(x) \approx \frac{f(x+h) - 2f(x) + f(x-h)}{h^2}$$ (6-2)

where h = interval in the x-axis.

Determination of flap shrinkage

A linear segment of data that was closest to the origin, and longer than 5% strain, was identified. The deflection point at the end of this linear region was taken as the point of flap shrinkage.

6.3. **Method – Mechanical testing**

In order to study the proposed methodology, proof-of-concept experiments were conducted on rubber sheets, followed by the validation experiments on animal models.

6.3.1. Materials

Large Theraband® sheets (yellow color grade) with average stiffness of 0.8 MPa at 50% strain were used in a rubber sheet experiment; the stiffness was close to that of the elastic deformation region of skin. Pig skin trials were also undertaken due to the similarity of skin structure to human model. Prior to the experiments, four piglets (three to six months old) were freshly slaughtered at the animal facility according to strict university ethics regulations.

6.3.2. Mechanical testing – Rubber

Two Theraband® sheets were stretched biaxially and then attached by double-sided tape onto a 120 x 120mm fixed frame (on all 4 sides); this condition emulated skin covering a human body in pre-tension. One rubber sheet was stretched biaxially by approximately 18% expansion while the other sheet was expanded by 25%. The test setup is similar to that shown in Figure 3-12. In order to ensure that the rubber sheet was stretched uniformly over the frame, a square grid was stamped onto the sheet prior to stretching; after stretching, the dimensions of the grid were measured to verify that stretching was done uniformly. Extensometer measurements in the compressive direction were conducted at the centre of the sheets by attaching the pads to the surface using double-sided adhesive tapes, where the width of the gap between the fixed and movable pads was 25mm. During measurement, the pads were brought to 15mm at a rate of 0.6 mm/s, and the force-displacement data was recorded.

Using a universal tensometer (Instron, model no. 5440), the force-extension measurement of a rubber strip was obtained. The specimen was cut into a dumbbell-shape with an effective test size of 25 x 12mm. This test size was chosen to be the

same as that of the test size in the extensometer experiment on large sheets; the same measurement speed of 0.6 mm/s was also used. The purpose of this experiment was to determine the rubber tensions at 18% and 25% expansions; these values would be used to compare against those estimated by the extensometer on large sheets.

6.3.3. Mechanical testing – Pig skin

Animal hair was shaved off to ensure maximum adhesion between skin and device pads. Three specific test sites (abdomen, upper thigh and upper shoulder) were chosen to cover a variety of anatomical regions (refer to Figure 6-5). These sites were also relatively flatter and where the skin slides over the muscle layer with ease.
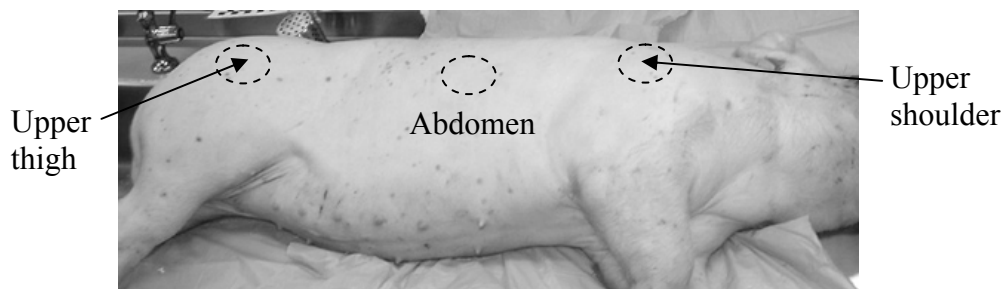
Figure 6-5: Test sites of the pig model

Before each measurement, the skin surface was also stamped with a standard square grid (100 x 100mm) as shown in Figure 6-6. Individual grid lines, 10mm apart, were used as reference dimensions to calculate the post harvest shrinkage. After which, uniaxial tests in the compressive direction were carried out by attaching the pads of the extensometer to the skin surface using double-sided adhesive tapes, where the width of the gap between the fixed and movable pads was 25mm. The pads were then brought to 15mm at a rate of 0.6 mm/s, and the force-displacement data was recorded. At each test site, extensometer measurements were performed both parallel and perpendicular to the Langer's line; the Langer's directions were estimated invasively (refer to technique described in Section 4.6.1). Experimental sites were preconditioned

by two successive loading-unloading cycles, and data from the third cycle was taken as the actual measurement. Necessity for such preconditioning was explained in Section 4.3.
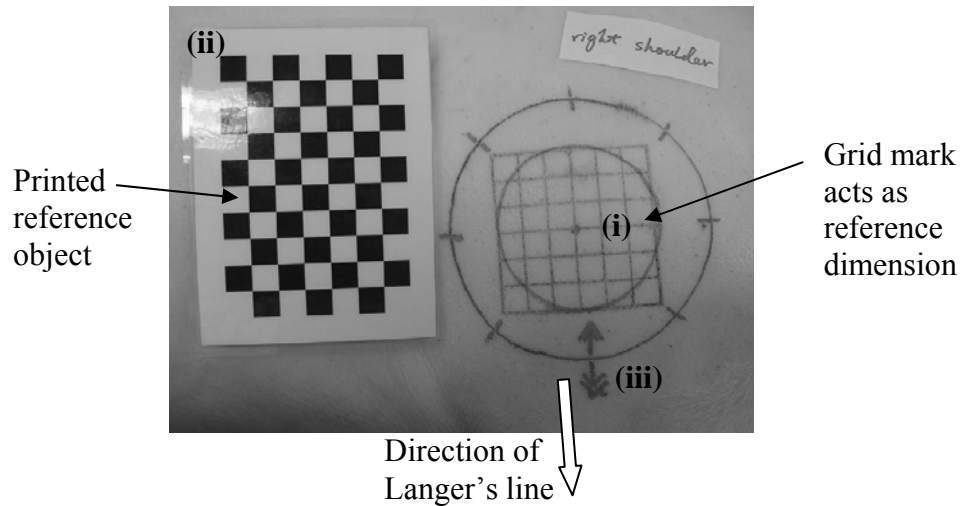
Figure 6-6: Photograph of a test site before measurement, showing (i) stamped grids, (ii) reference object for post dimension analysis, (iii) marked Langer's line pre-determined invasively

After the measurements, the skin flap (dermis-fat layers) was excised at the fascia-subcutaneous junction. The harvested flap was then placed in a tray that contained a thin layer of saline solution to stop the evaporation of water, and to prevent the further associated shrinkage. The saline also prevented the underlying fat layer from sticking to the tray surface (which otherwise would affect the shrinkage). The final size of the grids was then measured immediately by a Vernier caliper to determine the percentage shrinkage parallel and perpendicular to the Langer's line. The thickness of the flap was also measured by a thickness gauge. A total of 41 sets of measurements were taken.

6.4. <u>Results</u>

6.4.1. Rubber experiments

The measured data of 18% and 25% biaxially expanded Theraband® sheets are shown in Figure 6-7 and Figure 6-8 respectively. Note that the formula used for plotting the horizontal axes (shrinkage %) in both graphs is defined by equation (6-3). Based on the terms in this equation, the 18% expanded rubber would shrink ~15%, while the 25% expanded rubber would shrink 20%.

$$Shrinkage = \frac{\Delta l}{l_0} \times 100\% \qquad (6\text{-}3)$$

where l_0 = initial pad separation (25 mm),
  Δl = pad displacement.
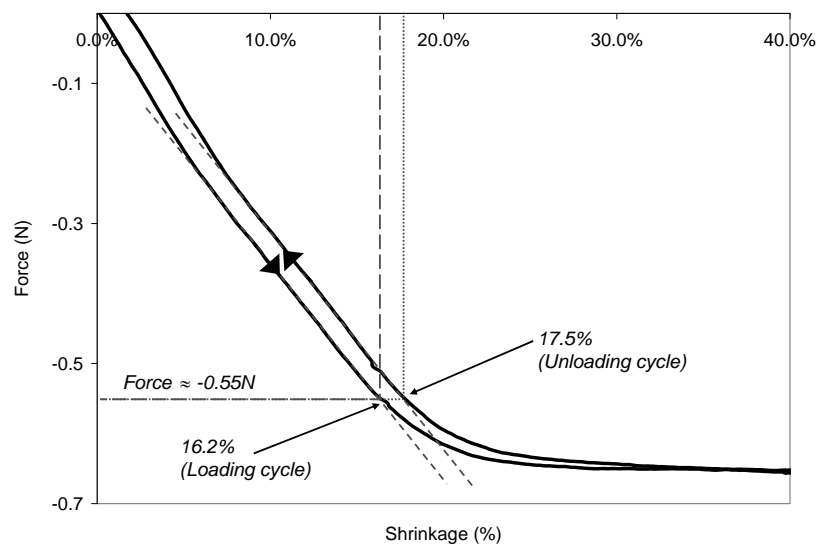
Figure 6-7: Tensile data of 15% shrunken rubber; transition points at 16.2% and 17.5%; the natural tension is estimated to be 0.55N.
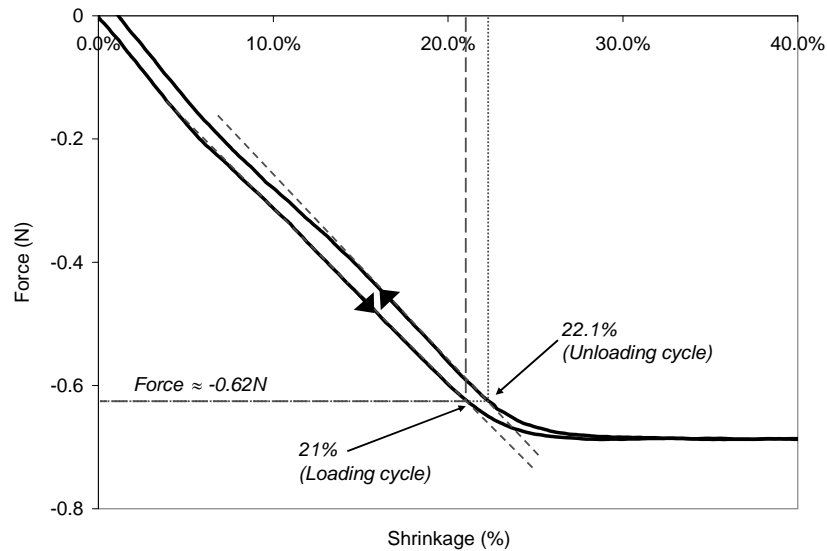
Figure 6-8: Tensile data of 20% shrunken rubber; transition points at 21% and 22.1%; the natural tension is estimated to be 0.62N.

From the figures, it was observed that the absolute force steadily increased until near the natural length, after which the force leveled off to almost flat after that. Hence, two distinct regions are observed, and they meet near the natural length. This behavior was expected, and is described as "case 1" in the proposed hypothesis section at 6.2. In the first region where the absolute force steadily increased, the internal tension was being measured by the load cell as the rubber was brought to its natural length. In the second region, the rubber had moved together beyond its natural length, and so it sagged loose between the pads; hence, no change in measured force in this region. Note that the loading curve refers to the initial compressive force-displacement data when the pads on the material surface move towards each other, while the unloading refers to the returning of the pads back to their initial position.

$$\text{Absolute Error} = \left| \text{Actual shrinkage\% – predicted shrinkage\%} \right| \qquad (6\text{-}4)$$

The results of the predicted shrinkages and the absolute errors are summarized in Table 6-1; the absolute errors were calculated using equation (6-4). It was found that

the overall average absolute error of predicted shrinkages is 1.7% for all the cycles. For natural tensions, it was found from the Instron measurements (*in vitro*) on the rubber strip that the *actual* natural tensions were 0.49N and 0.44N for the loading and unloading cycles respectively for the 15% shrinkage case; for the 20% shrinkage case, the *actual* natural tensions were 0.62N and 0.57N for the respective cycles. The results of the estimated natural tensions and errors are summarized in Table 6-2. The overall average error was found to be 11.5%. Finally, the results for the elastic modulus are summarized in Table 6-3; based on the tensometer *in vitro* data, the *actual* elasticity of the rubber was 0.97 MPa near the starting strain. The overall average error was found to be 18.5%.

Table 6-1: Results of predicted shrinkages of stretched rubber

Experiment set	Cycle type	Actual shrinkage	Predicted shrinkage	Absolute error
Theraband® with 15% shrinkage	Loading	15%	16.2%	1.2%
	Unloading	15%	17.5%	2.5%
Theraband® with 20% shrinkage	Loading	20%	21.0%	1.0%
	Unloading	20%	22.1%	2.1%

Table 6-2: Results of estimated natural tensions (NT) of stretched rubber

Experiment set	Cycle type	Actual NT	Estimated NT	Error (%)
Theraband® with 15% shrinkage	Loading	0.49N	0.55N	12.2%
	Unloading	0.44N	0.55N	25.0%
Theraband® with 20% shrinkage	Loading	0.62N	0.62N	0.0%
	Unloading	0.57N	0.62N	8.8%

Table 6-3: Results of estimated elastic modulus of stretched rubber. Only the results from loading data are shown since the unloading data has almost the same values.

Experiment set	Actual elasticity	Estimated elasticity	Error (%)
Theraband® with 15% shrinkage	0.97 MPa	1.25 MPa	28.9%
Theraband® with 20% shrinkage	0.97 MPa	1.05 MPa	8.1%

6.4.2. Animal experiments – Natural length

A compressive force-displacement data of a pig skin is shown in Figure 6-9. As expected, the results show that the force-displacement data yields a linear profile and the gradient changes near the expected natural length. However, this linear relationship was only seen after an unexpected small initial deflection at the origin, for both the loading and unloading curves.
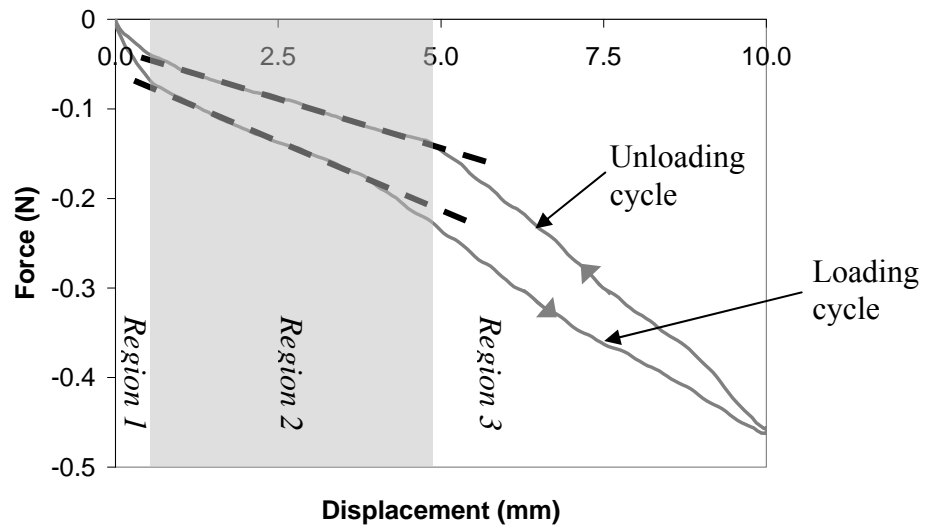
Figure 6-9: A typical force-displacement data, showing three distinct regions. Region 1- small initial concave region that may be attributed to unwanted force contribution due to experimental site; Region 2- the linear elastic region of skin; Region 3- beyond the natural length, where slopes differ from that of region 2.

As discussed earlier in the proposed hypothesis section, all three types of curves were observed from the animal experiments and are given in Figure 6-10 to Figure 6-14. The data in Figure 6-10 and Figure 6-11 deflect upward after the natural length (NL) were reached (deemed to fit case 1). Figure 6-12 and Figure 6-13 show the typical case 2 where the curves deflect downward, while Figure 6-14 shows a case 3 where the curve only deflects at a much later stage beyond the natural length. It should be noted that case 3 was encountered in only one measurement out of the total of 41 measurements collected in the experiment (or 2% of all data).
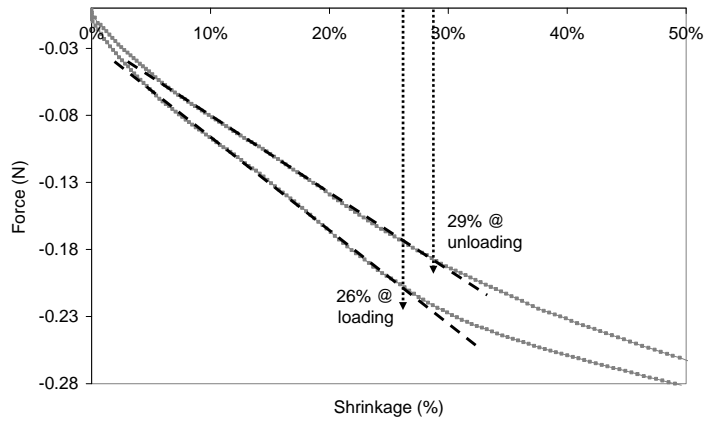
Figure 6-10: Sample data where curves deflect upward after NL; the actual shrinkage here is 26%.
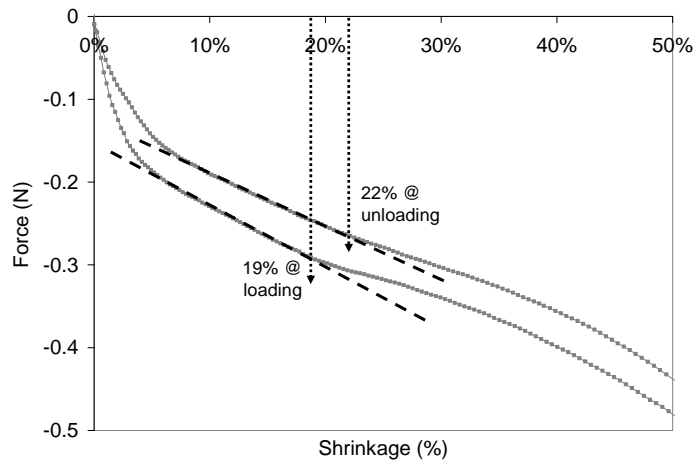
Figure 6-11: Sample data where curves deflect upward after NL; the actual shrinkage here is 20%.
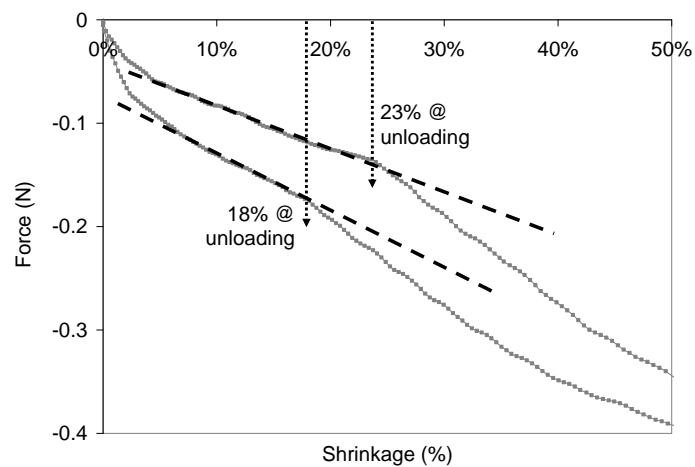
Figure 6-12: Sample data where curves deflect downward after NL; the actual shrinkage here is 20%.
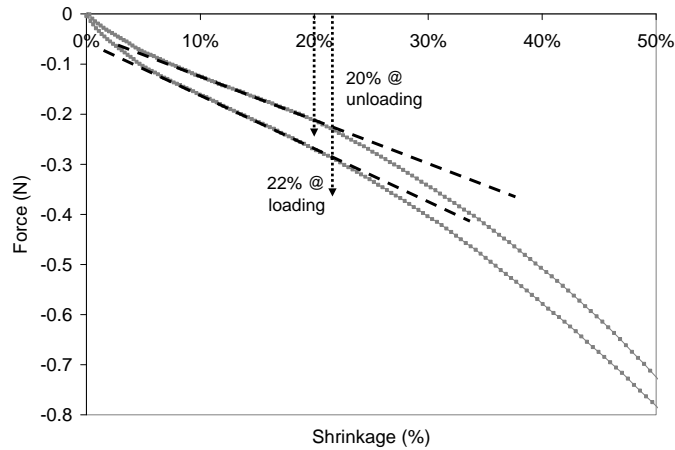
Figure 6-13: Sample data where curves deflect downward after NL; the actual shrinkage here is 24%.
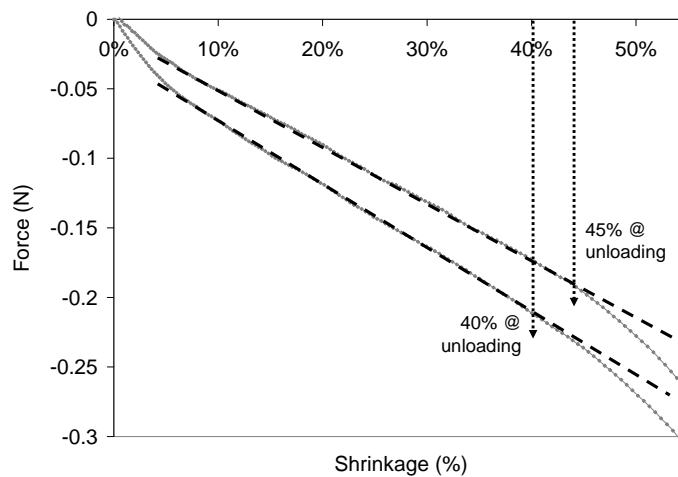
Figure 6-14: Sample data where curves deflect at a much later stage beyond NL; the actual shrinkage here is 17%.

It was found that the actual shrinkage did not generally lie between predictions made from the loading and unloading cycles. In fact, it was found to be closer to the prediction made from unloading data. This observation may be related to the viscoelastic nature of skin. At the start of a loading phase, skin tissue is typically under its own natural tension and may undergo simultaneous time and strain–dependent changes to dissipate some of the applied compressive strain energy. Therefore, the natural length may be miscalculated. During the unloading phase, the deflection point corresponding to the natural length is expected to be at where skin

(from a relaxed state) begins to tense and stretch back into the linear elastic region. Therefore, one would expect the latter case to be closer to the natural length of a harvested flap, and which was also observed experimentally.

Figure 6-15 shows the result of the predicted against actual shrinkage (in percentage), where prediction was made from the respective unloading curves. The given results were from the 3 anatomical sites (shoulder, abdomen and thigh). Ideally, all the data should lie on the y = x line, and any deviation from this line will indicate prediction error; this line is represented as the black solid line in Figure 6-15. The points between the black dashed lines have an absolute error of ±7.5% with the ideal black line; the points between the grey dash-dot lines have an absolute error of ±15% with the ideal black line. The tabulated results are given in the Appendix.
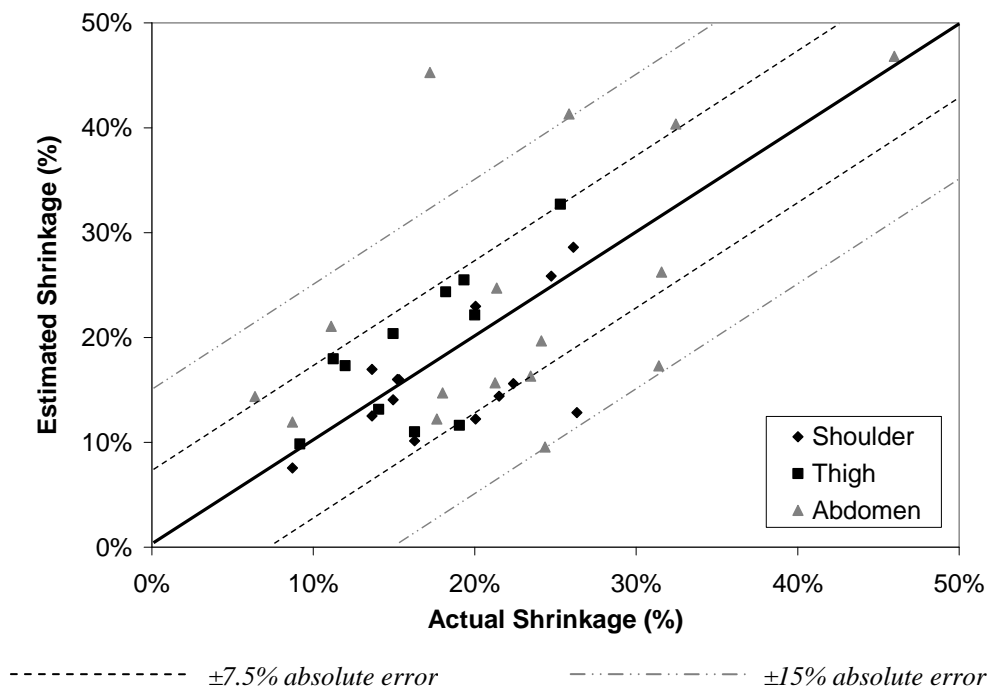
Figure 6-15: Scatter gram of predicted vs. actual shrinkage; black solid, black dashed and grey dash-dot lines have absolute errors of 0%, ±7.5% and ±15% respectively.

It was found that among the 41 sets of data analyzed, 40 of the predictions were made within an absolute error of 15% between the actual and estimated shrinkage. In most

predictions (35 out of 41 data sets, or 85%), the absolute errors were found to be within 7.5%. There was also no evidence of systematic under- or over-estimation observed, which suggested unbiased results. The average absolute error between actual and estimated shrinkage in all data was calculated to be 6.0%, with a standard deviation of 5.3%. There was only one case where shrinkage was over-estimated with an absolute error of 28%. This may be due to experimental error, or attributed to the structural property of this examined skin site, or may be a "case 3" (as explained in the proposed hypothesis section). It should be emphasized that such case has only been observed once. This also highlights the necessity to repeat the measurements.

A histogram plot of the absolute error is shown in Figure 6-16. The plot resembles a typical Gaussian distribution.
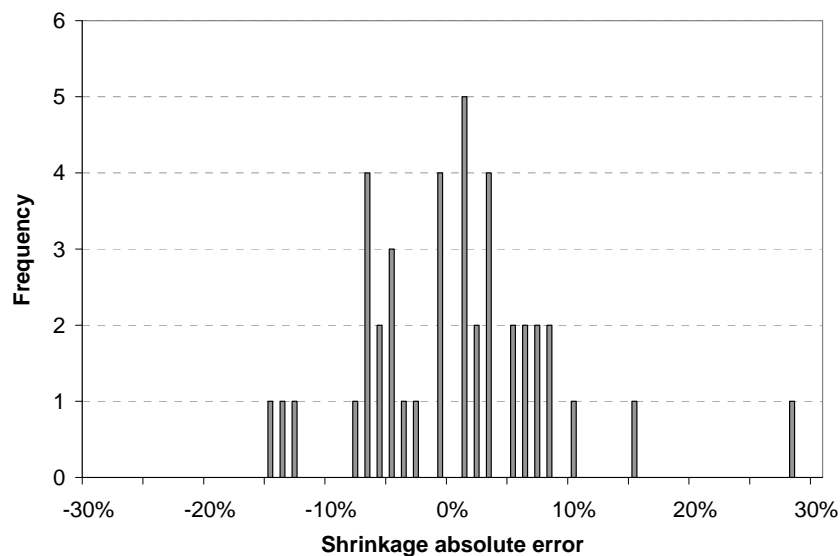
Figure 6-16: Histogram plot of the absolute error.

6.4.3. Animal experiments – Natural tension and elastic modulus

Figure 6-17 shows a sample force-displacement data. In this example, the natural tension measured is 11.3 N/m, given that the width of the extensometer's load cell pad is 12mm (refer back to Figure 3-5). Using a skin thickness of 1.0 mm, the elastic

modulus as given by equation (6-5) is 0.05 MPa. In general, it was found that the natural tension measured at the various skin sites and directions with respect to the Langer's line was of the order of 10 N/m, while the elastic modulus was between 0.01 and 0.1 MPa.

$$E = \frac{\sigma}{\varepsilon} \qquad \text{where } \sigma = \frac{T_N}{t \times w} \qquad (6\text{-}5)$$

where T_N = natural tension (0.135N),
  ε = strain (0.23),
  t = skin thickness (1 mm),
  w = extensometer pad width (12 mm).
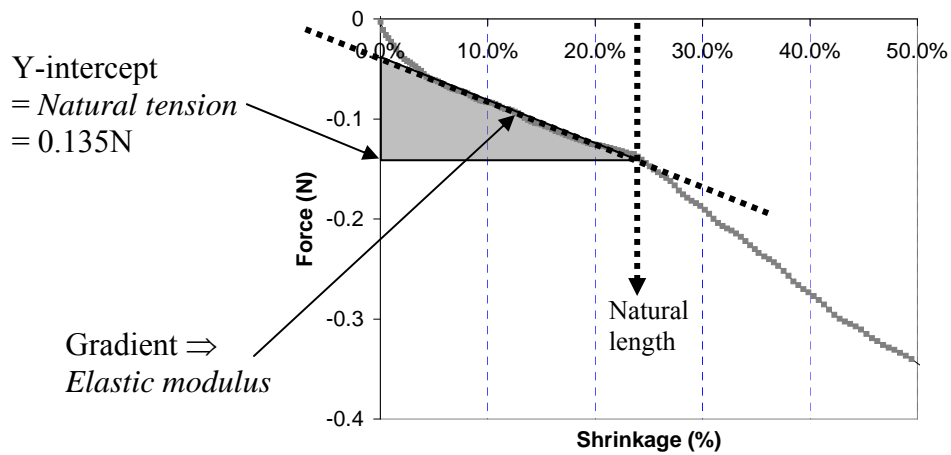
Figure 6-17: Deducing the natural tension and elastic modulus from the compressive force-displacement data (after determining the natural length).

6.5. Discussion

6.5.1. Shrinkage prediction

In the results from the experiments on pre-stretched rubber and pig skin, it was found that the compressive force-displacement data produced the trends that were described at the proposed hypothesis section in 6.2, i.e. a gradient deflection near the natural length. Therefore, this verified the hypothesis that the natural length may be deduced from the measured data.

In the rubber experiments, the proposed method produced results with an average absolute error of 1.7% between the actual and predicted shrinkages. This proof-of-concept study demonstrated that the method was capable of predicting the natural length of stretched rubber sheets with high accuracy. In the validation experiments on pigs, the method was shown to produce results with an average absolute error of 6%. This result was deemed clinically acceptable by the doctors involved in this study; the result may be close to what an experienced surgeon would estimate subjectively. Also, there is no observable correlation between the Langer's line and result accuracy.

It is expected that predictions on pig skin were poorer than on rubber sheets. As given in the Results Section (6.4.2) of the pig experiments, 6 of the 41 measurement predictions have absolute errors of more than 7.5% from the actual shrinkage; among them, one data significantly over-predicts the shrinkage by more than 15% absolute error. Therefore, the proposed method occasionally produces relatively larger errors. The challenges of non-invasive measurement of skin flap properties *in vivo* are numerous. Skin flap is a complex structure that is thick and multiply-layered, and the extensometer took measurement from the top skin surface. Despite the fact that the top skin layer has a dominant stiffness over the underlying fat layer (refer to Section 4.2), the contribution from the latter is not negligible. Furthermore, the flap does not slide on the fascia with zero friction. In addition, the stretching of the surrounding skin will still affect the forces measured by the extensometer, despite the use of a shield pad. Due to these physical constrains, the properties measured *in vivo* will certainly have errors, and this may explain why exact answers are difficult to obtain. The method can, however, be refined for greater accuracy, and this is the work of future research to be described at the final chapter.

6.5.2. Skin shrinkage observation

Even though there are references to the expansion behavior of skin flaps in literature (Stell, 1980, 1982; McGregor *et al*, 1970), only shrinkage was observed during this trial (refer to Figure 6-18). Furthermore, it was observed that there was no evidence that the minimum shrinkage have preferential orientation along the Langer's line. Nevertheless, it was noticed that circular planned excision produced an elliptical skin flap and the major axes of ellipse either lie along or orthogonal to the Langer's line. This observation further affirms the literature that states that a skin area has at least two axes of symmetries (Alexander *et al*, 1975, 1977; Lanir *et al*, 1974). Note that the ellipticity of a shrunken flap was validated by capturing an orthogonal image of the flap using a camera, followed by software fitting of an ellipse over the outline of the flap in the image; in all experiments, the outlines of fitted ellipses were found to follow the outlines of the shrunken flaps.
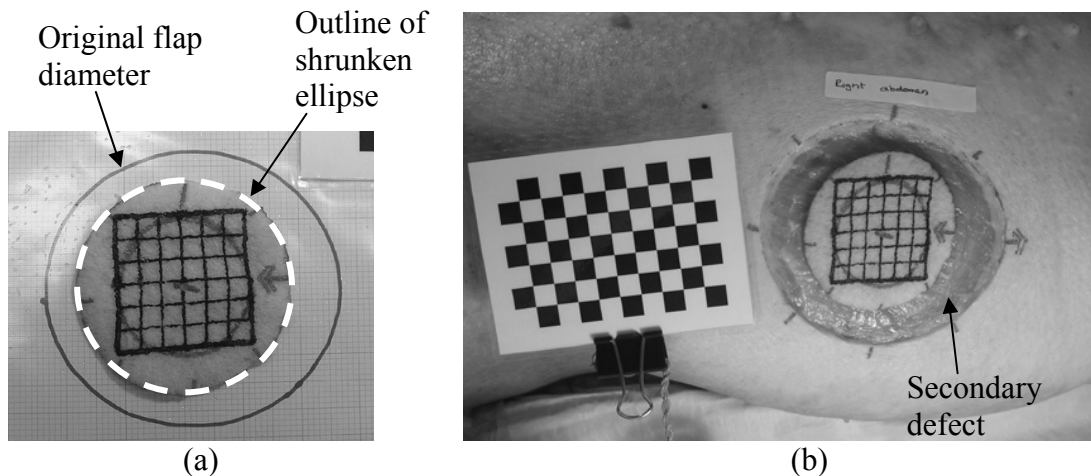
Figure 6-18: Photos of flap and secondary defect after harvest, showing (a) shrinkage of circular flap to an ellipse; (b) expansion of secondary defect.

It was thought that thickness of the skin flap may have some influence on the degree of shrinkage. However, linear regression coefficient values of 0.49 (abdomen), 0.04 (thigh), and 0.01 (shoulder) are inconclusive because they show no clear correlation

(see data in Figure 6-19, which shows poor linear fit between flap shrinkage and thickness at each test site).
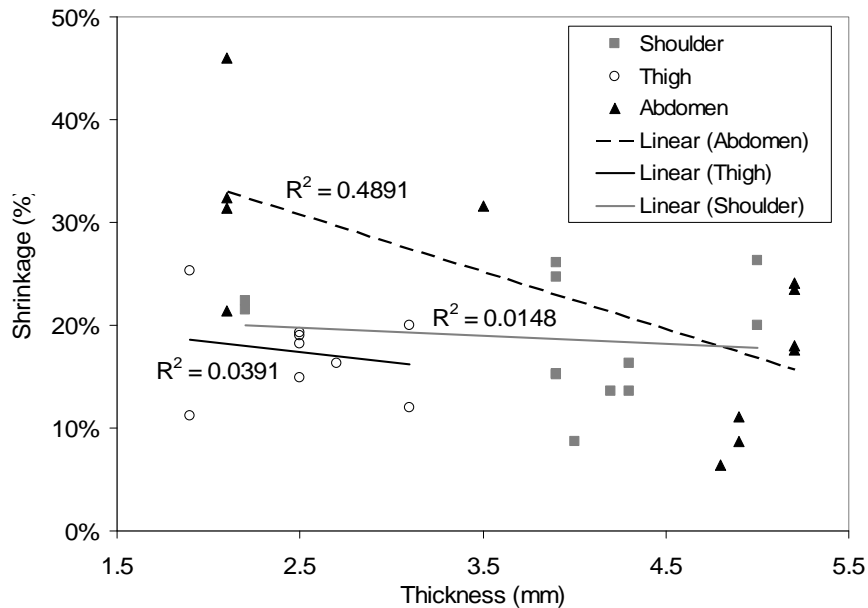
Figure 6-19: Data of flap shrinkage vs. flap thickness, where linear regression fitting is used to assess their relationship at each test site

6.5.3. Data analysis algorithm

The algorithm employed here utilized gradient analysis to locate the linear section in the data to predict the natural length. This method was chosen since it was straightforward and simple, thus ensuring that the algorithm procedure was not too sensitive or dependent on too many parameters. It was found experimentally that varying these algorithm parameters by ±15% did not affect the results significantly; an exception was the $p = 0.9$ value for the MATLAB® *CSAPS* spline function, where it was found that $p = 1.0$ gave too little smoothing. Thus, this finding indicated that the used algorithm was not too sensitive to the chosen parameters. Besides using gradient analysis to detect linear data, there are also other possible algorithms, such as Hough transform. The suitability of other methods can be explored in future work.

6.5.4. Direction of data deflection

In the proposed hypothesis (refer to Figure 6-1), the data is expected to deflect upward or downward near the natural length. Table 6-4 summarizes the number of data sets for each of the deflection directions and the mean thicknesses of the skin flaps at the corresponding anatomy sites. It was found that both deflection behaviors are present among the 41 data sets, and they are also present in each of the anatomy sites. In addition, there is no observable correlation between the direction of Langer's line and the deflection behavior.

Table 6-4: Site, skin thickness and number of data for each deflection direction

Deflection direction	Anatomy site	Mean thickness	Number of data
Deflect downward	Shoulder	4.3mm	7
	Thigh	2.7mm	4
	Abdomen	4.1mm	15
Deflect upward	Shoulder	3.3mm	7
	Thigh	2.4mm	7
	Abdomen	2.1mm	1

It can also be observed from the results that the data generally deflect upward for thinner flaps (below 3.3mm), and downward for thicker flaps (above 4.1mm). This observation may suggest that when the thicker flaps fold together, the folded subcutaneous tissues (which are in relatively larger amount) would press and squeeze together to build up forces faster with applied compressive strain, thus resulting in the downward deflection. In contrast, for thinner flaps in which there is less tissue, such event may take place at a greater applied compressive strain. Thinner flaps may relax or buckle up at the skin surface just beyond the natural length, thus the upward deflections are produced.

Among the downward deflection results, there are four data (at the thigh) where the flap is relatively thin at 2.7mm, but the curve did not deflect upward as expected. In

this case, there may be other factors affecting the forces during measurement, as discussed earlier about the complexity of *in vivo* skin measurement. It should also be noted that this happened to less than 10% of all the data.

Figure 6-20 shows the results of data which deflect downward. This belongs to "case 2" and "case 3" deflection type that was discussed at the proposed hypothesis in section 6.2.1; in "case 3", the shrinkage is over-estimated. As observed, there are several results which are over-estimated beyond an absolute error of 7.5%, and these may belong to the "case 3" type. In contrast, none of the results for the upward deflection data (or "case 1") is over-estimated by more than 7.5%. Figure 6-21 shows these upward deflection results.

±7.5% absolute error   ±15% absolute error
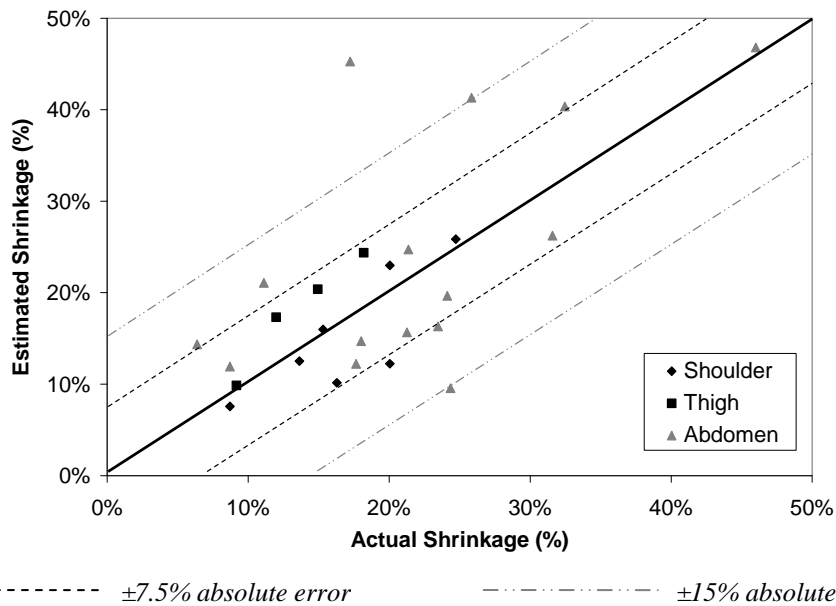
Figure 6-20: Scatter gram of predicted vs. actual shrinkage for results where data curve deflects downward ("case 2" and "case 3").
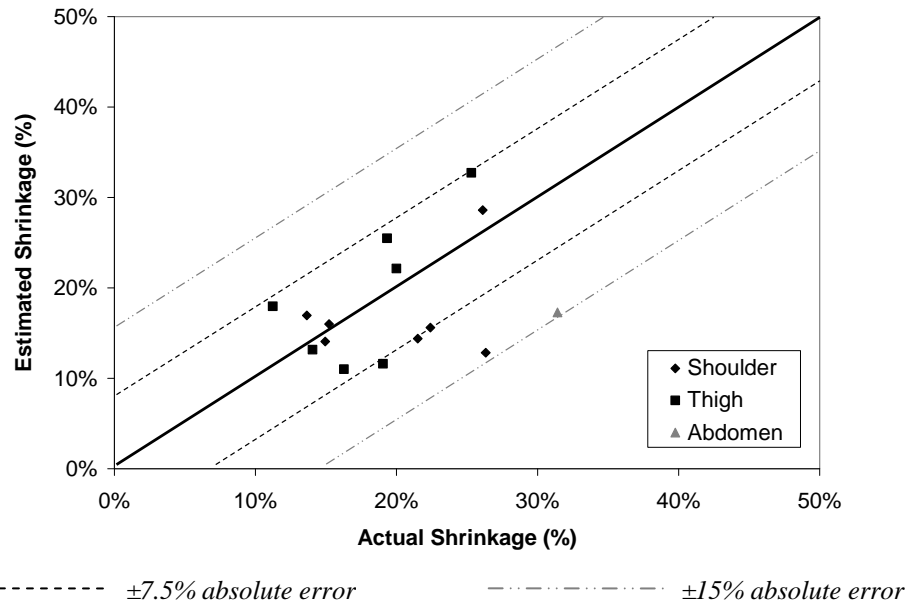
Figure 6-21: Scatter gram of predicted vs. actual shrinkage for results where data curve deflects upward ("case 1").

6.5.5. Natural tension and elastic modulus of skin

Various groups attempted to measure the natural tension and elastic modulus of skin *in vivo*. However, as discussed in the literature review, the techniques used were deemed to be inaccurate due to a variety of instrument design and measurement methodology problems. In this research work, the natural tensions measured *in vivo* for the rubber sheet experiments have an average precision of 88.5% from the actual values; the actual values were determined *in vitro*. For the elastic modulus, the measurement's average precision was 81.5%. Hence, this proof-of-concept trial demonstrated that the proposed method was capable of estimating the natural tension and elastic modulus of biaxially pre-tensioned rubber sheets with good accuracy.

In the animal experiments, the magnitude of natural tensions measured *in vivo* were of the order of 10 N/m, and this is of the same order of magnitude as the tensions measured by Alexander and Cook, and Diridollou (Alexander *et al*, 1977; Cook *et al*, 1975; Diridollou *et al*, 2000). The elastic modulus measured were between 0.01 and

0.1 MPa, and this range is also within range of the *in vivo* values given in literature (Diridollou *et al*, 2000). It was also noted that the elastic modulus found in literature ranged from 0.02 to 57 MPa, and so the values obtained in this study are at the lower end of the range. This was expected since it was discussed at the literature review at Section 2.4.1 that existing devices typically also measure unwanted peripheral forces (due to deformation of surrounding skin), thus resulting in higher measured values.

To verify the accuracy of the natural tension and elastic modulus found, skin flap samples were harvested after each *in vivo* measurement for *in vitro* testing on an Instron tensometer. This test involved pulling the shrunken skin flap samples back to their original pre-harvested length, and then determining the tension and elastic modulus from the resulting force-displacement data; these values were then compared with the *in vivo* ones. However, the validation tests were conducted unsuccessfully, as the results obtained from the tensometer were found to be inaccurate or inconsistent. The reasons for the test failure were deemed to be due to the following:

- A tensometer with grippers that tightened by screws was available at the site of the animal experiments. However, those grippers were found to cause skin sample slippage during pulling, and so the results obtained were inaccurate. A tensometer with pneumatic grippers was found to be most appropriate for testing skin samples, but it was unavailable at the test site.

- It was found that the hydration state of the skin flap should be kept the same pre- and post- harvest, so that the biomechanical properties of the samples do not change. If the samples were left exposed to the atmosphere after harvest and not tested immediately, then the loss of moisture would cause the tissue to stiffen. On the other hand, if the samples were hydrated by submergence in saline, they may

swell and become softer. Ideally, the skin samples should be tested at the tensometer *immediately* after harvest.

- The low force measurement condition and small size of the skin samples caused handling difficulties, including sample cutting, preparation and placement precision at the grippers.

Therefore, the accuracy of the *in vivo* results was not verified experimentally at this round of animal experiments; this will be the work of future research. However, this trial successfully showed proof-of-concept in rubber sheets, and that the results obtained in animals were within range of those values given in literature.

6.5.6. Explanation of initial curve

During the experiments, it was noticed that the majority of the measurements gave an unexpected small initial non-linear region near the origin (refer to region 1 in Figure 6-9). This curve, which was concave, generally ranged from 0% to 7% strain. It was also observed that on flatter skin regions, such as the abdomen, this curve was short (typically from 0% to 2% strain). In more curved regions such as the shoulder, this curve extended longer (typically to 7% strain). An example of the initial curve regions of an abdomen vs. a shoulder is shown in Figure 6-22, where the initial curve is almost non-existent at the abdomen; at the shoulder, this curve extends from 0% to 4% strain before becoming straight.
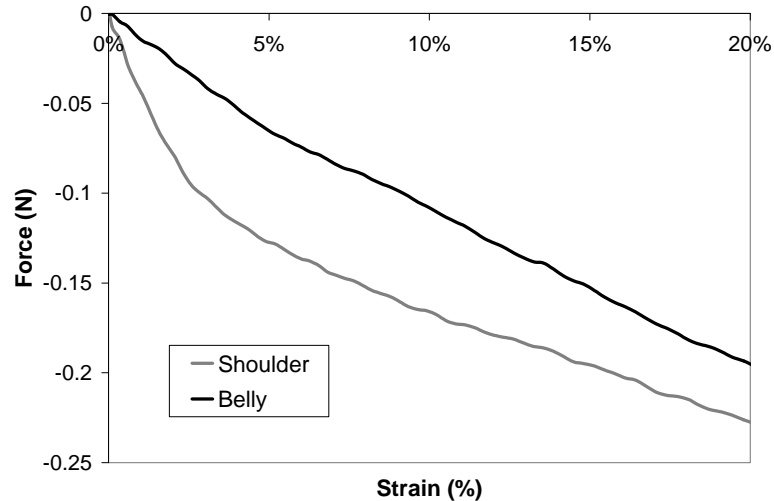
Figure 6-22: Zoomed in data showing the initial regions at an abdomen and shoulder region.

Hence, it was possible that the curvature of the studied site may be partly responsible for the unexpected results. As illustrated in Figure 6-23, when the extensometer was placed on a curved region, the pads entrapped more tissue than the distance between them. This excess tissue may have produced additional forces that resisted the initial movements of the pads, hence explaining the initial concave nature of the curve.
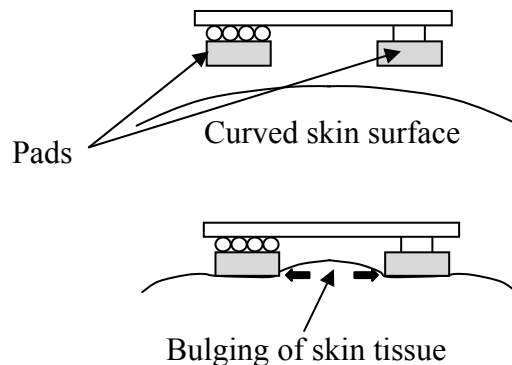
Figure 6-23: Illustration of unavoidable bulging of tissue in between the pads at a curved site.

To prove this proposition, a set of experiment was devised and conducted on the inner thigh of a volunteer. In the first measurement, a small weight of 100g was added to the extensometer so that the pads pressed down on the skin with greater pressure than usual. In this configuration, observed bulging between the pads was apparent. The

second measurement was carried out under the normal condition, whereby the device rested on the skin under its own weight of 2.45N. In the last measurement, the extensometer was slightly lifted up from the skin surface to make skin tissue between the pads to be flat. In all experiments, the extensometer was rigidly held in their respective positions by the articulated arm. The result is shown in Figure 6-24.
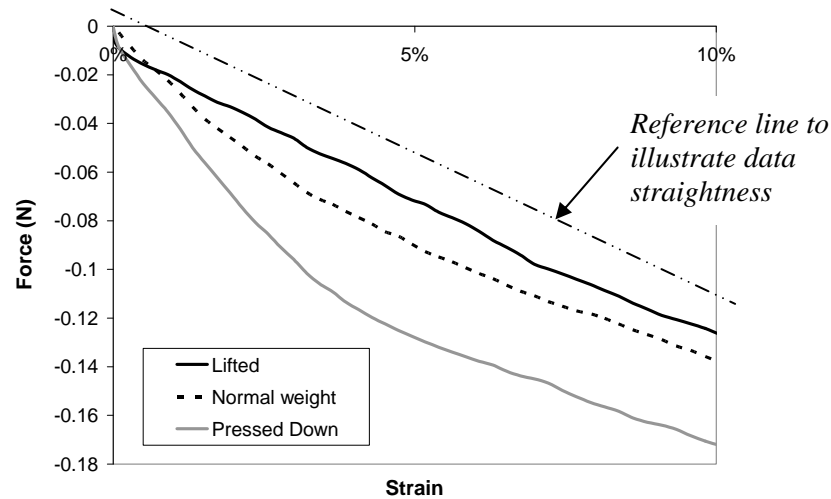
Figure 6-24: Data showing the trend of the initial region when the extensometer is (i) pressed down, (ii) resting under its normal weight, and (iii) lifted.

As expected, the initial curved region was pronounced when the extensometer was pressed down, whilst the curve disappeared when the device was lifted up. This observation led to the conclusion that the initial curve was partly due to the bulging of skin between the pads. Although lifting the extensometer removed the unexpected curved region, it may create additional downward pulling forces that may affect the force measurement, and subsequently the accuracy of the shrinkage estimation.

Another possible cause may be static friction between the skin layers, whereby the cohesive forces must be overcome before the skin layers can slide smoothly. Furthermore, yet another explanation may be that the skin on the body was at the second phase of the stress-strain state instead of the first (refer back to Figure 2-5). In

the second phase, the stress-strain behavior is curved upward and therefore, this curve region may be captured during measurement. However, this possibility was ruled out after *in vitro* stress-strain measurements of harvested pig skin, which reaffirmed that the skin on the body was within the first linear phase.

In order to reduce the size of the initial curve region in the data, the bulging skin between the device pads can be minimized. This can simply be achieved by constructing a lighter device, such as by using fewer and lighter components.

6.6. **Summary**

In conclusion, one can say this proposed method of non-invasive analysis of the compressive force-displacement data measured using a custom designed extensometer can quantitatively estimate skin flap shrinkage, natural tension and Young's modulus of elasticity along the measurement direction. The method was first tested on rubber sheets and produced results with high accuracy. For flap shrinkage estimation, the validation experiments on piglets have been shown to produce results with an average absolute error of 6%, which was considered clinically acceptable by the doctors involved in the study.

CHAPTER 7
SKIN FLAP SURGICAL PLANNER

7.1. <u>Introduction</u>

The shrinkage prediction method described at the previous chapter takes measurement at a small local area of the skin (25mm length of skin between the extensometer pads). This area is small compared to the size of an actual flap during a surgery. Therefore, one concern is whether the shrinkage estimated by the localized measurement can represent the shrinkage of a much larger flap. This chapter will address this issue. In addition, the described method only estimates shrinkage along the device's measurement direction, and not the overall shrinkage in *all* directions. This chapter will present an integrated methodology that allows surgeons to predict the overall shrinkage of a large flap easily.

7.2. <u>Method – shrinkage across flap</u>

In order to identify and establish the relationship between shrinkage of small flaps (localized) and that of larger flaps, pig skin trials were undertaken. Prior to the experiment, two piglets (six months old) were freshly slaughtered at the animal facility according to strict university ethics regulations. Three specific test sites (abdomen, upper thigh and upper shoulder) were chosen on each animal; these sites were the same anatomical sites as the shrinkage prediction experiments in the previous chapter. Five concentric circles of diameters 120, 100, 80, 50 and 25 mm are drawn by marker on the pig skin at each test site, as shown in Figure 7-1. The smallest diameter of 25 mm was the same size as the measurement region between the extensometer

pads; circles larger than 120 mm were not drawn because these larger diameters would go beyond the relatively flat regions chosen.

Figure 7-1: Impression of concentric circles of 120, 100, 80, 50 and 25 mm diameters, drawn prior to flap harvest.

Circular flaps of diameter 120mm were then harvested to determine the associated shrinkage along and perpendicular to the Langer's line; the Langer's line was determined invasively nearby (refer to method described in section 4.6.1), as well as interpreted from the axes of the shrunken ellipse after flap harvest. The flaps were harvested at the fascia-subcutaneous junction, and placed in a tray that contained a thin layer of saline solution to stop the evaporation of tissue fluid, and to prevent the underlying fat layer from sticking to the tray surface. Subsequently, for each large flap, smaller concentric flaps of diameters 100, 80, 50 and 25mm were cut out from the marked outlines progressively to determine the respective shrinkages.

The Langer's lines play a role in affecting shrinkage behavior. In a large flap where the Langer's lines vary significantly across the flap, the shrinkage behavior as well as the uniaxial biomechanical properties may not be uniform across the flap. Hence, the shrinkage behavior at any one localized position may not represent the shrinkage behavior somewhere else on the flap. To find out the directional influence of the Langer's lines, their directions at various positions across each tested flaps were

determined. This was done by finding the direction of the Langer's line at the corresponding anatomical sites on the *opposite* side of the animals' bodies; the Langer's lines were estimated invasively.

7.3. <u>Results</u>

It was found that the Langer's line direction across each measured flap varied only within 20 degrees of each other. Therefore, it can be concluded that the directional influence of the shrinkage behavior was relatively uniform across the flaps.

The results obtained for the experiments on shrinkage of concentric flaps for both animals are given in Figure 7-2. It can be seen that the shrinkages across the various diameters of each flap do not differ much. The mean and standard deviation of the shrinkage across the concentric diameters for each of the six flaps are shown at Table 7-1. It was found that the overall average standard deviation of the shrinkage across the various concentric diameters was only 0.8%, which is small.
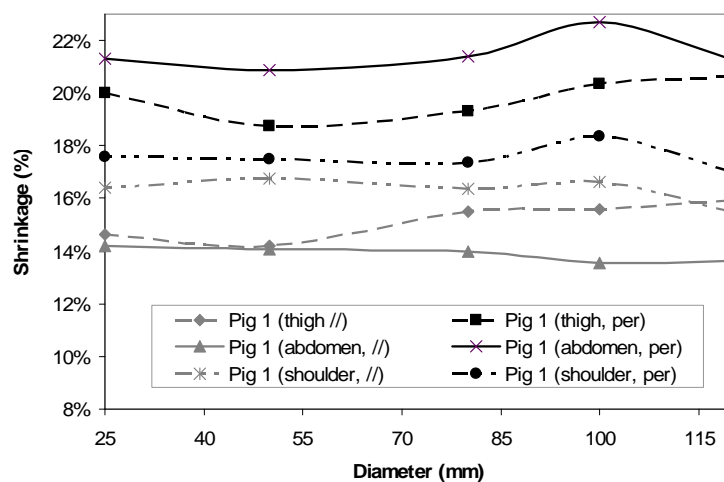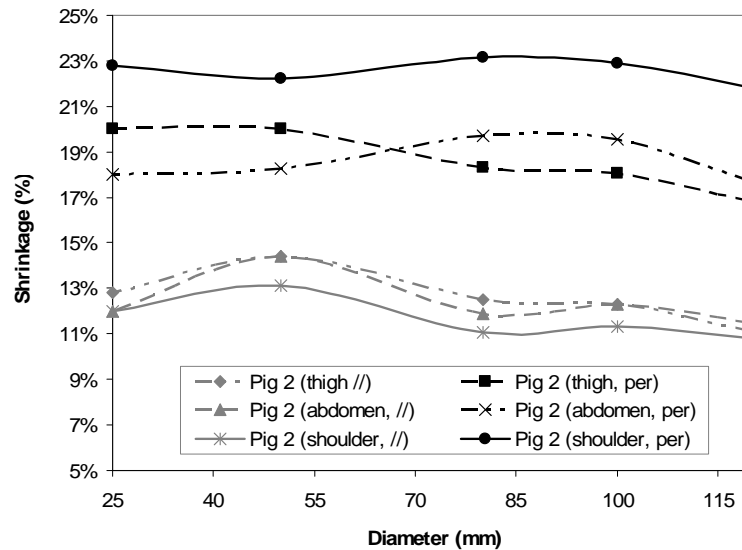
Figure 7-2: Percentage shrinkage plotted against flap diameter at parallel and perpendicular to the Langer's line for pigs 1 and 2.

Table 7-1: Result of flap shrinkage across the concentric diameters, at parallel and perpendicular to the Langer's line (LL)

Site and direction	Mean shrinkage	Standard Deviation
Pig 1 (thigh), parallel LL	15.2%	0.7%
Pig 1 (thigh), perpendicular LL	19.8%	0.8%
Pig 1 (abdomen), parallel LL	13.9%	0.3%
Pig 1 (abdomen), perpendicular LL	21.5%	0.7%
Pig 1 (shoulder), parallel LL	16.3%	0.5%
Pig 1 (shoulder), perpendicular LL	17.6%	0.5%
Pig 2 (thigh), parallel LL	12.6%	1.2%
Pig 2 (thigh), perpendicular LL	18.6%	1.4%
Pig 2 (abdomen), parallel LL	12.4%	1.1%
Pig 2 (abdomen), perpendicular LL	18.6%	0.9%
Pig 2 (shoulder), parallel LL	11.7%	0.9%
Pig 2 (shoulder), perpendicular LL	22.6%	0.5%
Average standard deviation		0.8%

7.4. Discussion

7.4.1. Shrinkage prediction based on localized measurement

The results showed that the shrinkage variation across the flaps was minimal. Hence, this trial demonstrated that the localized shrinkage estimated by the device was able to represent the shrinkage of a much larger area up to a diameter of 120mm, which was the dimension limit set in this trial. It should be noted that this assumption may only

apply to skin flap which has the Langer's line generally in the same direction across the flap. This is usually the case at large flatter skin surfaces, such as the human abdomen region. For a flap in which the Langer's line varies greatly across, the shrinkage across the flap may be non-uniform and so the shrinkage behavior may not be well represented at the midpoint.

7.4.2. Method of predicting shrinkage of circular flap

The result obtained from this study and reports in literature show that circular skin flap shrinks to an elliptical shape or remain circular after harvest (Reihsner *et al*, 1995; Langer, 1978; Thacker *et al*, 1977). Either way, since it will possess at least two axes of symmetries, it is then possible to model the shrinkage behavior of a circular flap prior to surgery by simply estimating the shrinkage in multiple different directions and then fitting an ellipse onto the result. This ellipse outlines the shrunken dimension and orientation of a circular flap, up to a diameter of 120mm. Furthermore, the major axis of the ellipse corresponds to the direction of the Langer's line, and so this is another method to estimate the Langer's line direction non-invasively; refer to Chapter 5 for the preferred method.

In the simplest case, the flap shrinkage can be estimated at three directions 60 degrees apart (refer to Figure 7-3). Then an ellipse can be fitted onto the result. The mathematical derivation is given as follows.
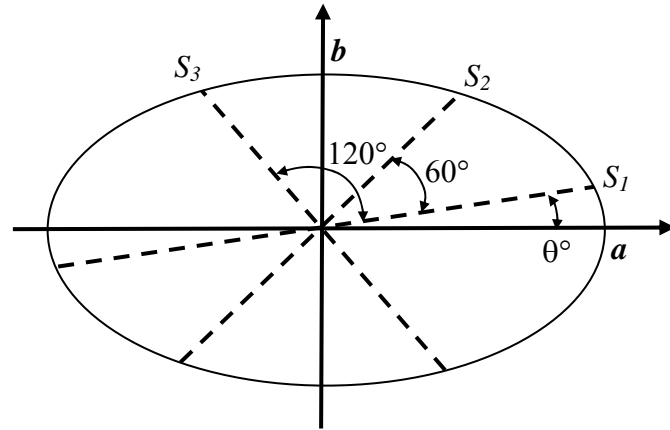
Figure 7-3: An illustration of three data points (S_1, S_2 and S_3) on the ellipse, where they are separated by 60°.

The equation of an ellipse in polar coordinates is given by:

$$\frac{S_i^2 \cos^2 \theta}{a^2} + \frac{S_i^2 \sin^2 \theta}{b^2} = 1 \qquad (7\text{-}1)$$

where S_i = data point on the ellipse (predicted shrinkage value),
    a = major axis,
    b = minor axis,
    θ = angle between point S_i and the major axis.

By choosing a suitable sampling angle interval, such as 60°, one can ensure that the three data points cover more than one quadrant of the ellipse for maximum fitting accuracy. The set of equations in (7-2) can be obtained by substituting the predicted shrinkage values S_1, S_2 and S_3 into equation (7-1). A numerical solution of the three unknowns (a, b and θ) can then be computed that will satisfy all three equations.

$$\begin{aligned}
S_1^2 a^2 \sin^2 \theta + S_1^2 b^2 \cos^2 \theta &= a^2 b^2 \\
S_2^2 a^2 \sin^2 (\theta + \alpha) + S_2^2 b^2 \cos^2 (\theta + \alpha) &= a^2 b^2 \\
S_3^2 a^2 \sin^2 (\theta + 2\alpha) + S_3^2 b^2 \cos^2 (\theta + 2\alpha) &= a^2 b^2
\end{aligned} \qquad (7\text{-}2)$$

where S_1, S_2, S_3 = data points,
    α = angle of sampling interval,
    θ = angle between data point S_1 and the major axis.

If the direction of the Langer's line is estimated using the method described in Chapter 1, the fitting accuracy can be maximized by choosing S_1 to be approximately along the Langer's line (so that θ is small), and then choosing a 45° sampling interval. This ensures that the three data points will cover much of one quadrant of an ellipse.

The ellipse outlines the final shape and size of a circular flap, up to a diameter of 120mm; larger diameter limits may be possible, though the animal trial only experimented with flaps up to 120mm diameter. For an irregularly shaped flap up to a maximum span of 120mm, it can be assumed to shrink geometrically in the same manner as a circular flap, and so the final shape and size can be computed accordingly. On the other hand, for a large flap with non-uniform Langer's line direction such that the biomechanical properties across the flap may be non-uniform, more complex geometric analysis and extensometer measurements at multiple points may be needed. This would be the work of further research.

7.5. **Summary**

The extensometer measurement and data analysis estimate shrinkage at a small localized region of the skin. It has been demonstrated in this chapter that the localized predicted shrinkage can represent that of a larger flap that has reasonably uniform Langer's line directions. As a result of this finding, it is then possible to estimate the shrinkage behavior of a large flap using an elliptical model. This is achieved by estimating the flap shrinkage in at least 3 different directions and then fitting the results onto an ellipse.

Thus, an integrated method has been described which combines extensometer measurements in multiple directions followed by data analysis to estimate skin flap shrinkage. This method potentially provides surgeons an objective and reliable way to plan a flap transplant surgery prior to the actual operation.

CHAPTER 8
CONCLUSIONS

8.1. <u>Introduction</u>

The overall goal of this project was to develop a surgical planning methodology to aid the prediction of skin flap shrinkage prior or during a flap transplant surgery. There were three objectives defined for this thesis work. The first objective was to develop a device to measure the *true* uniaxial biomechanical properties of skin *in vivo* non-invasively. The second and third objectives were to develop a set of methods that integrates with the device to measure the relevant skin properties, including the Langer's line direction, natural tension, Young's modulus of elasticity, and most importantly, flap shrinkage. This chapter concludes the thesis, and discusses the contributions made and the recommendations for future work.

8.2. <u>Contributions</u>

8.2.1. New measurement device

The literature review indicated that for uniaxial measurements, existing non-invasive devices are unable to measure the *true* uniaxial biomechanical properties accurately. In this research, a new device in the form of an extensometer was developed. This device used a shield pad that has been demonstrated by FEM simulation, rubber sheets and animal (pig) experiments to be effective in removing peripheral forces due to stretching of surrounding skin during measurement, thus obtaining biomechanical properties that were significantly closer to the actual *in vitro* ones. A model was also developed to model residual peripheral forces during the shield pad device

measurement, and has been shown in rubber sheets to be effective in bringing the measured data even closer to the *in vitro* ones. Aside from the shield pad, the new device also incorporated a standardization protocol into its design and operation. The parameters that were standardized include the pad dimensions, their initial separation, measurement strain rate, device contact pressure on the skin, and means of holding the device during measurement. This standardization was designed to enable reliable and consistent results to be obtained.

This new device, which has been patented and published, will allow the future study of skin biomechanics, especially directionally dependent properties, to be conducted more accurately.

8.2.2. New method to estimate direction of Langer's line

Stark observed that the terminal stiffness of skin in various directions exhibited periodicity when plotted (Stark, 1977), although the data points did not always conform to a regular geometrical form, such as an ellipse. His work was revisited in this research work, and it was found that the terminal stiffness did fit an ellipse in verification experiments done on soft leather, pig and human skin. It was deemed that Stark's result did not fit an ellipse because the skin may not have been stretched beyond the 2nd phase (of the stress-strain curve) in some instances; hence, the gradient at the 3rd phase was computed with error. It was thus established that terminal stiffness can be approximated to be orthotropic.

The new observation led to the development of a non-invasive *in vivo* method to predict the direction of the Langer's line. This method simply involved measuring the

force-extension data of skin at three directions using the extensometer, and fitting the computed terminal stiffness onto an ellipse; the major axis of the ellipse coincides with the Langer's line. Using the terminal stiffness is more reliable than other properties such as limit strain because terminal stiffness is related to the orientation of the collagen network, which is a material constant, whereas the limit strain may vary according to external factors. In verification experiments on animals, the precision is found to be within 4° of the actual direction, thus demonstrating the high accuracy of this method. In this research, accurate determination of the Langer's line (or lines of tension) is useful. Firstly, it can be used to estimate the general shape and direction of skin flap shrinkage. Also, the Langer's line coincides with the principal stress axis of a flap, which is needed for finite element analysis to model flap shrinkage; this is a parallel study to this thesis work (Jeyapalina and Lim, 2005).

The biomechanical properties of skin are often investigated during clinical trials, for example to assess correlations between diseased/damaged and healthy skin tissues. Often, directional differences of skin are overlooked during the planning and evaluation of these experiments. This research has demonstrated the importance of directional variations in relation to the structural make up of skin. Therefore, it should be stressed that when studying the biomechanical properties of skin, it is essential to design experiments to minimize variation within the results by considering the directional variations.

8.2.3. New method to estimate natural tension and elastic modulus

There are numerous works done to estimate the natural tension of skin (Alexander *et al*, 1977; Cook *et al*, 1975; Emmanuelle *et al*, 2007; Diridollou *et al*, 2000), but each

had shortcomings, as described in the literature review in Chapter 2. In this research work, a new method was developed to estimate the natural tension and elastic modulus of skin. This method involved measuring the compressive force-displacement profile of skin using the extensometer, and extracting the answers from the data after the natural length was determined. In the experiments on pre-tensioned rubber sheets, the proposed method has been shown to be accurate in estimating the natural tension and elastic modulus. In the experiments on pig skin, the results obtained have been shown to be within the values stated in literature. Unlike the rubber sheet experiments, the results from the pig study were not verified (by comparing with the data from *in vitro* measurements), and this will be the work of future research; in fact, based on the literature review, animal experiments by other research groups were also not verified by any *in vitro* means.

Accurate measurement of the natural tension and elastic modulus is important for finite element modeling, which is a project that is done in parallel to this work (Jeyapalina and Lim, 2005). The result from a modeling simulation can be used to complement the methodologies presented in this thesis. Furthermore, having an accurate technique to measure natural tension is useful in the study of skin biomechanics. Most biomechanics research on skin today revolves around finding the relationship between skin elasticity and physiological/pathological characteristics, such as healthy vs. diseased or damaged tissues, wound healing, aging, gender, and others. Thus, it will be interesting to study the role of natural tension as well.

8.2.4. New method to predict skin flap shrinkage

A method was developed to predict the shrinkage of skin flap (along the measurement direction) by analyzing the compressive force-displacement data measured using the extensometer. To the best of our knowledge, there is no existing work done in this area. Proof-of-concept studies on pre-stretched rubber sheets produced highly accurate results of average 1.7% absolute error between the actual and predicted shrinkages, while validation studies on animal skin produced results of average 6% absolute error. An integrated technique was also developed to predict the entire shrinkage behavior of a large flap with relatively uniform Langer's line direction. This involved three extensometer measurements followed by fitting the analyzed results into an elliptical model. The technique was applicable for flaps up to 120mm in span; flaps of larger size were not experimented.

The demonstrated accuracy of shrinkage prediction may be close to what an experienced surgeon would estimate subjectively, thus indicating the potential usefulness of this method as a clinical tool for training or surgery. With additional understanding, animal and human trials, and computerized measurement, this method may be simplified further in order for surgeons to plan the size and shape of a donor flap effectively before surgery. This would not only improve the quality of the surgery, but would also give surgeons more valuable stress-free time for planning their surgical procedures.

8.3. Recommendations for future work

During the research work, several limitations and shortcomings were identified. The areas of improvements proposed to address them are discussed as follows.

8.3.1. Device design improvement

Several design issues emerged during device testing. Firstly, the weight of the device was found to cause the skin between the pads to bulge, thus contributing to the initial curve in the force-displacement data (refer to Section 6.5.5). To reduce this problem, a lighter device can be designed, such as by using smaller and lighter components. Secondly, it is deemed that the current design in which the pads are offset to one side of the device can be improved so that the weight is more evenly distributed about all the pads. A new design using a pulley-belt mechanism is proposed, so that the pads can be positioned closer to the center of mass of the device (see Figure 8-1).
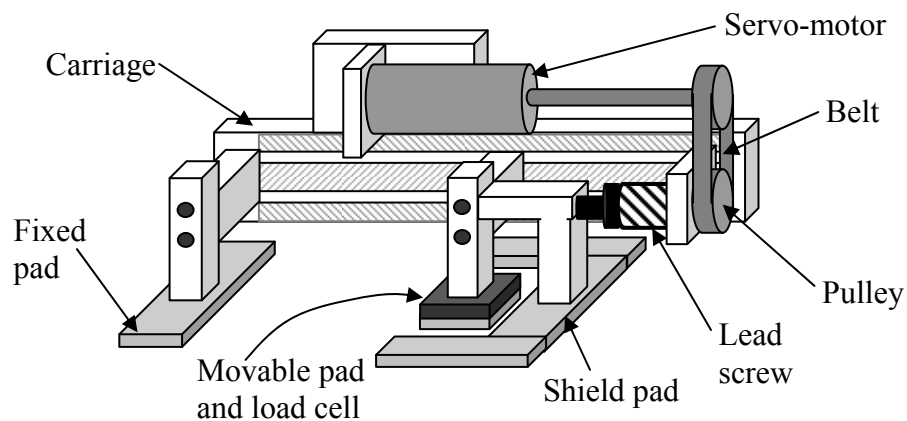
Figure 8-1: Schematic drawing of improved extensometer design.
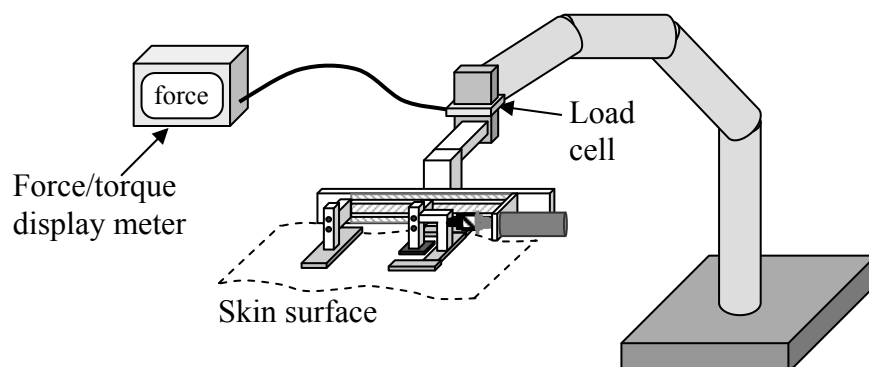
Figure 8-2: Schematic drawing of new articulated arm attachment.

As part of the standardization procedure, the current design utilized a linear sliding mechanism at the articulated arm to ensure the extensometer pressed onto the skin with a standard weight (refer to Section 3.3.4). The limitation of this design was that measurements must be done with the device at a horizontal position. To improve versatility so that measurements can be done in other positions, a pressure transducer can replace the slide attachment to ensure a constant pressure (see Figure 8-2). The device's position should be carefully adjusted prior to measurement such that the extensometer sits on the skin surface with almost zero pressure.

8.3.2. Data analysis algorithm

The algorithm to identify the natural length of skin used simple gradient analysis to locate linear sections in the measured data (refer to Section 6.2.3). Other methods of analysis can also be explored, such as Hough transform.

8.3.3. Verify natural tension and elastic modulus

In Section 6.2.2, a method of estimating the natural tension and Young's modulus of elasticity is described. The accuracy of this method was validated for the rubber experiments using *in vitro* tests, but the same validation test was not conducted successfully in the animal trials. The reasons were due to difficulties encountered in handling and gripping the small skin samples at the screw-type clamps of the available Instron tensometer, and keeping the tissue hydration state constant. Therefore, future work will include finding more effective means of conducting the *in vitro* tests. One such improvement is to have a tensometer (with pneumatic grippers) in the same room as the pig experiment so that the *in vitro* measurements can be conducted immediately after harvest. This ensures that the hydration state is constant.

8.3.4. Human and animal trials

Results obtained from animal experiments cannot be applied completely to the human patient (Kenedi *et al*, 1975). Thus, if the method is deem feasible and accurate after further animal trial, the next stage will be the human clinical trials.

8.3.5. Patient-shrinkage database

At the animal experiments, 15% of the data have absolute errors of more than 7.5% from the actual shrinkage, and this is not ideal. The shrinkage prediction method can be refined for greater accuracy, such as implementing the improvements suggested above. Another suggested method is to *cross check* the predicted results against other methods of shrinkage prediction. One such method already described is finite element analysis to model flap shrinkage.

Another cross check method proposed is the use of database analysis. Presently, surgeons plan the flap transplant from experience. In general, they based their judgment of the flap shrinkage on physiological factors such as age, gender, body mass index, location of the donor site, and manual tactile pinch test on the patient's skin (to estimate elasticity). Experienced surgeons can usually give a reasonably good estimate of the shrinkage; junior surgeons, on the other hand, need adequate training and experience to achieve the same success. This observation suggests that it is then feasible to build a clinical database of patients' physiological information, and correlate that to the shrinkage observed during surgery; these data can be collected in a clinical trial. The manual pinch test presently used to estimate skin elasticity can be replaced by an objective extensometer measurement. Once built and studied, this

database can be used to produce statistical predictions of the expected flap shrinkages by inputting the relevant patient data. The result can then be used to complement the surgical planning methodology presented in this thesis. To the best of our knowledge, no study such as this has been embarked.

8.4. <u>Summary</u>

The work presented in this thesis is part of a large project to develop an integrated skin flap surgical planner. This work involved the development of instrumentation and measurement methodologies to aid the prediction of skin flap shrinkage, and the ideas presented have been verified by actual experiments. Other parts of the project involved finite element modeling, clinical database collection, optical imaging, and computer graphical visualization. During the extensive literature survey, no existing work to develop such surgical planner has been found. Thus, it is believed that the research done in this thesis has moved this goal forward. In the context of developing a clinically approved surgical planner to be used in hospitals, the work done so far is considered preliminary as the critical human clinical trials is yet to begin.

APPENDIX

A1. <u>Introduction</u>

This section includes information of the research work which is not described in detail in the main chapters so as to facilitate reading. These information include experimental data, details of experimental set up, and calculation examples.

A2. <u>Load cell calibration for extensometer</u>

Section 3.3 refers to the calibration of the load cell on the extensometer during device development. The load cell (refer to Figure 3-8) was connected to a strain gauge amplifier, and the voltage changes with respect to the force measured were read from a computer using a data acquisition card. During the load cell calibration process, the relationship between voltage and force measured using this system was determined. The calibration process was performed by hanging standard weights (known) onto the load cell and recording the voltage read-out with respect to the weight (refer to Figure A-1). This calibration process was conducted in both directions along the measurement axis of the load cell.
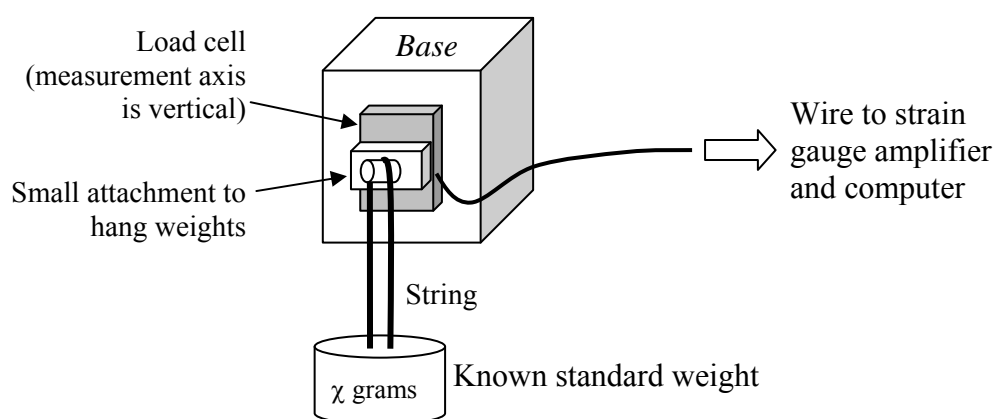
Figure A-1: Illustration of load cell calibration set up

It was found that the voltage had a linear relationship with respect to the weight in this system (refer to the data in Figure A-2). The formula for this relationship was then input into the computer program so that the computer would directly compute the force measured by the load cell during measurement.
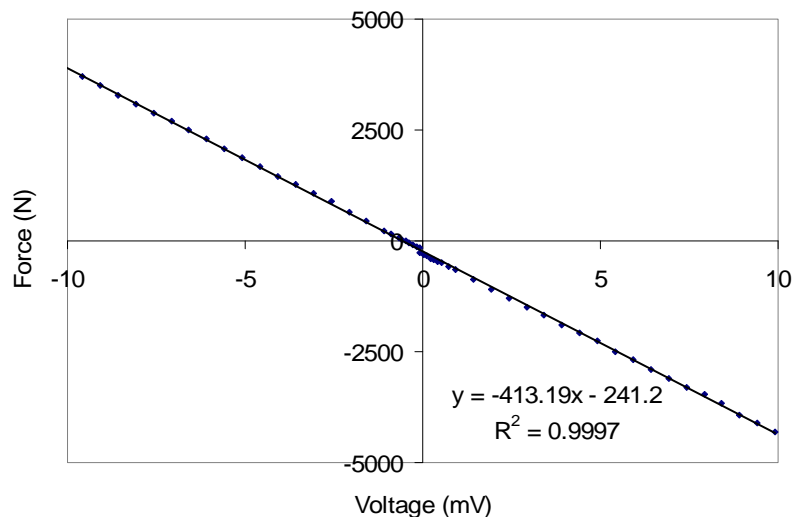
Figure A-2: Calibration data showing force loaded vs. voltage

A3. **Modeling of residual peripheral forces**

Section 3.4.2 describes the modeling of residual peripheral forces $F_{peripheral}$ that are present during extensometer measurement. In this model, the total force experienced by the extensometer's load cell is given by equation (3-3), where $\pm\alpha$ represents the coverage angle of $F_{peripheral}$. To determine the influence of the coverage angle in this model, the shield-pad data (compensated for $F_{peripheral}$) for the various values of α were compared against the *in vitro* data of the rubber sheet experiment, as given in section 3.6.3; ideally, the compensated data should match closely with the *in vitro* data. The results for both the yellow and grey theraband experiments are summarized in the following table, where the errors (mean square difference) of the $F_{peripheral}$ compensated data against the *in vitro* data are computed for the various coverage angles α.

Table A-1: Errors of $F_{peripheral}$ compensated data against *in vitro* data for various coverage angles $\pm\alpha$

Coverage angle α	Error [N^2] (mean square difference)	
	Yellow theraband experiment	Grey theraband experiment
30°	0.012872	0.229678
45°	0.007195	0.010222
60°	0.031235	0.054659
75°	0.045961	0.104782
90°	0.048378	0.113689

From the results, it was determined empirically that $\alpha = 45°$ produced better results than other angles considered. Moreover, 45° is a reasonable value, and it is unlikely that the range of angles will cover as far as the entire 90°.

A4. **Computation of terminal stiffness**

Section 5.3.3 describes a method of estimating the Langer's line direction from the terminal stiffness of the tensile data measured in 3 directions. The definition of terminal stiffness is described in Figure 2-6 as the slope of the terminal region (third phase, linear portion) of the tensile data.

Figure A-3: Sample data illustrating the computation of terminal stiffness from the slopes of the tensile data

An example of the computation of the terminal stiffness is shown in Figure A-3. The terminal region of one set of data is first identified, and then a line is fitted over those data using linear regression. The slope of the fitted line is then the value of the terminal stiffness. In the leftmost curve in the figure, the terminal stiffness is calculated to be 2.9744 N/mm. The R-squared value of each linear fit is also computed to ensure that the value is at least 0.99 for a good fit.
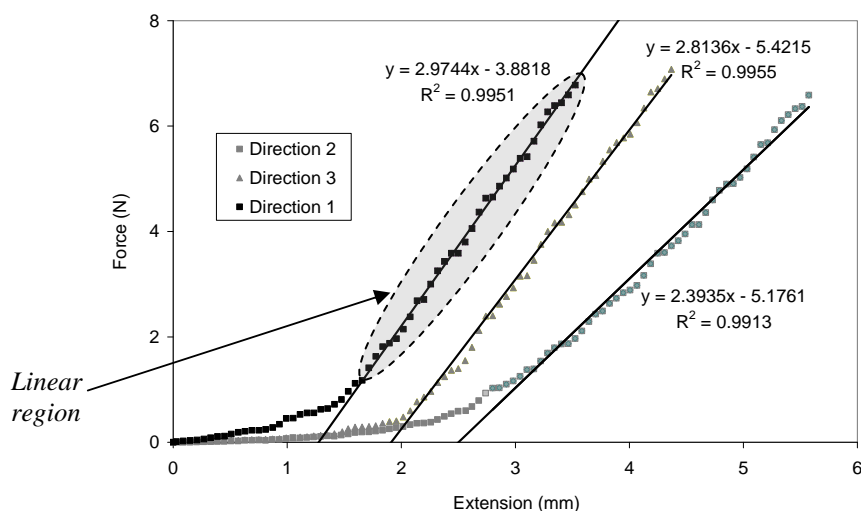
A5. Results of shrinkage prediction in animal experiments

Section 6.4.2 describes the outcome of the animal experiments to predict flap shrinkage, where the results of the predicted against actual shrinkage is shown graphically in Figure 6-15. For the purpose of reference, a table that shows the numerical results of all 41 sets of measurements is given as follows.

Table A-2: Results of predicted against actual shrinkage of animal experiments. Note that "LL" represents Langer's line.

Experiment setting	Actual Shrinkage	Predicted shrinkage	Absolute error
Shoulder			
Pig 1 – Left side, along LL	20.05%	22.98%	2.93%
Pig 1 – Left side, perpendicular LL	14.94%	14.07%	-0.87%
Pig 2 – Right side, along LL	15.31%	15.99%	0.68%
Pig 2 – Right side, perpendicular LL	24.73%	25.85%	1.12%
Pig 2 – Right side, along LL (site 2)	26.11%	28.60%	2.49%
Pig 2 – Right side, perpendicular LL (site 2)	15.22%	16.00%	0.78%
Pig 2 – Left side, along LL	13.64%	16.96%	3.32%
Pig 3 – Left side, along LL	22.40%	15.61%	-6.79%
Pig 3 – Left side, perpendicular LL	21.51%	14.40%	-7.11%
Pig 3 – Right side, along LL	26.32%	12.84%	-13.48%
Pig 3 – Right side, perpendicular LL	20.05%	12.23%	-7.82%
Pig 4 – Right side, along LL	8.70%	7.56%	-1.14%
Pig 4 – Left side, along LL	13.64%	12.52%	-1.12%
Pig 4 – Left side, perpendicular LL	16.28%	10.15%	-6.13%
Thigh			
Pig 1 – Left side, along LL	14.05%	13.16%	-0.89%
Pig 1 – Left side, perpendicular LL	9.17%	9.85%	0.68%
Pig 2 – Right side, along LL	18.20%	24.36%	6.16%
Pig 2 – Right side, perpendicular LL	19.33%	25.49%	6.16%
Pig 2 – Left side, along LL	16.28%	11.01%	-5.27%
Pig 3 – Left side, along LL	25.31%	32.72%	7.41%

Pig 3 – Left side, perpendicular LL	11.23%	17.97%	6.74%
Pig 3 – Right side, along LL	20%	22.14%	2.14%
Pig 3 – Right side, perpendicular LL	11.98%	17.31%	5.33%
Pig 4 – Left side, along LL	14.94%	20.38%	5.44%
Pig 4 – Left side, perpendicular LL	19.05%	11.62%	-7.43%
Abdomen			
Pig 1 – Left side, along LL	25.84%	41.31%	15.47%
Pig 1 – Left side, perpendicular LL	17.23%	45.27%	28.04%
Pig 1 – Right side, along LL	24.35%	9.56%	-14.79%
Pig 1 – Right side, perpendicular LL	21.26%	15.67%	-5.59%
Pig 2 – Right side, along LL	18.01%	14.71%	-3.30%
Pig 2 – Right side, perpendicular LL	24.12%	19.67%	-4.45%
Pig 2 – Right side, along LL (site 2)	17.65%	12.22%	-5.43%
Pig 2 – Right side, perpendicular LL (site 2)	23.46%	16.32%	-7.14%
Pig 2 – Left side, along LL	6.38%	14.37%	7.99%
Pig 3 – Left side, along LL	31.41%	17.30%	-14.11%
Pig 3 – Left side, perpendicular LL	45.99%	46.82%	0.83%
Pig 3 – Right side, along LL	32.45%	40.35%	7.90%
Pig 3 – Right side, perpendicular LL	21.36%	24.72%	3.36%
Pig 4 – Right side, along LL	31.58%	26.24%	-5.34%
Pig 4 – Left side, along LL	11.11%	21.08%	9.97%
Pig 4 – Left side, perpendicular LL	8.70%	11.93%	3.23%

REFERENCE

Agache, P., Monneur, C., Leveque, J.L., De Rigal, J., 1980. Mechanical properties and Young's modulus of human skin *in vivo*. Archives of Dermatological Research 269, 221-232.

Agache, P., 1992. Noninvasive assessment of a biaxial Young's modulus of human skin *in vivo*. 9th International Symposium on Bioengineering of Skin, Sendai, Oct 19-20.

Agache, P., 2004. Part 1: skin structural components: physiology and metrology. In: Agache, P., Humbert, P. (Eds.), Measuring the Skin, Springer-Verlag Berlin, Heidelberg, New York. pp 21-410.

Alexander, H., Cook, T.H., 1975. The measurement of natural tension in human skin, 28th ACEMB, New Orleans, USA, Sept 20-24, 178.

Alexander, H., Cook, T.H., 1976. Variations with age in the mechanical properties of human skin *in vivo*. In: Kennedi, R.M. (Eds.), Bedsore biomechanics. McMillan Press, Bath. pp 109-118.

Alexander, H., Cook, T.H., 1977. Accounting for natural tension in the mechanical testing of human skin. Journal of Investigative Dermatology 69, 310-314.

Ashton, H., 1962. Critical closing pressure in human peripheral vascular beds. Clinical Science 22, 79–87.

Attenburrow, G.E., 1993. The rheology of leather - a review. Journal of Society of Leather Technologists and Chemists 77, 107-114.

Baker, M.R., Bader, D.L., Hopewell, J.W., 1988. An apparatus for testing the mechanical properties of skin *in vivo*: its application to the assessment of normal and irradiated pigskin. Bioengineering of Skin 4, 87-103.

Barel, A.O., Lambrecht, R., Clarys, P., 1998. Mechanical function of the skin: state of the art. In: Elsner, P., Barel, A.O., Berardesca, E., Gabard, B., Serup, J., (Eds.), Skin bioengineering techniques and applications in dermatology and cosmetology. Current Problems in Dermatology 26. Karger, Basel. pp 69–83.

Barron, J.N., Emmett, A.J.J., 1965. Subcutaneous pedicle flaps. British Journal of Plastic Surgery 5, 171-180.

Berardesca, E., Elsner, P., Wilhelm, K and Maibach, H. (Eds.), 1995. Bioengineering of the skin: Methods and instrumentation. CRC Press, Boca Raton, London, New York.

Blocker Jr., T.G., Mithoefer, J., 1950. The pattern flap, Plastic and Reconstructive Surgery 5, 163-167.

Barrett-Brown, J., Cannon, B., Graham, W.C., Lischer, C.E., Scarborough, C.P., Davis, W.B., Moore, A.M., 1945. Direct Flap Repair of Defects of the Arm and Hand – Preparation of Gunshot Wounds for Repair of Nerves, Bones and Tendons. Annals of Surgery 122(4), 706-715.

Burton, A.C., 1951. On the physical equilibrium of small blood vessels. American Journal of Physiology 164, 319-329.

Cannon, B., Lischer, C.E., Davis W.B., Chasko, S., Moore, A., Murray, J.E., McDowell, A., 1947. The use of open jump flaps in lower extremity repairs. Plastic Reconstructive Surgery 2, 336-341.

Chui, C., Kobayashi, E., Chen, X., Hisada, T., Sakuma, I., 2004. Combined compression and elongation experiments and non-linear modelling of liver tissue for surgical simulation. Medical and Biological Engineering and Computing 42, 787-98.

Clark, J.A., Cheng, J.C., Leung, K.S., Leung, P.C., 1987. Mechanical characterisation of human postburn hypertrophic skin during pressure therapy. Journal of Biomechanics 20, 397-406.

Clark, J.A., Cheng, J.C., Leung, K.S., 1996. Mechanical properties of normal skin and hypertrophic scars. Burns 22, 443-446.

Coakley, W.A., McCoy, S.M., Kelleher, J.C., 1950. The use of direct forearm flaps in resurfacing defects of the soft tissues of the lower extremities. Plastic Reconstructive Surgery 6, 413-424.

Cook, T., Alexander, H., 1975. The measurement of natural tension in human skin. In 28th Annual Conference on Engineering in Medicine and Biology, New Orleans.

Cox, H.T., 1941. The cleavage lines of the skin. British Journal of Surgery 29, 234-240.

Crawford, B.S., 1965. The management of tube pedicles. British Journal of Plastic Surgery 18(4), 387-96.

Daly, C.H., 1969. The role of elastin in the mechanical behavior of human skin. In proceedings of 8th ICMBE, Chicago, IL.

Daly, C.H., 1982. Biomechanical Properties of dermis. Journal of Investigative Dermatology 79, 17-20.

Danielson, D. A., 1973. Human skin as an elastic membrane. Journal of Biomechanics 6(5), 539-546.

Danielson, D.A., Natarajan, S., 1975. Tension field theory and the stress in stretched skin, Journal of Biomechanics 8, 135-142.

Dickson, B.C., 2004. Venous thrombosis: on the history of Virchow's triad. University of Toronto Medical Journal 81, 166-171.

Diridollou, S., Black, D., Lagarde, J.M., Gall, Y., 2000. Sex and site-dependent variations in the thickness and mechanical properties of human skin *in vivo*. International Journal of Cosmetic Science 22, 421–435.

Diridollou, S., Patat, F., Gens, F., Vaillant, L., Black, D., Lagarde, J.M., Gall, Y., Berson, M., 2000. *In vivo* model of the mechanical properties of the human skin under suction. Skin Research and Technology 6, 214-221

Elsner, P., Berardesca, E., Wilhelm, K., Maibach, H. (Eds.), 2002. Bioengineering of the skin: skin biomechanics. CRC Press, Boca Raton, London, New York, Washington D.C.

Emmanuelle, J., Josse, G., Fouad, K., Camille, G., 2007. A new experimental method for measuring skin's natural tension. Skin Research and Technology, *(online early article)*.

Escoffier, C., 1989. Age related mechanical properties of human skin: an *in vivo* study. Journal of Investigative Dermatology 93, 353-357.

Evans, J.H., Siesennop. W.W., 1967. Controlled quasi-static testing of human skin *in vivo*. In Digest of the 7th International Conference on Medical and Biological Engineering. Stockholm.

Fawcett, D.W. (Ed.), 1986, A Textbook of histology-11th edition, W.B Saunders Company, Philadelphia.

Foutz, T.L., Stone, E.A., Abrams, C.F. Jr., 1992. Effects of freezing on mechanical properties of rat skin. American Journal of Veterinary Research 53(5), 788-92.

Fung, Y.C. (Ed.), 1996. Biomechanics: Mechanical properties of living tissues. Springer-Verlag, New York.

Gibson, T., Kenedi, R.M., Craik, J.E., 1965. The mobile micro architecture of dermal collagen. British Journal of Surgery 52, 764-770.

Gibson, T., Stark, H., Evans, J.H., 1969. Directional variation in extensibility of human skin *in vivo*. Journal of Biomechanics 2, 201-204.

Grahame, R., Holt, P.J.L., 1969. The influence of ageing on the *in vivo* elasticity of human skin. Gerontologia 15, 121-139.

Gunner, C.W., Hutton, W.C., Burlin, T.E., 1979a. The mechanical properties of skin *in vivo*- a portable hand held extensometer. British Journal of Dermatology 100, 161-163

Gunner, C.W., Hutton, W.C., Burlin, T.E., 1979b. An apparatus for measuring the recoil characteristics of human skin *in vivo*. Medical and Biological Engineering and Computing 17, 142-144

Hendriks, F.M., Brokken, D., van Eemeren, Oomens, C.W. J., Baaijens, F.P.T., Horsten, J.B.A.M., 2003. A numerical-experimental method to characterize the non-linear mechanical behavior of human skin, Skin Research and Technology 9, 274-283.

Hudson-Peacock, M.P., Matthews, J.N.S. and Lawrence, C.M., 1995. Relation between size and skin excision, wound and specimen. Journal of the American Academy of Dermatology 32, 1010-1015.

Jeyapalina, S., Lim, K.H., Ho, H.N., Poston, T., Chew, C.M., Chen, C.Y., Rappel J.K., Lim, B.H., 2005. Directional dependent *in vivo* mechanical behavior of human skin. In Proceedings of the 12th International Conference on Biomedical Engineering, Singapore.

Jeyapalina, S., Lim, K.M., Chen, C.Y., Chew, C.M., Lim, K.H., Ho, H.N., Poston, T., Selvanayagam, C., Lim, B.H., 2005. A finite element model for estimating skin flap shrinkage. In Proceedings of the 12th International Conference on Biomedical Engineering, Singapore.

Jobert, A.J., 1849. Chirurgie Plastique, pp. 5, 13, 58, 59, 60, 62, 76 and 77. Vailliere, Paris.

Kenedi, R. M., Gibson, T., Evans, J. H., Barbenel, J. C., 1975. Tissue mechanics. Physics in Medicine and Biology 20(5), 699-717.

Kolodney M.S., Wysolmerski, R.B., 1992. Isometric contraction by fibroblast and endothelial cells in tissue culture: a quantitative study. The Journal of Cell Biology 117, 73-82.

Kovarik, C., Stewart, D., Cockerell, C., 2005. Gross and histologic postmortem changes of the skin. American Journal of Forensic Medicine and Pathology 26(4), 305-8.

Langer, K., 1862. Zur Anatomie Und Physiologie Der Haut II. Die Spannung der C tis. *Sitzungsberichte der Mathematisch Naturwissenschaftlichen Akademie Wein*, 45(1), 133-188.

Langer, K., 1978 A. On the anatomy and physiology of the skin: I. The cleavability of the cutis. British Journal of Plastic Surgery 31, 3-8.

Langer, K., 1978 B. On the anatomy and physiology of the skin: II. Skin tension. British Journal of Plastic surgery 31, 93-106.

Lanir, Y., Fung, Y.C., 1974. Two dimensional mechanical properties of rabbit skin II: experimental results. Journal of Biomechanics 7, 171-182.

Lanir, Y.; Skalak, R., Chien, S., (Eds.), 1987. Skin Mechanics. Handbook of Bioengineering. McGraw-Hill, New York.

Larrabee, W. F. Jr., Sutton, D., 1986. A finite element model of skin deformation. II. An experimental model of skin deformation. Laryngoscope 96(4), 406-412.

Leveque, J.L., De Rigal, J., Agache, P., Monneur, C., 1980. Influence of ageing on the *in vivo* extensibility of human skin at a low stress. Archives of Dermatological Research 269, 127-135.

Lim, K.H., Ho, H.N., Chew, C.M., Chen, C.Y., Jeyapalina, S., Teo, C.L., Lim, B.H., 2006. Non-invasive *in vivo* measurement of skin flap shrinkage. In Proceedings of the XVth International Conference of Mechanics in Medicine and Biology. Nanyang Technological University, Singapore.

Manschot, J.F.M., Brakkee, A.J.M., 1986. The measurement and modeling of the mechanical properties of human skin *in vivo*, 1. The measurement. Journal of Biomechanics 19, 511-515

Masquelet, A.C., Gilbert, A., 1995. An atlas of flaps in limb reconstruction. Martin Dunitz, London.

McGregor, I.A., Jackson, I.T., 1970. The extended role of the delto-pectoral flap. British journal of plastic surgery 23, 173-185.

Panisset, F., 1992. Le stratum corneum: sa place dans la function me´canique de la peau humaine *in vivo*. MD thesis, Franche-Comte´ University, France.

Reihsner, R., Baloghi, B., Menzel, E. J., 1995. Two-dimensional elastic properties of human skin in terms of an incremental model at the *in vivo* configuration. Medical Engineering and Physics 17, 304-313.

Rodrigues, L., 2001. Part 2 EEMCO Guidance to the *in vivo* assessment of tensile functional properties of the Skin Part 2: Instrumentation and test modes. Journal of pharmacological and biophysiological research 14. 52-67.

Rose, E.H., Ksander, G.A., Vistnes, I.M., 1976. Skin tension lines in the domestic pig. Plastic Reconstructive Surgery 57, 729-32.

Sanders, R., 1973. Torsional elasticity of human skin *in vivo*. Pflügers Arch 342, 255-260.

Sanders, J.E., Goldstein, B.S., Leotta, D.F., 1995. Skin response to mechanical stress: adaptation rather than breakdown- A review of the literature, Journal of rehabilitation research and development 32, 214-226.

Sawhney, C.P., 1977. The influence of skin tension on the contraction of open wounds and skin grafts in rabbits. British Journal of Plastic Surgery 30, 115-117.

Serup, J., Jemec, G.B.E, Grove, G.L., 2006. Handbook of non-invasive methods and the skin, 2nd edition. CRC Press, Boca Raton, London, New York.

Silver, F.H., Siperko, L.M., Seehra, G.P., 2003. Mechanobiology of force transduction in dermal tissue. Skin Research and Technology 9, 3-23.

Stark, H.L., 1977. Directional variations in the extensibility of human skin. British Journal of Plastic Surgery 30, 105-114.

Stell, P.M. 1980. The effect of varying degrees of tension on the viability of skin flaps in pigs. British Journal of Plastic Surgery 33, 371-376.

Stell, P.M., 1982. Retraction of skin flaps, Clinical Otolaryngology 7, 45-49.

Strauch, B., Yu, H.L., 1992. Atlas of Microvascular Surgery: Anatomy of Operative Approaches. Thieme Medical Publishers, New York.

Sun, Q., Lin, S.F., Al-Saeedea, S. Ruberte, L., Nam, E., Hendrix, R., Makhsous, M., 2005. Soft Tissue Stress in Buttock-Thigh of a Seated Individual Elucidated by a 3D FE Model. In proceedings of 28th Annual RESNA Conference, Atlanta, GA.

Thacker, J.G., Lachetta, F.A., Allaire, P.E., Edgerton, M.T., Rodeheaver, G.T. and Edlich, R.F., 1977. *In vivo* extensometer for measuring of the biomechanical properties of human skin. Review of Scientific Instruments 48, 181-185.

Van Ee, C.A., Chasse, A.L., Myers, B.S., 2000. Quantifying skeletal muscle properties in cadaveric test specimens: effects of mechanical loading, postmortem time, and freezer storage. Journal of Biomechanical Engineering 122(1), 9-14.

Vescovo, P., 1998. Validation de methods de measure des mod modules d'élasticité de la peau humaine. Diplôme d'Etudes Approfondies, Université de Franche-Comté.

Virchow, R.L.K.; translators: Matzdorff, A.C., Bell, W.R., 1998. Thrombosis and Emboli. Science History Publications, Canton, Massachusetts.

PUBLISHED WORKS

A list of patents and publications by the thesis author is given as follows.

Patents

Lim, K.H., Poston, T., Ho, H.N., Chew, C.M., Chen, C.Y., Jeyapalina, S., Lim, B.H., 2008. Apparatus and method for measuring *in vivo* biomechanical properties of skin. Patents No. US2008200842, EP1906831 and WO2007004993.

Journals

Lim, K.H., Chew, C.M., Chen, P.C.Y., Jeyapalina, S., Ho, H.N., Rappel, J.K., Lim, B.H., 2008. New extensometer to measure *in vivo* uniaxial mechanical properties of human skin. Journal of Biomechanics 41, 931-936.

Lim, K.H., Jeyapalina, S., Ho, H.N., Chew, C.M., Chen, P.C.Y., Teo, C.L., Lim, B.H., 2008. Non-invasive prediction of skin flap shrinkage: a new concept based on animal experimental evidence. Journal of Biomechanics 41(8), 1668-1674.

Journals (under review)

Lim, K.H., Jeyapalina, S., Ho, H.N., Rappel, J.K., Chew, C.M., Chen, P.C.Y., Teo, C.L., Lim, B.H., 2008. Skin flap surgical planner – a new *in vivo* non-invasive method to estimate skin flap shrinkage. Journal of Biomechanics.

Jeyapalina, S., Lim, K.H., Ho, H.N., Poston, T., Chew, C.M., Chen, P.C.Y., Rappel, J.K., Lim, B.H., 2008. A non-invasive approach for predicting Langer's line. Skin Research and Technology.

Conferences

Lim, K.H., Ho, H.N., Chew, C.M., Chen, C.Y., Jeyapalina, S., Teo, C.L., Lim, B.H., 2006. Non-invasive *in vivo* measurement of skin flap shrinkage. In Proceedings of the XVth International Conference of Mechanics in Medicine and Biology. Nanyang Technological University, Singapore.

Lim, K.H., Ho, H.N., Chew, C.M., Chen, C.Y., Jeyapalina, S., Teo, C.L., Lim, B.H., 2006. New extensometer to measure *in vivo* uniaxial mechanical properties of human skin. In Proceedings of the XVth International Conference of Mechanics in Medicine and Biology. Nanyang Technological University, Singapore.

Lim, K.H., Ho, H.N., Chew, C.M., Chen, C.Y., Jeyapalina, S., Teo, C.L., Lim, B.H., 2005. New uniaxial extensometer to measure *in vivo* mechanical properties of human skin. In Proceedings of the 12th International Conference on Biomedical Engineering, Singapore. *(* Won best paper award)*

Jeyapalina, S., Lim, K.H., Ho, H.N., Poston, T., Chew, C.M., Chen, C.Y., Rappel J.K., Lim, B.H., 2005. Directional dependent *in vivo* mechanical behavior of human skin. In Proceedings of the 12th International Conference on Biomedical Engineering, Singapore.

Jeyapalina, S., Lim, K.M., Chen, C.Y., Chew, C.M., Lim, K.H., Ho, H.N., Poston, T., Selvanayagam, C., Lim, B.H., 2005. A finite element model for estimating skin flap shrinkage. In Proceedings of the 12th International Conference on Biomedical Engineering, Singapore.